PURDUE UNIVERSITY

MIT

NUMERICAL SIMULATION OF SOLUTE TRANSPORT IN RANDOMLY HETEROGENEOUS POROUS MEDIA: MOTIVATION, MODEL DEVELOPMENT, AND APPLICATION

by

ANDREW F. B. TOMPSON

EFSTRATIOS G. VOMVORIS

and

LYNN W. GELHAR

RALPH M. PARSONS LABORATORY
HYDROLOGY AND WATER RESOURCE SYSTEMS

DEPARTMENT

OF

CIVIL

ENGINEERING

SCHOOL OF ENGINEERING
MASSACHUSETTS INSTITUTE OF TECHNOLOGY
Cambridge, Massachusetts 02139

Report Number 316

February, 1988

R88-05

NUMERICAL SIMULATION OF SOLUTE TRANSPORT IN RANDOMLY HETEROGENEOUS POROUS MEDIA: MOTIVATION, MODEL DEVELOPMENT, AND APPLICATION

by

ANDREW F.B. TOMPSON
EFSTRATIOS G. VOMVORIS
LYNN W. GELHAR

RALPH M. PARSONS LABORATORY

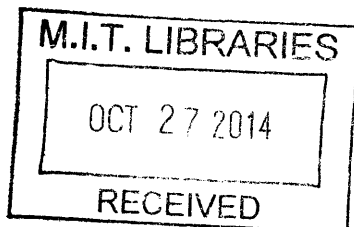HYDROLOGY AND WATER RESOURCES SYSTEMS

Report Number 316

FEBRUARY 1988

ABSTRACT

A particle tracking, or "random walk" solute transport model is developed to study detailed contaminant movements through large, synthetic heterogeneous flow systems in porous media. Such simulations can be used to examine the large time and spatial effects of the variable flow field on the expanding solute plumes. More specifically, the large scale experimental dispersive behavior can be compared with theoretical predictions based upon stochastic analyses. The particle tracking model is developed from first principles and is shown to be the most computationally efficient model for this type of application. Computational issues regarding the model's implementation are discussed, including the choice of time steps, boundary and initial conditions, and conversion of solutions to concentration fields. The model is applied to some simple test problems and then to two large, three-dimensional, heterogeneous, saturated flow systems. The results of these preliminary investigations are analyzed and compared with results of stochastic theories. They are also used to plan more comprensive simulations to be carried out in the future.

- 2 -

ACKNOWLEDGEMENTS

Table of Contents

List of Figures

List of Tables

1. INTRODUCTION

1.1 Scope. This report is intended to review the design, development and implementation of a detailed solute transport model for use in studying contaminant movements through large heterogeneous flow systems in porous media. The model is based upon a particle tracking or "random-walk" approach and is meant to be applicable to large, three-dimensional problems dealing with the transport of dilute solutions of conservative materials through saturated or unsaturated flow regions. The interest in carrying out these simulations stems from a desire to examine the *detailed* spatial and temporal effects of developing solute plumes in heterogeneous porous media. Although such investigations can be carried out and analyzed in many different ways, we specifically wish to compare the results of these simulations and their mean characteristics directly with the large scale, mean predictions of several stochastic transport theories [e.g., *Gelhar et al.*, 1979, *Matheron and de Marsily*, 1980, *Gelhar and Axness*, 1983, *Dagan*, 1984, *Gelhar*, 1984, and *Mantoglou and Gelhar*, 1987a,b,c]. As developed, the transport model can also be implemented in another way for the solution of larger-scale, *mean* transport equations, as developed in the stochastic theories. Applications of this sort would involve larger-scale, mean velocities and effective dispersion coefficients and would form an integral part of a new, practical, and more credible modeling approach [*Gelhar*, 1986,1987].

1.2 Background. It is well known that subsurface porous materials can exhibit a large degree of natural variability, in terms of both their specific type and spatial distribution. Geologic formations that act as flow conduits are often characterized by highly variable three-dimensional structures consisting of layers, lenses, and perhaps, fractures in various materials ranging from sands and gravels to clays or rocks. Corresponding to these material fluctuations is a similar variablility in the characteristic hydraulic parameters used for the description of both flow and transport in porous media scale balance equations [e.g., *Hassanizadeh and Gray*, 1979a, b]. Although these balance laws are phrased in terms of spatially variable coefficients, their use in classical numerical models to obtain reliable, large scale predictions of flow and transport (in space and time) through variable media can be hampered by several factors. In many cases, geologic properties can vary over spatial scales too small to be accurately resolved (much less physically measured) in a discretized numerical model [e.g., *Gelhar*, 1984]. Depending on the medium and problem size, such a detailed representation could conceivably require an immense number of nodes ($\sim 10^9$?) to account for the necessary detail over the flow domain. A usual procedure in these situations is to consider a number of homogeneous layers or zones and treat hydraulic variabilities element- or node-wise in a traditional finite element or finite difference grid. Such an approach ostensibly ignores the effects of any fine variations of the

hydraulic parameters *within* the elements or *between* the nodes. However, it will typically involve the fitting of smooth solution(s) through measured points with partially manipulated, representative parameters. This process basically accounts in some part for measurement errors in the parameters as well as the aforementioned sub-grid scale variabilities, although it is neither quantitative nor predictive in nature. The resultant solutions essentially represent an averaged behavior on a scale closer to the size of an element, grid increment, or length scale of the input parameter variation. They do not necessarily reflect variabilities of quantities defined around the laboratory or representitive elementary volume (REV) scale if significant heterogeneities of these parameters exist within computational elements.

The idea behind many of the stochastic approaches mentioned above is to try to quantitatively account for the effects of these small scale parameter variabilities so that they can be reliably included in large scale predictive models without any extravagant data acquisition or grid resolution expense. The usual theoretical approach employs a simple *model* representation of the smaller scale variabilities and attempts to mathematically discern the resulting effects on, say, the flow and concentration fields. The locally variable hydraulic parameter distributions are represented mathematically as realizations of stationary spatially correlated random fields [*Vanmarcke*, 1983]. Each field is characterized in an approximate way by its first two statistical moments, namely the mean, variance about the mean, and a correlation structure with an associated set of integral or correlation length scales [*Gelhar*, 1984]. Although the hydraulic parameters are not truly "random", this construct seems to be an appropriate approximation in many problems where the parameter variability about an unchanging (or perhaps linearly varying) mean is roughly constant (i.e., "locally stationary") over the flow domain of interest [e.g., *Ababou, et al.*, 1985, *Gelhar*, 1987].

The ultimate objective is to use this sort of parameter representation as an input to the classical balance equations mentioned above. Corresponding to the mean values of the input parameters will be mean, or smoothed output fields (i.e., head, velocity, concentration) that satisfy larger scale, mean balance equations phrased in terms of these quantities and effective (or, large scale) hydraulic parameters. The effective coefficients embody the influence of the small-scale variability otherwise not directly present in the mean equations. These averaged balance equations are the ones meant to be used in everyday practice. They would be solved numerically in the familiar fashion for the mean (e.g., *smoothed*) output fields as discussed above, and they would employ the effective coefficients derived from the theory. The variability of the true (or locally measured) values about the predicted mean solution as well as the effective parameters can be quantified in terms of the statistical parameters used to describe the variable medium. Measurement of the statistical quantities is meant to be much easier than mapping out the entire distribution of the hydraulic parameters themselves. This process, in a sense, systemizes the usual ad-hoc modeling procedures described above. It also

provides a framework for judging the reliability of these models in terms of a different fitting procedure: instead of trying to force the numerical (mean) solution to fit all the measurements (quantities now seen to be representative of different scales), one now tries to fit the measurements within a "band" around the mean solution, the width of the band being related to the predicted local variability discussed earlier. These methods are analogous to similar procedures utilized in the study of turbulence [*Monin and Yaglom*, 1975].

1.3 Scales. Implicit in all of this work is a conscious recognition of two distinct spatial scales, although many others could be hypothesized. The first is the familiar "REV" or local scale around which the traditional porous media continuum variables, balance equations and numerical models are developed [*Hassanizadeh and Gray*, 1979a, b]. Most laboratory studies as well as many kinds of field measurements are made (more or less) at this scale. Point head observations, multilevel concentration samples, some hydraulic conductivity evaluations and laboratory dispersivity measurements serve as examples. Here we are not considering the differences between theoretically-based REV scales and those based around the scale of a measuring instrument [see the discussions of *Cushman*, 1984, *Baveye and Sposito*, 1984, and *Whitaker*, 1986]; such effects can be treated routinely within a stochastic framework, however, by incorporating an appropriately weighted linear filter to represent spatial averaging. The second spatial scale is the larger "ensemble" or "mean" scale about which the mean balance equations, effective coefficients, and smoothly varying solutions discussed in the stochastic literature are defined. Although not formulated in a volumetric sense, quantities formulated about this scale are meant to be representative of regions larger than an REV, and would typically be different than the smaller scale counterparts if significant variabilities of the small scale processes exist. This is essentially the scale around which many traditional models with manipulated parameters and smoothly varying results are centered, even though it is not usually recognized as such, and is the one implied above when mean or averaged balance equations are discussed.

1.4 Objectives. The primary aim of the present and complementary [e.g., *Ababou, et al*, 1985] numerical investigations is to develop a flow and transport model to solve the *local* balance equations for fluid mass, momenta and solute mass in a large, three-dimensional saturated or unsaturated domain characterized by heterogeneous distributions of hydraulic parameters. It is then desired to analyze the behavior of the local solutions and compare them with larger scale results predicted by the stochastic theories mentioned above.

To be consistent with the fundamental hypotheses of the stochastic theories [e.g., *Gelhar*, 1984, *Mantoglou and Gelhar*, 1987a,b,c] the variable hydraulic parameter field(s) will be modeled as realizations of spatially correlated random fields. Flow fields will be developed for independent

study as well as input to the transport model here. The local transport simulations will be used to examine large time and spatial effects of the variable flow fields on a developing solute plume, and, in particular, investigate the nature of the mean, large scale dispersive behavior. The stochastic results of *Gelhar et al.,* [1979], *Gelhar and Axness,* [1983], *Dagan* [1984], and *Gelhar,* [1987] generally indicate that this behavior can be described by an asymptotic Fickian relationship in terms of constant macrodispersivities and the spatial gradient of the mean (large scale) concentration. Other topics, such as the specific influence of locally variable dispersivities on these phenomena, the concentration variability or variance, as well as the specific effects of the kind of underlying correlation structure selected to represent the variable hydraulic parameters can be studied.

The local simulations will focus on the generation of a large single replicate of the hydraulic parameters over space and the use of this "artificial" domain for the flow and transport studies. This is similar in concept to the approach of *Cole, et al.* [1985] who consider saturated two-dimensional flow and transport in a "numerical groundwater laboratory" characterized by five distinct kinds of materials distributed according to a cross sectional photograph of an actual alluvial deposit. Their model computed flow on a grid of roughly $260,000$ nodes and used a particle tracking technique for transport based only upon a constant local diffusion coefficient. Our approach has been designed to consider three-dimensional problems for both saturated and unsaturated problems with up to as many as 10^7 nodes and will involve local transport equations based upon velocity dependent dispersion coefficients. Our approach is similar also to those of *Schwartz,* [1977], *Smith and Schwartz,* [1980], and *Uffink,* [1983] who consider saturated two-dimensional problems based on conductivities distributed either in layers, as grid-like inclusions in an otherwise homogeneous medium, or randomly in space as done here. All of these investigations use particle tracking methods to model solute movement.

Unlike *Smith and Schwartz,* [1980], however, we will not consider Monte Carlo analyses which involve repeated simulations of the same flow and transport problem in the same region with different realizations of the conductivity field (with identical statistics). This approach can be useful for identifying "worst case" scenarios and it is, of course, the proper arena for numerical verification of any ensemble stochastic theory. Our approach is a pragmatic one, however, and is designed to simultaneously test both the theory and the implicit ergodic hypothesis that allows one to use ensemble theory to approximate the behavior of a single realization. This rationale is practical for the following reason: as repeated aquifer realizations do not occur in the real world, assessment of the utility of the mean or averaged balance equations as well as the theoretical predictions of local variability might best be made under the circumstances for which they ultimately are meant to be used: a "single replicate" of a large, statistically homogeneous porous medium.

A secondary objective of this study is to review the theoretical and computational aspects of particle tracking methods with regard for their use in this and other transport investigations.

1.5 Report Outline. In the next two sections, specific details of the problem setups will be reviewed, including a review of the governing equations, physical system, and the choice of the particle tracking technique for our transport simulations. In sections 4 and 5, the theoretical basis of the "random-walk" model will be presented in brief and a discussion of its relative merits and disadvantages will be given, from both a theoretical and computational point of view. Section 6 will review a number of applications of the simulator to a preliminary selection of model problems. The relevant results will be compared with predictions of stochastic theories. Section 7 will include further comments on these and future problems and a discussion of other potential applications of this model.

2. PHYSICAL SYSTEM AND GOVERNING EQUATIONS

2.1 Local System and General Balance Laws. Consider a porous medium composed of a rigid solid phase partially saturated with both an air and water phase. Let the water phase contain a dilute solution of a non-reacting and non-sorbing chemical species such that the overall bulk fluid properties such as viscosity and density remain unchanged by the presence of the solute. Furthermore, assume that this medium is locally homogeneous so that a single representative elementary volume (REV) can be defined and used everywhere in some domain Ω to define local scale continuum balance equations for the mass and momenta of each phase as well as the solute mass [*Bear*, 1972; *Hassanizadeh and Gray*, 1979 a, b]. Attention here will be restricted to the isothermal balances of fluid mass and momentum and solute mass in Ω, the first and last of which are given by

$$\frac{\partial}{\partial t}(\rho\theta) + \nabla\cdot(\rho\theta v) = 0 \tag{1}$$

$$\frac{\partial}{\partial t}(\rho\theta\omega) + \nabla\cdot(\rho\theta v\omega) + \nabla\cdot J = 0 \tag{2}$$

The variables in (1) and (2) are microscopically averaged (REV) continuum quantities associated with the porous medium and are defined at all points x in Ω. They will be considered as local porous medium properties (as opposed to larger scale mean or effective properties referred to elsewhere) and are defined by

ρ =   constant, mass averaged fluid density,

$\theta(x,t)$ =   fluid void fraction, or porosity,

$v(x,t)$ =   mass averaged fluid seepage velocity,

$\omega(x,t)$ =   mass averaged mass fraction of the chemical species, and

$J(x,t)$ =   mass averaged, nonadvective flux vector of the chemical species.

It is also assumed that the local fluid momentum balance is given by the modified form of Darcy's law,

$$\theta v = q = -K\nabla(h + z) \tag{3}$$

Here,

$q(\mathbf{x},t)$ = Θv = the Darcy fluid mass flux,

$K(\mathbf{x},t)$ = a local, scalar hydraulic conductivity,

$h(\mathbf{x},t)$ = $p(\mathbf{x},t)/\rho g$ = the local pressure head, g being the magnitude of the gravitational acceleration and $p(\mathbf{x},t)$ being the gauge pressure relative to atmospheric, and

z = the elevation above some reference datum (specifically along a direction parallel with the gravity vector).

The coordinate system $\mathbf{x} = x_i = (x,y,z)$ is assumed orthogonal, z being in the vertical, and fixed with the medium.

Three constitutive approximations for Θ, K, and J are adopted to further describe and simplify the porous medium under study. The moisture content and conductivity are chosen to closely parallel the work of *Mantoglou and Gelhar* [1987a,b,c]:

$$\Theta = \begin{cases} \Theta_r & h - h_r \le (\Theta_r - \Theta_0)/C & \text{(unsaturated)} \\ \Theta_0 + C(h - h_r) & (\Theta_r - \Theta_0)/C < h - h_r < 0 & \text{(unsaturated)} \\ \Theta_0 & h - h_r \ge 0 & \text{(saturated)} \end{cases} \qquad (4)$$

$$K = \begin{cases} K_s\, e^{\alpha(h - h_r)}, & h - h_r < 0 & \text{(unsaturated)} \\ K_s & h - h_r \ge 0 & \text{(saturated)} \end{cases} \qquad (5)$$

where

$\Theta_0(\mathbf{x})$ = the saturated fluid void fraction, or effective porosity, at $\mathbf{x}$,

$C(\mathbf{x})$ $\equiv$ $\partial\Theta/\partial h$ = a linearized soil moisture capacity at $\mathbf{x}$,

$\alpha(\mathbf{x})$ = a linear characteristic $\ln K$ -- h slope at $\mathbf{x}$,

$K_s(\mathbf{x})$ = the saturated hydraulic conductivity at $\mathbf{x}$, a scalar,

Θ_r = a constant, dry or residual moisture content, and

h_r = a small, positive constant residual pressure head above which saturated flow exists.

Notice that in the special case of saturated flow, $\Theta(\mathbf{x},t) \equiv \Theta_0(\mathbf{x})$, and the head and velocity fields will be steady (if the boundary conditions are time independent). The local nonadvective flux is assumed to obey a general Fickian relationship [*Bear*, 1972]:

$$J = -\rho\theta\, \mathbb{D}\cdot\nabla\omega \tag{6}$$

where $\mathbb{D}(\mathbf{x},t)$ is the widely used velocity-dependent hydrodynamic dispersion tensor for an isotropic medium:

$$\mathbb{D} = (\alpha_T V + D)\mathbb{I} + (\alpha_L - \alpha_T)\mathbf{v}\mathbf{v}/V \tag{7}$$

Here, $V(\mathbf{x},t)$ is the magnitude of the velocity, $\alpha_L(\mathbf{x})$ and $\alpha_T(\mathbf{x})$ are local longitudinal and transverse dispersivities, respectively, and $D(\mathbf{x})$ is a molecular diffusion coefficient that includes the effects of the medium tortuosity. Groundwater velocities V are typically on the order of 10^0-10^2 cm/day in magnitude (i.e., 10^{-5}-10^{-3} cm/sec). As measured in local laboratory situations, the magnitudes of α and D are $O(1)$ cm and $O(10^{-5})$ cm^2/sec, respectively.

2.2 Larger Scale System and Mean Balance Laws. All of the material coefficients introduced above (θ_0, K_s, C, α, D, α_L, and α_T) represent some aspect of the local (REV scale) medium behavior. If the local medium characteristics vary over regions much larger than the REV scale, these properties would most generally become spatially dependent. Spatial heterogeneity in the saturated conductivity K_s (or its natural logarithm), for example, is well documented, and variabilities in other hydraulic parameters or fields are also widely reported [e.g., *Gelhar*, 1984, 1987, *Hoeksema and Kitanidis*, 1985, *Wierenga, et al.*, 1985, *Yeh, et al.*, 1985b, *Yeh, et al.*, 1986].

In the stochastic models discussed above, attention is generally focused on the influence of the spatial variation of $\ln(K_s)$ on the hydraulic flow fields. The characteristic length over which fluctuations of $\ln K_s$ are observed is the correlation or integral scale, λ (Figure 1). This quantity can be dependent on direction and is used to parameterize the statistical (or, correlation) model of the variable medium. Depending on the medium, the magnitude of λ can range anywhere from 0.1 to 1000 meters [*Gelhar and Axness*, 1983, *Gelhar*, 1984, 1987, *Hoeksema and Kitanidis*, 1985]. Observations of the $\ln(K_s)$ process generally indicate that it can vary about a mean or trend $F(\mathbf{x})$ that can remain constant or vary linearly over a much larger scale L, perhaps on the order of 1 to 10 kilometers, and that this itself can be dominated by a larger regional scale L_F, indicative of a nonlinear nature of the trend [*Gelhar*, 1986]. The degree of local variability about $F(\mathbf{x})$ is measured by the standard deviation statistic σ_f of $\ln(K_s)$. This can range from 0.2 (uniform media) to 5 or more (very heterogeneous media).

Because we intend to compare our results to large scale stochastic theories based upon stationarity assumptions, interest here will be limited to those systems that possess some degree of local stationarity; i.e., ones where λ/L and σ_f/L are much smaller than unity [*Gelhar*, 1987]. Thus,
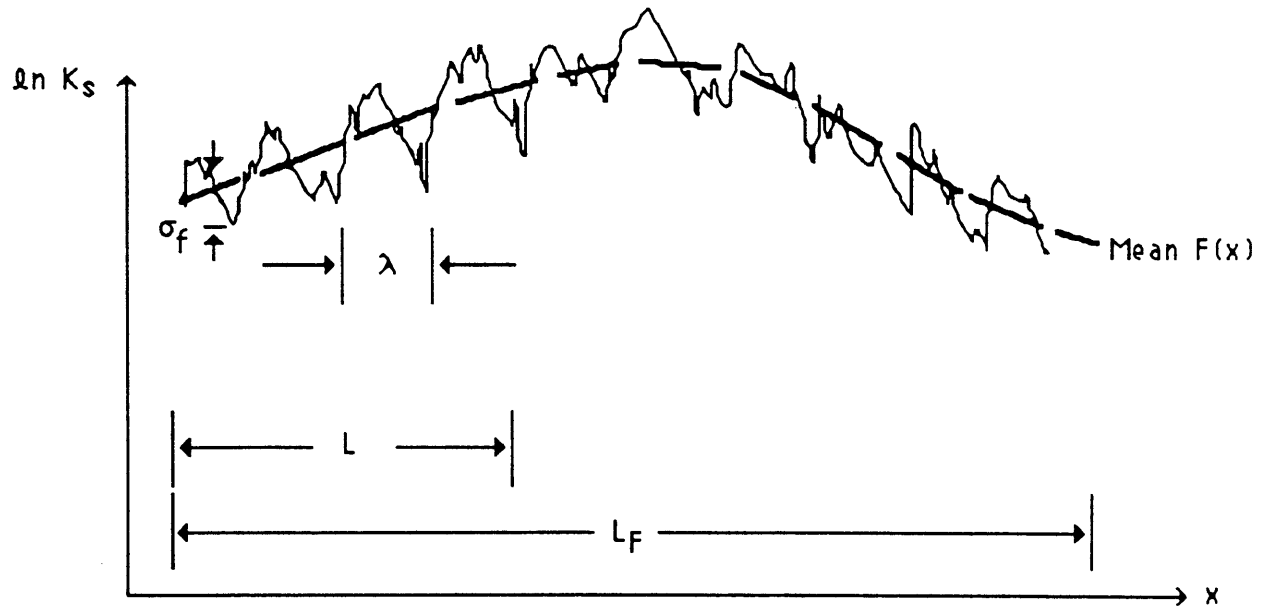
$$\lambda \approx 0.1 - 1000\,m$$

$$L \approx 1 - 10\,km$$

$$L_F \approx 10\,km \text{ or higher}$$

Figure 1:   Scales of $\ln K_s(x)$

domains of length less than or equal to L are usually considered. The $\ln(K_s)$ variability over such a region is usually approximated by

$$\ln K_s(x) = F(x) + f(x) \tag{8a}$$

where $F(x)$ is the mean or expectation of $\ln(K_s)$, at most a linear function, and $f(x)$ is a perturbation from the mean. The perturbation is modeled as a zero-mean stationary random field with a correlation structure $R_{ff}(\xi)$. The variance σ^2_f is simply $R_{ff}(0)$. Although every random field possesses an infinite set of moments, it is only the first two, namely $F(x)$ and $R_{ff}(\xi)$, that are used to specify the degree of variability and structure of the natural system and $\ln(K_s)$. Because of this approximation, it is not necessary to know the exact form of the joint probability distribution function associated with f. Nevertheless, a large body of evidence suggests that the marginal densities of K_s are log-normal [*Freeze*, 1975], so the $\ln K_s$ process will be considered as a normally distributed random field.

For unsaturated systems, the influence of the spatial variation of $\alpha(x)$ and/or $C(x)$ is also included in the stochastic models of *Yeh, et al.* [1985a, 1986] and *Mantoglou and Gelhar,* [1987a]. Their spatial behavior is similarly approximated:

$$\alpha(x) = A + a(x) \tag{8b}$$

$$C(x) = \Gamma + \gamma(x) \tag{8c}$$

Here, A and Γ are the constant means of α and C, respectively, and $a(x)$ and $\gamma(x)$ are stationary, spatially correlated random fields. For simplicity, the correlation models of a and γ are presumed to differ from R_{ff} by multiplicative constants $(\sigma^2_a/\sigma^2_f$ or $\sigma^2_\gamma/\sigma^2_f)$, and cross covariances between a, γ, and f are either assumed to be perfect or nonexistent. For lack of other information, they will also be modeled as normally distributed fields.

As mentioned in §1.4, there exists a set of mean hydraulic output fields that correspond to the means of the parameter fields and their modeled variabilities. These are conserved according to a set of larger scale, mean balance equations similar in form to those in §2.1. The form of the larger scale equations is generally found by inserting the model parameter representations (8) into the balance laws (1), (2), and (3) and forming the mean or expected value of these equations under the joint probability distribution used to model the variabilities of f, a, and γ. These laws will be approximate because only the first and second order moments of f, a, and γ are used to characterize their distributions in the theoretical analyses. They can be thought of as filtered equations, affected

by the small scale equations and parameter variabilities, and typically are meant to be used over regions of scale L (Figure 1) where the parameter variabilities are approximately stationary. Although we will not be solving the mean equations in this investigation, they are presented below for consistency in the discussion. The forms are somewhat general and are only meant to convey the essence of the approach used in the saturated and unsaturated theories.

Corresponding most generally to equations (1) and (2) are the mean balances of fluid and solute mass:

$$\frac{\partial}{\partial t}(\rho\overline{\theta}) \; + \; \nabla\cdot(\rho\overline{\theta v}) \; = \; 0 \tag{9}$$

$$\frac{\partial}{\partial t}(\rho\overline{\theta}\,\overline{\omega} \; + \; \hat{R}) \; + \; \nabla\cdot(\rho\overline{\theta v}\,\overline{\omega}) \; + \; \nabla\cdot(J_{local} \; + \; J_{macro}) \; = \; 0 \tag{10}$$

where the density ρ is still assumed locally constant. The fluid momentum is conserved in terms of a mean form of Darcy's equation (3):

$$\overline{\theta v} \; = \; \overline{q} \; = \; -\mathbb{K}\cdot\nabla(\overline{h} + z) \tag{11}$$

Here, $\overline{\theta}(x,t)$, $\overline{q}(x,t)$, and $\rho\overline{\omega}(x,t) \equiv \overline{c}(x,t)$ are the large scale, mean quantities, representative of behavior in spatial regions on the order of a correlation scale. Corresponding to the constitutive relationships (4) and (5) are the larger scale forms

$$\overline{\theta} \; = \; \begin{cases} \theta_r & \overline{h} - h_r \leq (\theta_r - \theta_0 - \hat{E})/\Gamma & \text{(unsaturated)} \\[2mm] \theta_0 \; + \; \Gamma(\overline{h} - h_r) + \hat{E} & (\theta_r - \overline{\theta_0} - \hat{E})/\Gamma < \overline{h} - h_r < 0 & \text{(unsaturated)} \\[2mm] \theta_0 & \overline{h} - h_r \geq 0 & \text{(saturated)} \end{cases} \tag{12}$$

$$\mathbb{K} \; = \; \begin{cases} K_G\,\mathbb{g}_u & \overline{h} - h_r < 0 & \text{(unsaturated)} \\[2mm] K_G\,\mathbb{g}_s & \overline{h} - h_r \geq 0 & \text{(saturated)} \end{cases} \tag{13}$$

where $\overline{h}(x,t)$ is a mean pressure head.

In the formulations (9) - (13), new or modified quantities appear that reflect the influence of the local variabilities on the large scale processes. The estimation of functional forms and parameterizations for them generally constitutes a closure problem and is one of the fundamental goals of any stochastic model aimed at quantifying larger scale phenomena. The effective hydraulic

conductivity, $\mathbb{K}$, for example, is most generally tensorial (and perhaps nonlinear) in nature and is written in terms of the geometric mean of the saturated conductivity, $K_G(x) = e^{F(x)}$, and a function of the statistical quantities used to characterize the modeled medium. In saturated applications, $\mathbb{g}_s$ generally depends on σ^2_f and the correlation scales, λ_i [Gelhar and Axness, 1983; Gelhar, 1987] and is essentially constant. In the unsaturated approaches of Mantoglou and Gelhar [1987a,b,c], for example, $\mathbb{g}_u(x,t)$ depends on σ^2_a, σ^2_f, the local head variance σ^2_h, A, Γ, λ_i, as well as the mean pressure head, $\overline{h}$, its spatial gradient, and its partial time derivative.

The terms $\hat{R}(x,t)$ and $\hat{E}(x,t)$ are two other new effective quantities that are means of two perturbation terms. The first, $\hat{R} = \rho\overline{\theta'\omega'}$, (where $\theta' \equiv \theta - \overline{\theta}$ and $\omega' \equiv \omega - \overline{\omega}$) represents the influence of the variabilities of moisture on the mean solute transport, a process that has, to date, not been studied in detail. The second, $\hat{E} \equiv \overline{\partial h'}$, where $h' \equiv h - \overline{h}$, represents the effect of pressure head variabilities on the mean moisture content, and has been discussed briefly by Mantoglou and Gelhar [1987a,b,c] and Mulford [1986].

Contributions to the mean nonadvective flux from local dispersion, J_{local}, are often excluded from larger scale models [e.g., Dagan, 1984], or treated approximately. Its overall effect on the mean transport is frequently thought to be small, however it is believed to influence the structure of J_{macro} in some cases. Gelhar and Axness [1983] and Mantoglou and Gelhar [1987a,b,c], model J_{local} as in (6) and (7), where D is ignored and θV is replaced by the mean flux $\overline{q}$ and its components, such that

$$J_{local} \approx -\rho\mathbb{E}_{local}\cdot\nabla\overline{\omega} \qquad (14a)$$

The tensor $\mathbb{E}_{local}$ is essentially $\theta\mathbb{D}$ of equation (6) evaluated in terms ot the mean components of the flux, $\overline{q}$, where D is neglected. The large scale nonadvective flux $J_{macro} \equiv \rho\overline{q'\omega'}$, is the result of local, porous medium velocity fluctuations and is believed to be quite important in the overall transport process, both in saturated and unsaturated systems. Within the framework of a simple perturbation expansion that ignores products of three or more deviation terms, J_{macro} is generally found to behave approximately according to a Fickian-like relationship

$$J_{macro} \approx -\rho\mathbb{E}_{macro}(t)\cdot\nabla\overline{\omega} \qquad (14b)$$

where $\mathbb{E}_{macro}(t)$ is usually written in terms of the so-called marcrodispersivity tensor, $q\mathbb{A}(t)$, with q being the magnitude of the mean flux, $\overline{q}$. The specific nature of the components of $\mathbb{A}(t)$ is discussed in detail in Gelhar and Axness, [1983], Dagan, [1984], Gelhar, [1987], and Mantoglou and Gelhar [1987a,b,c] to which the reader is encouraged to refer. It will suffice to say here that certain

components of $\mathbb{A}(t)$ have been evaluated in closed form for certain kinds of problems under specific simplifying assumptions and appear to take on constant asymptotic values for large solute travel time or distances, in effect making (14b) an exact Fickian relationship. Since they originate from stochastic models, these are strictly *ensemble* results and only make sense in the familiar, single replicate forum in an ergodic (large scale) sense. According to this approach, the nature of the mean solute dispersion at small travel times or distances is embodied in a time dependence of the macrodispersivity $\mathbb{A}(t)$. Although some expressions have been developed for some time-dependent components of $\mathbb{A}(t)$, it will generally be difficult to confirm these results exactly in single replicate situations, whether they be found experimentally (as in our computations) or in field experiments. A specific demonstration of the use of the asymptotic, effective dispersivity tensor in a large-scale, mean simulation will be presented in section 6.

For the most part, the large scale asymptotic effect has been borne out in many physical situations and theoretically to varying degrees [e.g., *Gelhar*, 1986], although some theoretical results occasionally indicate otherwise [e.g, *Matheron and deMarsily*, 1980]. It is the subject of a great deal of debate and will be discussed further in section 5 and the applications in section 6.

2.3 Discretized Local Domain. Let us return now to the local simulation problems and consider how to appropriately define the large and heterogeneous flow region. In order to obtain statistically meaningful local output fields for the single replicate simulations, a flow and transport domain Ω_c (a subset of Ω) must be considered whose characteristic length L_i in the i-th coordinate direction is much larger than the corresponding correlation scale of the $\ln(K_s)$ field in the same direction ($L_i \gg \lambda_i$). This is chosen to ensure that variabilities in the output fields have sufficient room to develop in space in the absence of boundary effects. Similarly, it is also desired to have a computational resolution Δx_i much less than λ_i ($\Delta x_i \ll L_i$) so that detailed local behavior on a scale close to the REV can be modeled. The choice of Δx_i may also be affected by the degree of variability (e.g., σ^2_f) of the local parameter distributions. A relatively smooth variation in the parameter values is required so that physical behavior within a cell or element is representative of the small scale (REV) as well as to make the ensuing computations more tractable [*Ababou, et al.,* 1985].

The choices $L_i \approx 25\lambda_i$ and $\lambda_i \approx 4\Delta x_i$ have been postulated by *Ababou, et al.,* [1985] as a possible domain discretization that roughly satisfies the above constraints (Figure 2). More recent suggestions have considered raising L_i to $30\lambda_i$ *or* λ_i to $5\Delta x_i$. The ideal three-dimensional problem would be equivalently discretized in all three directions and could thus possess anywhere from one- to as many as ten-million ($10^6 - 10^7$) nodes. The sheer size of this problem will imply that extreme care be taken in the design and use of the numerical simulators for flow and transport.
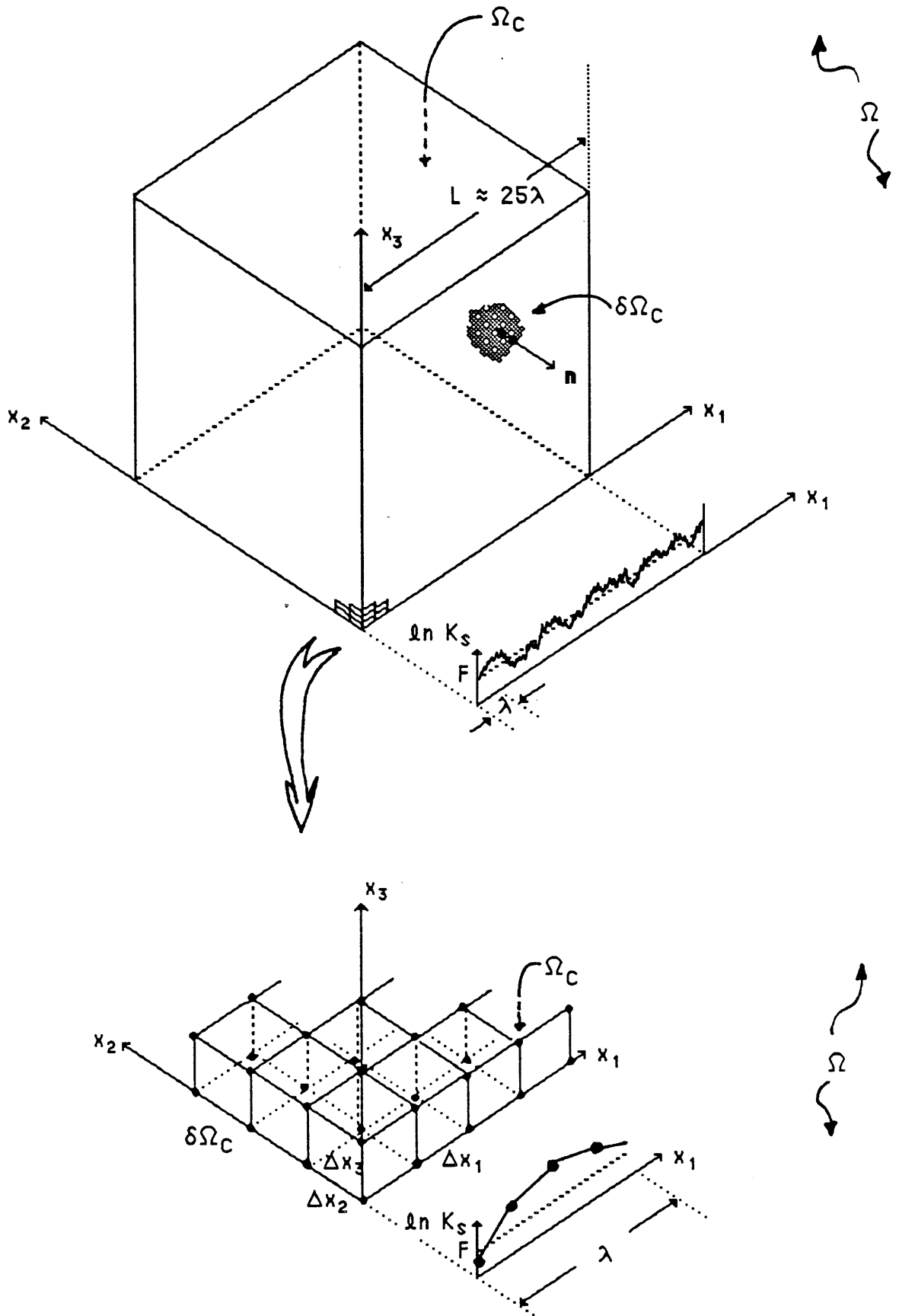
Figure 2:   Computational grid

2.4 Local Saturated Problem. Given the random distribution of the saturated conductivities $K_s(x)$ in space, the general flow problem on the finite domain Ω_C with suitable conditions on the boundary $\partial\Omega_C$ will simply involve the solution of (1) and (3), using (4) and (5). Combination of (1) and (3) with ρ = constant yields an equation for the saturated head field:

$$\nabla \cdot [K_s \nabla (h + z)] = 0 \tag{15}$$

The velocities can be derived from

$$\theta_0 v = q = -K_s \nabla \cdot (h + z) \tag{16}$$

For saturated problems, our operating hypotheses will presume that spatially variable porosities θ_0 are either small or unimportant in the overall flow and transport process (paralleling the stochastic work of *Gelhar and Axness*, 1983, *Dagan*, 1984, *Mantoglou and Gelhar*, 1987a, for example), and their effects will not be included in the current analyses. In this case, the saturated transport equation with ρ = constant becomes

$$\frac{\partial}{\partial t}(\rho\omega) + \nabla \cdot (\rho v \omega) - \nabla \cdot [\mathbb{D} \cdot \nabla (\rho\omega)] = 0 \tag{17}$$

which can be solved on Ω_C given the velocity field and suitable auxiliary conditions for ω or the mass concentration defined by $c = \rho\omega$. Notice that local models based upon (17) will be able to include the effects of a spatially variable dispersion tensor $\mathbb{D}(x,t)$. The spatial dependence could arise from locally variable velocities, dispersivities, diffusion coefficients, or a combination of all three. These options could be retained for comparisons with stochastic theories based upon no local dispersion [e.g., *Dagan*, 1984], spatially constant dispersion coefficients [e.g., *Gelhar and Axness*, 1983, *Mantoglou and Gelhar*, 1987a,b,c], or spatially variable coefficients [e.g., *Gelhar, et al.*, 1979].

2.5 Local Unsaturated Problem. The general unsteady flow problem implies

$$\frac{\partial}{\partial t}(\rho\theta) - \nabla \cdot [K \nabla (h + z)] = 0 \tag{18}$$

must be solved on Ω_C with appropriate auxiliary conditions in conjunction with the state equations (4) and (5). In the most general case, it will be necessary to specify the randomly correlated distributions of $\alpha(x)$, $\gamma(x)$, as well as $K_s(x)$. The velocities or fluxes can be found from (4), (5), and

$$\theta v = q = -K \nabla \cdot (h + z) \tag{19}$$

The transport simulations will be based upon

$$\frac{\partial}{\partial t}(\rho \theta \omega) + \nabla \cdot (\rho \theta v \omega) - \nabla \cdot [\theta \mathbb{D} \cdot \nabla (\rho \omega)] = 0 \tag{20}$$

assuming the velocity and moisture fields as well as a sufficient set of auxiliary conditions are supplied. The density is again assumed constant. If desired, this more general formulation would be capable of simulating saturated/unsaturated systems, as well as systems with variable porosities; these possibilities, however, will not be considered here.

2.6 Auxiliary Conditions. Most flow simulations will involve the specification of two kinds of conditions on the boundary $\partial \Omega_c$, usually a combination of Dirichlet conditions (specified h) or second-type normal flux conditions (specified $n \cdot \nabla (h + z)$, n being an outward normal vector to $\partial \Omega_c$). When used, the specified flux is often set to zero, although this is by no means necessary. In addition, the unsaturated problem is time dependent and will require an initial condition for h in Ω_c. Auxiliary conditions on θ can be based upon those for h and the state equation (4). The transport problem will require an initial condition for ω or c in Ω_c as well as Dirichlet (specified ω or c) or flux (specified $n \cdot \nabla \omega$) conditions on $\partial \Omega_c$. Nonzero Dirichlet or flux conditions are usually associated with mass inflow to Ω_c. Because it is physically impossible to know concentrations or solute fluxes at downstream or outflow boundaries at future times, the boundaries are typically assumed to be remote and far removed from any solute mass during the period of simulation. Fixed zero Dirichlet or flux conditions can be applied here to satisfy the necessity of auxiliary conditions without affecting the true solution.

3. SELECTION OF COMPUTATIONAL MODELS

3.1 Generation of Parameter Fields. As mentioned ealier, the heterogeneous parameter fields $K_s(x)$, $\alpha(x)$, and $C(x)$ to be used in the local flow simulations are to be modeled as spatially correlated random fields. These will be generated by a three-dimensional *turning bands* random field simulation technique, as discussed by *Mantoglou* [1987] and *Tompson, et al.* [1987]. The turning bands simulator generates single or multiple replicates of a normal $N(0,1)$ stationary random process $z(x)$ with zero mean, unit variance, and a user-supplied correlation structure $R_{ff}(\xi)$. Such fields can be manipulated to give realizations of the desired physical parameters. For example, the $\ln K_s(x)$ process in (8a) is modeled as an $N(F, \sigma^2_f)$ field, so the $K_s(x)$ field can be found from a realization $z(x)$ by

$$K_s(x) = exp[z(x)\sigma_f + F(x)] \tag{21}$$

If none of the three fields $\ln(K_s(x))$, $\alpha(x)$ and $\gamma(x)$ are cross correlated, then they should be generated from three independent replicates of the simulator. If they are all perfectly cross correlated, then they should only differ by a multiplicative constant from a single replicate. Although not considered in this and the theoretical analyses, the case involving the simulation of three fields partially cross correlated could be approached using a matrix method as discussed by *Mantoglou* [1987].

Other variable parameter fields that could be included in the flow or transport simulations include the saturated porosity θ_0 (which was earlier assumed constant) or the dispersion coefficients. These coefficients are based upon local dispersivities $\alpha_L(x)$ and $\alpha_T(x)$, velocities $v(x,t)$ and diffusion coefficients $D(x)$. Spatial variation in the velocities derives directly from the flow problem and the K_s distribution; variations in the dispersivities have been linked to the K_s field [*Gelhar, et al.,* 1979] and could be chosen otherwise if desired; and fluctuations in the diffusion coefficient are never considered because its contribution to large scale transport mechanisms is minute and usually neglected from the start in most analyses.

3.2 Flow Simulations. The flow simulations are based upon a simple 7-point finite difference discretization of the pressure equations (15) or (18 with 4 and 5) on the computational grid pictured in figures 2 and 3. The ultimate size of this problem has meant that extreme care be taken in the design of efficient iterative methods for solving the large algebraic systems as well as time stepping and iterative procedures for the nonlinear unsaturated problem. Further details of these formulations and

the subsequent analyses of the resulting head and flow fields are contained in the report of *Ababou,* [1987].

The size factor has also, in some sense, eliminated the possibility of using any kind of joint pressure-velocity approach for this problem. In terms of the transport simulations then, it will be necessary to know how the velocities $v(x,t)$ or fluxes $q(x,t)$ and moisture contents $\theta(x,t)$ can be defined from the pressure solutions. This will be discussed below in the context of the transport model adopted for use.

3.3 Transport Simulations: Choice of Numerical Approach. Because of the individual complexity and scope of both the flow and transport problems, it was decided to pursue the design and development of a transport model in somewhat of an independent manner. The approach would involve building a separate code that would run with minimal coupling to the flow code. The desire for added flexibility in the choice and design of the transport model was seen to outweigh the disadvantage of having to couple the two separate models when needed. A number of design features would be shared between the models. The computational domain Ω_c for each model will be identical in size and shape, and equivalent discretizations of this domain will be used (although, perhaps, in different contexts). This aids in satisfying the scale requirements reviewed in §2.3 and ensures that each model has an equivalent degree of spatial resolution.

There are a number of possible numerical approaches for solving the transport problem. It was decided to review a number of the more popular ones in use today and choose a method that best suited the needs of the current investigation. Most models fall into one of the following categories:

- Conventional finite difference or finite element methods [e.g., *Huyakorn and Pinder,* 1983, *Pinder and Gray,* 1977];

- Deforming finite element or moving mesh/characteristic techniques [e.g., *O'Neill,* 1981, *Ewing and Russell,* 1981, *Baptista, et al.,* 1984];

- Particle tracking/finite element or finite difference methods [e.g., *Konikow and Bredehoft,* 1978, *Pinder and Cooper,* 1970];

- Pure particle tracking based upon "random walk" approaches [e.g., *Ahlstrom, et al.,* 1977, *Prickett, et al.,* 1981, *Ackerer and Kinzelbach,* 1985, *Uffink,* 1987].

In order to make the choice of a numerical approach more clear, these methods will be discussed briefly in the context of the current study.

- <u>Conventional finite difference or finite element methods:</u> These techniques are probably the most frequently used in contemporary groundwater transport studies. However, if equations (17) or

(20) are to be accurately solved on the specific discretized computational domain Ω_C, then a number of potential problems would have to be reconciled. These include: (1) The nature of the most simple linear finite *element* approach implies that a 27-point connectivity for each equation be considered. This would involve almost four times as many matrix storage positions in the discretized matrix than in the flow problem and would have large implications on storage, matrix solution and time stepping techniques when a 10^7 node problem is considered (even as compared with the flow problem). Because of the tensorial nature of the dispersion coefficient $\mathbb{D}(x,t)$, the 27-point structure would be unavoidable with the finite *difference* method as well (Figure 3). (2) A tremendous amount of work will be devoted to the solution of the (ultimately) 10^7 equations per time step. Because of the uniformity of the grid (§2.3) and the fact that the boundaries will be generally distant from the solute (§2.6), a significant amount of this work will be spent on solutions in parts of Ω_C never traversed by solutes. (3) The grid Peclet number is defined by $Pe_G \approx V \Delta x_i / D$, where V is the velocity magnitude and D is a typical dispersion tensor component, say $\alpha_L V + D$. In cases where D / V is much smaller than α_L (§2.1) it is conservatively approximated by $Pe_G \approx \Delta x_i / \alpha_L$. This number can be basically thought of as a barometer of potential numerical problems that will occur from discretization of equations of the form (17) [*Pinder and Gray*, 1977, *Huyakorn and Pinder*, 1983]. A value greater than $2 - 10$ generally indicates poor propagation of certain large frequency spectral components of the numerical solution that can severely affect the solution near sharp fronts (i.e., the grid is too coarse to accurately transmit a sharp front at the given velocity). Because the spatial increment Δx_i is linked from the scale considerations to the correlation length λ, the Peclet number may likely be equal to or greater than 10, perhaps as large as 100. This case would arise if λ is estimated to be 5 meters and Δx_i is chosen as $\lambda / 5 = 1$ meter. With $\alpha \approx 0.1$ meters, $Pe_G \approx 10$. The only real way to circumvent this problem while still using a conventional method is to refine the mesh, a most impractical option for the current study. The remaining methods described below have been used, for the most part, as alternatives to traditional finite element or finite difference models when convection dominated (large Pe_G) problems are of interest.

• Deforming finite element or moving mesh/characteristic techniques: The deforming grid approach [e.g., *O'Neill*, 1981] generally tries to make the computational problem more "diffusive" in nature. The grid is moved or stretched relative to the fixed physical coordinates in some predetermined way such that the computational problem is transformed into one with a much smaller Pe_G. To our knowledge, such an approach has never been applied in a complicated three-dimensional problem, and to do so successfully may prove to be extremely difficult in terms of how to move the mesh in a field of variable velocities. The characteristic or Lagrangian approaches [e.g., *Ewing and Russell*, 1981, and *Baptista, et al.*, 1984] involve solving repeated diffusion equations over a
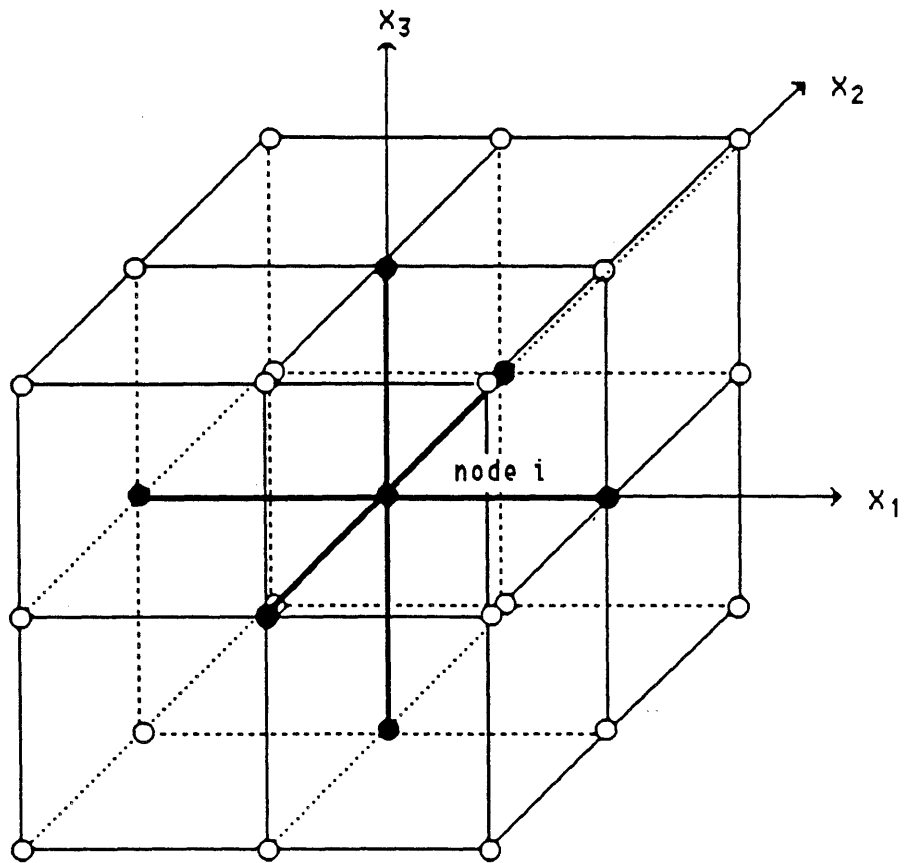
●   Nodes involved in finite difference approximation of flow
     equation at node i,

○   Additional nodes involved in finite difference approximation
     of transport equation at node i, (Also, nodes involved in any
     linear finite element approximation of either equation at node i),

Figure 3:   Computational cell for flow problem

transformed spatial frame in time (without the advection term), and use velocity information to trace out characteristics which map the spatial frame into the original, physical frame of reference. This allows the true motion of the solutes to be mapped out. The bulk of the work is really involved in solving for the characteristics, which could again be a very difficult problem in three-dimensions or in large systems.

• Particle tracking/finite element or finite difference methods: These techniques [e.g., *Pinder and Cooper*, 1970, *Konikow and Bredehoft*, 1978] involve the representation of the solute mass as a large collection of particles each of which is assigned a "value" of concentration. For a given time step, the solute mass is moved via two steps. The first moves the particles along streamlines computed from a velocity distribution. The second phase involves translating the concentration values of the particles to a discrete set of continuum concentrations defined at nodes on a fixed grid and solving a diffusion problem using a finite element or finite difference approach. When completed, the new node concentration values are used to reassign concentrations to particles which are again used to move the mass along streamlines. The procedure is somewhat awkward and suffers from mass conservation problems. These arise from the translation of particle concentrations to node concentrations and the use of particles to represent concentrations rather than mass. The method will also be limited by the number of particles used and the inelegant ways of treating source or sink terms (see next section).

• Pure particle tracking based upon "random walk" approaches: These methods [e.g., *Ahlstrom, et al.*, 1977, *Prickett, et al.*, 1981, *Ackerer and Kinzelbach*, 1985, *Uffink*, 1987] are similar to those above in that the solute mass is again represented by a large collection of particles. In this case, however, all particles represent identical, unchanging amounts of the mass. Each particle is displaced in two separate steps for each time step. The first involves a translation along a streamline or characteristic as above. The second involves a random displacement, the direction and magnitude of which is chosen so that the overall distribution of a cloud of particles will mimick the desired solution of (17) or (20). The method suffers from a similar need to use a large number (perhaps on the order of 10^4) particles to obtain consistent and reliable results. The treatment of source/sink terms is also complicated and a bit crude. In the absence of these kinds of terms, however, the technique is completely mass conservative and is not plagued with any large Pe_G problem. The algorithm is simple and can easily be applied in large, three-dimensional as well as unsaturated problems. The computational effort per time step is proportional to the number of particles and not the number of nodes, an advantage for our problem, and the storage requirements will be drastically reduced from any finite element or finite difference method.

Because of its ease of implementation, its mass conservative nature, and its ability to treat large Pe_G problems, the "random walk" particle tracking approach has been chosen for use in this study. Although the distribution of mass is based on particle locations and not on a continuum field of concentrations, the same kinds of information can be deduced from these results as in traditional continuum models if a suffucient number of particles are used and careful thought is given to the interpretation of the results. Extra consideration will also have to be given to the manner in which velocities are specified and derived from the numerical solution of the head equation.

In the next section, the theory behind this approach will be reviewed in a somewhat general manner and then discussed in terms of the current application.

4. Random Walk Model: Theoretical Highlights

4.1 Conceptual Aspects and Origin. The theoretical basis of the random walk model that will be employed here is quite general and has its origin in statistical mechanics literature that dates back to the early part of the century. The earliest development comes from Einstein's explanation of Brownian motion [see, for example, *Wax*, 1954, *Van Kampen*, 1981, *Gardiner*, 1985]. Much of that work has laid the foundation for a great deal of progress in what may be broadly classified now as the theory of stochastic differential equations. Interest in this broad field remains strong today and its use has seen far reaching applications in such diverse subjects as colloid chemistry and stellar motions [*Chandrasakhar*, 1954], quantum mechanics and chemistry, [*Van Kampen*, 1981, *Gardiner*, 1985], electrical signals and noise [*Wang and Uhlenbeck*, 1954, *Jazwinski*, 1970] and lasers and optics [*Haken*, 1983a]. Such theories have also been applied to the motion of fluids in porous media [e.g., *Scheidegger*, 1954, *Bhattacharya, et al.*, 1976] and are the foundation upon which random walk solute transport models [i.e., *Ahlstrom, et al.*, 1977, *Prickett, et al.*, 1981, *Uffink*, 1983, 1987, *Ackerer and Kinzelbach*, 1985] must rest. In what follows, we will briefly review the lines of thought contained in the mathematical developments that form the basis of the familiar "random walk"; the reader is urged to consult the works of *Jazwinski*, [1970], *Van Kampen*, [1981],*Haken*, [1983a, b], and *Gardiner*, [1985] for additional details, developments and applications.

We will consider a system described by a state variable $X(t)$ which changes, or more specifically, evolves probabilistically with time, t. As an example, X may represent the position in three-dimensional space of a particle. Such a system can be loosely classified as a stochastic process. Changes of the variable X in time (i.e., the motion of the particle) will be thought to be governed by both a deterministic, macroscopic set of coherent forces and a set of rapidly and irregularly fluctuating forces whose mean is zero. This kind of motion has generally been modeled by a simple equation of the form

$$\frac{dX}{dt} = A(X,t) + B(X,t) \cdot \xi(t) \tag{22}$$

which is commonly known as a nonlinear *Langevin* equation [*Gardiner*, 1985]. The vector $A(X,t)$ is a known function of the state (and perhaps time), and is used to represent the deterministic forces acting to change X. The second-order tensor $B(X,t)$ is also a known function of the state (and time) and will indicate directional characteristics of the random forces. In general, if X is an n-element position vector, B can be most generally an n by m matrix. For our purposes here, it will be sufficient to consider

it a square, n by n matrix. The vector function $\xi(t)$ is an idealized representation of the "rapidly" changing forces, the number of which is now limited to n. It is chosen such that $\xi(t)$ and $\xi(t^*)$ are statistically independent, or uncorrelated, for recognizably distinct times $t \neq t^*$. The idealistic qualities of $\xi(t)$ are embodied in the relationshps

$$< \xi(t)\xi(t^*)> = I \delta(t - t^*) \tag{23}$$

$$< \xi(t)> = 0 \tag{24}$$

where $<\cdot>$ denotes the expected value. As is, the model (22-24) has no strict meaning because of the infinte variance of $\xi(t)$. However, equation (22) can be integrated to form an integral equation that lends itself to a more clear interpretation:

$$X(t) - X(0) = \int_0^t A(X(s),s)\cdot ds + \int_0^t B(X(s),s)\cdot\xi(s)\, ds \tag{25}$$

The quantity

$$W(t) \equiv \int_0^t \xi(s)\, ds \tag{26}$$

is known as a *Wiener* process. Because the increments $dW(t) = W(t+dt) - W(t) = \xi(t)dt$ will have sharp jumps over small dt, the Wiener process cannot be differentiated (which confirms the inappropriate nature of equation 22). Integrals such as that in (26) or the second one in (25), however, can be viewed as Stieltjes integrals, which will then give meaning to the integrated forms of (22).

The differential form of (25) over a time span of dt takes the form

$$X(t + dt) - X(t) = A(X(t),t)\cdot dt + \int_t^{t+dt} B(X(s),s)\cdot\xi(s)\, ds \tag{27}$$

where the smooth nature of A allows its integral to be easily estimated as $A dt$. Because there can be "rapid" shifts in $\xi(t)$ over a time span of dt, no such approximation can be made immediately with the integral in the second term. It becomes necessary to make a special interpretation regarding what time to evaluate $B(X(t),t)$ in this expression. The so-called Îto assumption computes this integral with B evaluated explicitly at time t such that the integral is approximated as $B(X(t),t) \int_t^{t+dt} \xi(s)ds \equiv B\, dW$. In this context, B and $\xi dt = dW$ will remain uncorrelated. *Gardiner* [1985] thus refers to B as an *unanticipating* function. Under the alternatitive

- 3 2 -

Stratonovich interpretation, $\mathbb{B}$ is evaluated at $t+dt/2$, giving rise to a correlation between $\mathbb{B}$ and dW. The integral in this case becomes much more difficult to evaluate.

If we adopt the $\hat{I}$to interpretation, then the differential change (27) of the state X over an increment of time dt can thus be written as the stochastic differential equation

$$dX = A(X(t),t) \cdot dt + \mathbb{B}(X(t),t) \cdot dW(t) \tag{28}$$

where the macroscopic, or coherent change (or displacement) is given by $A\,dt$. The fluctuation or random component of change is given by $\mathbb{B} \cdot dW$. The tensor $\mathbb{B}(X(t),t)$ is a square coefficient matrix used to indicate the degree or magnitude of the random change of X along different coordinate directions. Although it can be most generally a function of the random state X, it, or more specifically, its functional form is deterministic. For our particle example, the fluctuation $\mathbb{B}(X(t),t) \cdot dW(t)$ may signify a pure diffusive displacement where $\mathbb{B}$ is a diagonal matrix whose components are proportional to the square root of the diffusion coefficient. The random Wiener process increments can be shown to have a mean of zero:

$$\langle dW \rangle = 0 \tag{29}$$

a mean square proportional to dt:

$$\langle dW\,dW \rangle = \mathbb{I}\,dt \tag{30}$$

as well as a number of other properties [*Gardiner*, 1985]. Recall that it is assumed in (30) that microscopic fluctuations that manifest themselves as $dW(t)$ over the macroscopic time scale dt occur over such small individual time scales ($\ll dt$) that the $dW(t)$ are uncorrelated in time. Notice, then, that $dW(t)$ is approximately $O(dt^{1/2})$. The $\hat{I}$to interpretation [*Haken*, 1983b, *Gardiner*, 1985] discussed above essentially means that the $X(t)$ used to calculate $\mathbb{B}(X(t))$ in (30) are such that $\mathbb{B}(X(t),t)$ and $dW(t)$ are uncorrelated. In a discrete sense, this means that $X(t_{n-1})$ is independent of $\Delta W(t_n) = W(t_n) - W(t_{n-1})$ so that

$$\langle \mathbb{B}(X(t),t) \cdot dW(t) \rangle = \langle \mathbb{B}(X(t),t) \rangle \cdot \langle dW(t) \rangle = 0 \tag{31}$$

Hence, the mean change in X (for example, the mean particle displacement) using the $\hat{I}$to assumption is due only to the coherent driving force, or

$$d<X(t)> \; = \; <A(X(t),t)>dt \; = \; A(X(t),t)dt \tag{32}$$

Consider the probability of finding the state of the system between X and $X + dX$ at time t given its initial state X_0 at time t_0, or more specifically, the corresponding density function $f(X,t \mid X_0,t_0)$. We wish to find a descriptive balance equation for this function based upon (28). To proceed, we consider first an arbitrary test function, $u(X)$, of the state variable X which does not depend explicitly on time. A stochastic differential equation for u can be found by a change of variables. The differential du is given by an approximate Taylor's expansion (using the indicial/summation notation, $i,j = 1,2,3$):

$$du \; \approx \; \frac{\partial u}{\partial X_i} dX_i \; + \; {}^1\!/_2 \; \frac{\partial^2 u}{\partial X_i \partial X_j} dX_i dX_j \tag{33}$$

Insertion of (28) yields

$$\begin{aligned}
du \; = \; & \frac{\partial u}{\partial X_i} \left[A_i(X,t)dt \; + \; B_{ik}(X,t)dW_k(t) \right] \\
& + \; {}^1\!/_2 \; \frac{\partial^2 u}{\partial X_i \partial X_j} \left[B_{ik}(X,t) B_{jm}(X,t) dW_k(t) dW_m(t) + \quad O(dt\,dW, \; dt^2) \right]
\end{aligned} \tag{34}$$

The last term in (34) can be disgarded by the differential nature of (34) and the properties of the Wiener process dW.

Assume now that the state of the system is known at a discrete set of times $(t_0, t_1, t_2, t_3, \ldots, t_n)$ where t_n is the current time and t_0 is the initial time. The states (the positions of a particle, for instance) are described by the sequence $(X_0, X_1, X_2, X_3, \ldots, X_n)$. The probability of finding this particular sequence given the initial state is described most generally by the joint conditional probability density function $P(X_n,t_n; X_{n-1},t_{n-1}; \ldots .X_1,t_1 \mid X_0,t_0)$. Integration of P over the space X^* spanned by all possible intermediate positions will yield the (marginal) conditional density of finding $X = X_n$ at $t = t_n$:

$$f(X_n,t_n \mid X_0,t_0) \; = \; \int\int\int \ldots \int_{X^*} P \; dX_1 dX_2 dX_3 \ldots dX_{n-1} \tag{35}$$

With the assumption that the $dW(t)$ are uncorrelated, the differential process defined by (28) is Markovian [*Jazwinski*, 1970, *Haken*, 1983b, *Gardiner*, 1985], and the integrations in (35) are greatly

simplified. The mean or expected value of $u(X_n)$ at $t=t_n$ given the initial position X_0 at t_0 can be written

$$\langle u(X_n) \rangle = \int\limits_{X_n} u(X_n) \left[\int \int \int ... \int\limits_{X^*} P \, dX_1 \, dX_2 \, dX_3 \, ... \, dX_{n-1} \right] dX_n$$

$$= \int\limits_{X_n} u(X_n) \, f(X_n, t_n \mid X_0, t_0) \, dX_n \qquad (36)$$

The time evolution of $\langle u(X_n) \rangle$ will be described by an average of (34). This can be found by multiplying (28) by $f(X_n, t_n \mid X_0, t_0)$ and integrating the result over X_n. In what follows, we will simply denote X_n by X (or the domain Ω) and $f(X_n, t_n \mid X_0, t_0)$ by $f(X, t)$. If the averaging procedure and time evolution of the system as expressed through du are exchanged, one finds:

$$d\langle u \rangle = \langle \frac{\partial u}{\partial X_i} A_i(X, t) \rangle \, dt + \langle \frac{\partial u}{\partial X_i} B_{ik}(X, t) \rangle \langle dW_k \rangle$$

$$+ \, ^1/_2 \langle \frac{\partial^2 u}{\partial X_i \partial X_j} B_{ik}(X, t) B_{jm}(X, t) \rangle \langle dW_k \, dW_m \rangle \qquad (37)$$

Assuming now that both $\mathbb{B}(X(t), t)$ and $u(X(t))$ are unanticipating functions (see above), they can be considered independent of the $dW(t)$ and their averages can be separated as in (37). The second term on the right vanishes by (29), and the remaining terms on the right can be integrated by parts using (30) and the assumption that $u(X)$ tends to 0 at $X = \pm\infty$. For instance, the first term on the right becomes

$$\langle \frac{\partial u}{\partial X_i} A_i(X, t) \rangle \, dt = \left[\int_\Omega \frac{\partial u}{\partial X_i} A_i(X, t) \, f(X, t) \, dX \right] dt \qquad (38)$$

$$= \left[\int_\Omega -u(X) \frac{\partial}{\partial X_i} [A_i(X, t) \, f(X, t)] \, dX \right] dt$$

while the term on the left becomes $d \, [\int_\Omega u(X) f(X, t) \, dX]$. The differential quotient of the resulting equation can be formed with dt, yielding

$$\int_{\Omega} u(X) \left[\frac{\partial f}{\partial t} + \frac{\partial}{\partial X_i}(A_i f) - \frac{\partial^2}{\partial X_i \partial X_j}(^1/_2 \, B_{ik} B_{jk} \, f) \right] dX = 0 \qquad (39)$$

Since u is arbitrary, the terms in the brackets must be zero, i.e.,

$$\frac{\partial f}{\partial t} + \frac{\partial}{\partial X_i}(A_i f) - \frac{\partial^2}{\partial X_i \partial X_j}(^1/_2 \, B_{ik} B_{jk} \, f) = 0 \qquad (40)$$

This is the desired balance or conservation equation for the probability density $f(X,t)$. Equations conserving these kinds of probability density functions are most generally known as *Fokker-Planck* equations.

4.2 Analogy to Solute Transport. The form of the Fokker-Planck equation (40) suggests that the distribution of particles that move according to an equation such as (28) satisfies a diffusive-type conservation law similar in form to the physical model equations used for solute transport such as (17) or (20). Indeed, suppose equation (28) can be used to follow or trace the motion of distinct, hypothetical "particles" of solute mass in a groundwater flow system. By "particle" we mean an infinitesimally small amount of "unbreakable" mass that can be identified at a continuum point X (§2.1) and able to move via the influence of pore scale velocities. Such particles do not occupy any identifiable volume and could coexist at the same point in space if need be.

In a discrete sense, (28) can be written using $X_n \equiv X(t_n)$ as

$$\Delta X_n = X_n - X_{n-1} = A(X_{n-1}, t_{n-1}) \cdot \Delta t + B(X_{n-1}, t_{n-1}) \cdot \Delta W(t_n) \qquad (41)$$

where A and B have been evaluated at the old time level. This will be consistent with the Îto integration rule used earlier.

Let us identify the position of any particle at time t_n by $X(t_n) \equiv X_n$. Consider first the motion of one particle initially located at X_0 at time t_0. Given the form of the macroscopic force A, independent, random fluctuation ΔW, and deterministic scaling tensor B, equation (41) can be used to move this particle through space over small discrete time steps Δt up to some fixed time T, whence the particle is located at a point X (Figure 4a). Each step will consist of a deterministic displacement $A \Delta t$ and an independent, random Markovian displacement $B \cdot \Delta W$. If this "experiment" is repeated with the same initial condition, macroscopic force A, and scaling tensor B many times (say, N), the particle will be located at different spatial locations at time T in each experiment (Figure 4b). The spatial density of these points will simply be the function $f(X,t)$ evaluated at $t=T$ which satisfies equation (40) according to a zero boundary condition $f(\infty, t) = 0$

- 36 -
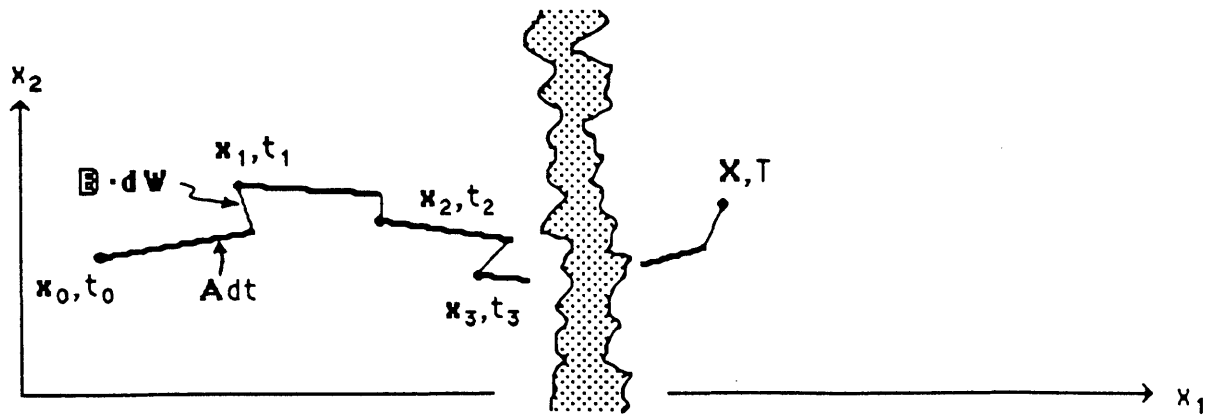
Figure 4a: One particle moving many steps to $\mathbf{X}, t$
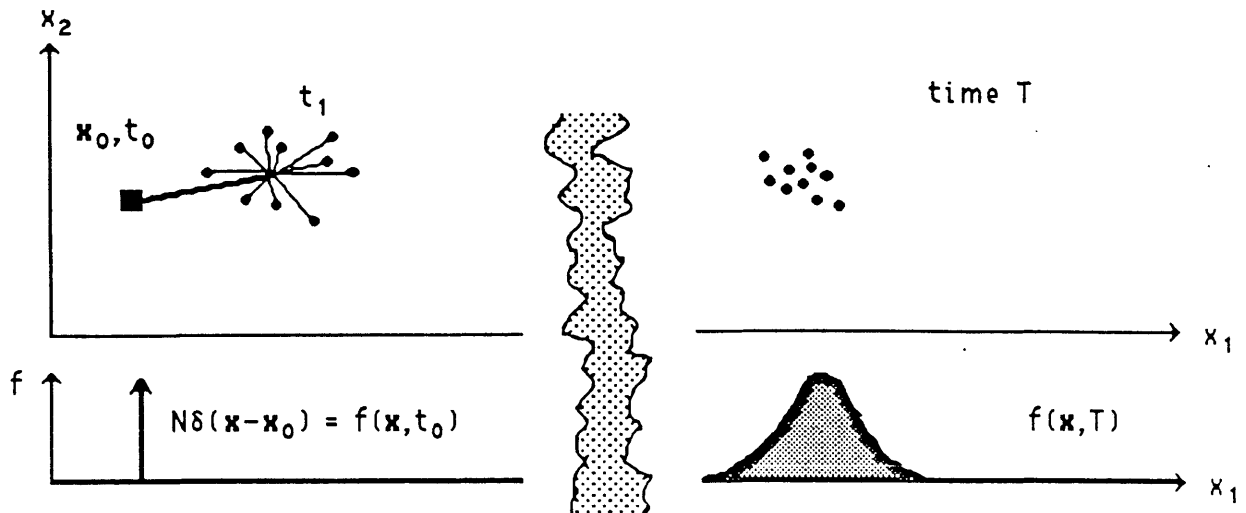
Figure 4b: N simulations of above experiment to a final time, T; *or*, one simulation of N particles all initially located at $\mathbf{X_0}, t_0$ up to a final time, T. Particle distribution functions shown also.
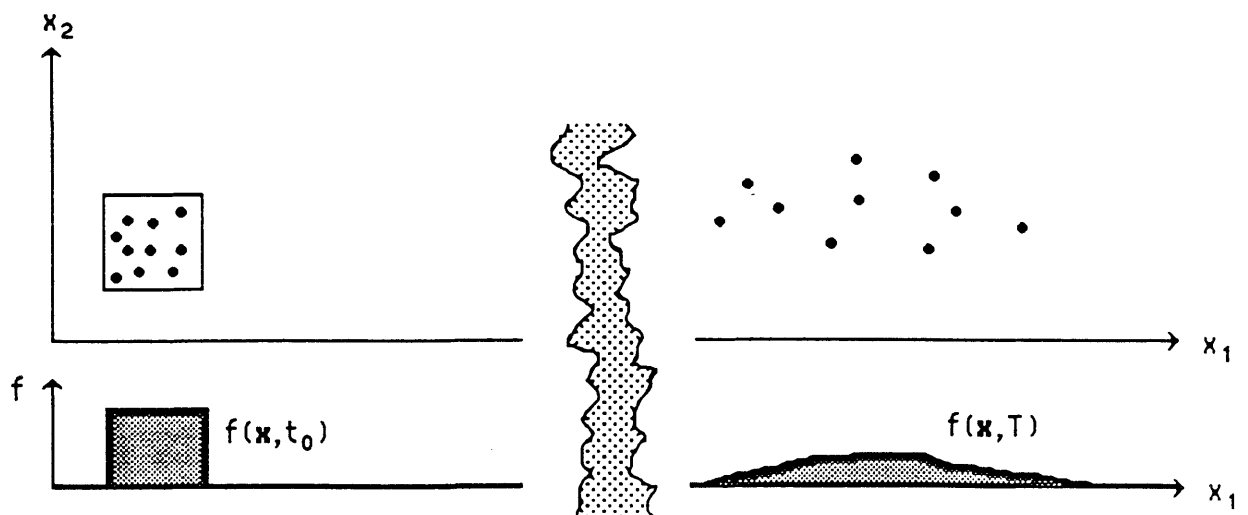
Figure 4c: Motion of N particles initially distributed over space according to $f(\mathbf{X}, t_0)$

on the (essentially) infinite domain and a "point source" initial condition of $f(X,t_0) = N\delta(X-X_0)$. In other words, the probability density for position at time T is just $f(X,T)$. The equivalence of the particle spread and the "ideal" nature of the function $f(X,t)$ will be exact only in the limit as N —> ∞ and Δt —>0.

Suppose now that a large number of N particles are all located at the same initial location X_0 and time t_0 and that each is individually moved according to (41) for each time step Δt up to the same end time, T. Let these particles represent a fixed amount of total solute mass, M, so that the individual particle mass changes with the number of particles chosen. Then the spatial distribution of all these particles will be just the same as in the previous example except that all of the particles will be present collectively at the end of one experiment instead of individually at the end of many (Figure 4b). Moreover, the same experiment could be run with the N particles distributed in space according to some other initial distribution $f(X,t_0)$ whence the resultant distribution would be a solution of (40) with the new initial condition (Figure 4c). Again, the connection between the theoretical function $f(X,t)$ and the specific distribution of N particles will be approximate and limited by the number of particles (or "individual" experiments) and the time step Δt (see section 5).

Given these N moving particles, the *expected* number of particles $,N_e,$ located in some small (infinitessimal) volume V_s centered at X at time t is approximately

$$N_e \approx N \cdot f(X,t) \cdot V_s \tag{42}$$

If each particle is of mass $m = M/N$, then the expected mass M_e in V_s is roughly $mN_e = MN_e/N$ using the particle approach. This quantity can be equated to the mass, M_t, computed in terms of familiar porous medium continuum quantities and used to form a relationship between the distribution function f and the mass fraction ω or concentration $c = \rho\omega$. The theoretical solute mass M_t in the infinitessimal volume V_s centered at X at time t is

$$M_t \approx \rho\omega(X,t)\theta(X,t) \cdot V_s \tag{43}$$

Using $M_t \approx M_e$, we find

$$\rho\omega(X,t)\theta(X,t) \approx mNf(X,t) = Mf(X,t) \tag{44}$$

Equation (44) can be used to form an analogy between the Fokker-Planck equation (40) and the solute transport balance equations (17) or (20). As the total solute mass M in Ω is assumed constant, equation (40) can be multiplied by $M = mN$ to express the Fokker-Planck equation in terms of the

solute mass $\rho\omega\theta$. Noting that $B_{ik}B_{jk} \equiv \mathbb{B}\cdot\mathbb{B}^T$, the chain rule can be used to rearrange the last term to give

$$\frac{\partial}{\partial t}(\rho\omega\theta) + \nabla\cdot[(A - \nabla\cdot(^1/_2\mathbb{B}\cdot\mathbb{B}^T))\rho\omega\theta] - \nabla\cdot[^1/_2\,\mathbb{B}\cdot\mathbb{B}^T\cdot\nabla(\rho\omega\theta)] = 0 \qquad (45)$$

It is now only necessary to choose $A(X,t)$, $\mathbb{B}(X,t)$, and $\Delta W(t)$ such that the Fokker-Planck equation (45), now phrased in terms of $\rho\omega\theta$, takes the form of the transport equations (17) or (20) that we wish to solve. In other words, it is desired to find the correct form of A, $\mathbb{B}$, and ΔW for the step equation (41) such that if a large number of particles are moved according to it, the resulting mass distribution will be equivalent to that given by the transport equations (17) or (20). It should be pointed out that the true physical model adopted for this study is given by equations (17) or (20). The point of these exercises is to use the step equation (41) to distribute particles in space and mimick the solution of the model continuum equations. This differs in intent from the work of *Bear* [1969] who adopts a step equation of the form (41) as the true physical model in order to derive an as yet unknown macroscopic law which turns out in the end to be of the form (40).

In the next sections, three sample problems will be examined to illustrate the choices of the step equation parameters. These will be chiefly concerned with modeling transport in a saturated medium with a scalar diffusion coefficient, and a spatially dependent dispersion tensor, as well as modeling transport in an unsaturated medium with a spatially dependent dispersion tensor.

4.3 Simple Diffusion. In this case, the balance law we seek to emulate through (41) derives from (17) where $\mathbb{D} \equiv D\,\mathbb{I}$, D being a constant coefficient of molecular diffusion:

$$\frac{\partial}{\partial t}(\rho\omega) + \nabla\cdot(\rho v\omega) - D\nabla^2(\rho\omega) = 0 \qquad (46)$$

Assuming the moisture content θ equals the constant saturated porosity, θ can be removed from (45) whence comparison with (46) reveals the desired relationships:

$$v(X_n,t_n) = A(X_n,t_n) \qquad \text{(macroscopic "force")} \qquad (47a)$$

$$D\,\mathbb{I} = {}^1/_2\,\mathbb{B}(X_n,t_n)\cdot\mathbb{B}^T(X_n,t_n) = {}^1/_2\,B_{ik}B_{jk} \qquad (47b)$$

It is immediately clear that $\mathbb{B}$ is the constant tensor

$$\mathbb{B} = \sqrt{2D}\ \mathbb{I} \qquad\qquad \text{(scaling tensor for random displacement)} \qquad (47c)$$

To use a step equation of the form (41) it will suffice to use (47a and c) along with a normalized random displacement that is $O\ (\Delta t^{1/2})$:

$$\Delta W(t_n) = Z_n \sqrt{\Delta t} \qquad\qquad \text{(normalized random displacement)} \qquad (47d)$$

where Z_n is a vector of three *independent* random numbers at t_n. These should be chosen from a distribution such that the discrete forms of (29) and (30) are satisfied, i.e.,

$$<Z> = 0 \qquad\qquad\qquad (48a)$$

$$<ZZ> = \mathbb{I} \qquad\qquad\qquad (48b)$$

It is only necessary for Z_n to have the statistical qualities given in (48), so many kinds of distributions might be implemented. One might use a normal $N(0,1)$ distribution [*Ahlstrom, et al.,* 1977] or a more simple uniform distribution $U(\pm\sqrt{3})$ spread over the range $\pm\sqrt{3}$ to determine each Z_i component.

The appropriate random walk equations to emulate the solution of (46) are

$$X(t_n) = X(t_{n-1}) + v(X_{n-1}, t_{n-1})\Delta t + Z_n \sqrt{2D\Delta t} \qquad (49)$$

4.4 Spatially Dependent Dispersive Transport under Saturated Conditions. In this case, the balance law we seek to emulate through (41) is simply equation (17):

$$\frac{\partial}{\partial t}(\rho\omega) + \nabla\cdot(\rho v\omega) - \nabla\cdot[\mathbb{D}\cdot\nabla(\rho\omega)] = 0 \qquad (50)$$

Upon division by the constant porosity θ_0, the Fokker-Plank equation (45) will be equivalent to (50) if A and $\mathbb{B}$ are chosen according to

$$v(X_n) = A(X_n, t_n) - \nabla\cdot[^1/_2\ \mathbb{B}\ (X_n, t_n)\cdot\mathbb{B}^T(X_n, t_n)] \qquad (51a)$$

$$\mathbb{D}(X_n, t_n) = {}^1/_2\ \mathbb{B}(X_n, t_n)\cdot\mathbb{B}^T(X_n, t_n) \qquad (51b)$$

In Appendix A, equation (7) is used in conjunction with (51b) to determine the components of the tensor $\mathbb{B}$ in terms of those of $\mathbb{D}$. Using this result along with (51a) and the random displacement (47c) yields the step equation

$$X(t_n) = X(t_{n-1}) + [v(X_{n-1}, t_{n-1}) + \nabla \cdot \mathbb{D}(X_{n-1}, t_{n-1})]\Delta t$$

$$+ \mathbb{B}(X_{n-1}, t_{n-1}) \cdot Z_n \sqrt{\Delta t} \qquad (52)$$

Use of the step equation (52) to move particles will result in a distribution of solute mass equivalent to that predicted by the model equation (17) or (50). Observe that the overall advective step will be smaller when the gradient of $\mathbb{D}$ is negative in the direction of v. This happens when $|v|$ is getting smaller in the positive v direction (e.g., towards a stagnation point) and it is seen that the dispersion gradient correction term attempts to keep particles away from these areas.

4.5 Spatially Dependent Dispersive Transport under Unsaturated Conditions. The appropriate physical model to be emulated by the random walk model in the unsaturated case is given by equation (20), rewritten here after having applied the chain rule to the third term:

$$\frac{\partial}{\partial t}(\rho\theta\omega) + \nabla \cdot [\rho\theta\omega(v + (1/\theta)\mathbb{D}\cdot\nabla\theta)] - \nabla \cdot [\mathbb{D}\cdot\nabla(\rho\theta\omega)] = 0 \qquad (53)$$

Comparison of (53) with the general Fokker-Planck equation (45) indicates that the terms A and $\mathbb{B}$ must be chosen in this situation according to

$$v(X_n) = A(X_n, t_n) - \frac{1}{2}\mathbb{B}(X_n, t_n) \cdot \mathbb{B}^T(X_n, t_n) - (1/\theta)\mathbb{D}(X_n, t_n) \cdot \nabla\theta$$

$$\mathbb{D}(X_n, t_n) = \frac{1}{2}\mathbb{B}(X_n, t_n) \cdot \mathbb{B}^T(X_n, t_n) \qquad (54a,b)$$

Use of the random displacement ΔW and equation (54a) leads to the following step equation for unsaturated transport:

$$X(t_n) = X(t_{n-1}) + [v(X_{n-1}, t_n) + \nabla \cdot \mathbb{D}(X_{n-1}, t_n) + (1/\theta)\mathbb{D}(X_{n-1}, t_n) \cdot \nabla\theta]\Delta t$$

$$+ \mathbb{B}(X_{n-1}) \cdot Z_n \sqrt{\Delta t} = 0 \qquad (55)$$

- 41 -

where the relationship between the components of $\mathbb{B}$ and $\mathbb{D}$ is given in Appendix A. Notice that a positive velocity component coupled with a negative moisture content gradient (i.e., it is drier in the direction of $\mathbf{V}$) will tend to counteract one another such that the overall advective term is smaller.

4.6 Other Comments. It should be reemphasized that the analogy used here simulates solute movements by moving minute, hypothetical particles of solute mass according to some sort of incremental step equation. The exact properties of these step equations ensure that the resulting particle (mass) distributions are approximately equivalent to the continuum distributions described by the model equations of section 2. It is the equivalence in form between these equations and the Fokker-Planck equation that makes this possible. The same analogy could be used to simulate the motion of *fluid* mass in unsaturated regions where a diffusive form of the flow equation is used [*Bhattacharya, et al.*, 1976]. It is important to recognize that this direct analog will break down if additional terms representing any kind of loss or gain of solute mass are included in the continuum balance equations of section 2. The step equations do not naturally add or subtract mass from the system. They are inherently mass conservative because they are related directly to the Fokker-Planck equation which theoretically (and necessarily) conserves *probability*. The only way to simulate loss or introduction of solute mass using these particle methods is to add a post processor which selectively adds or removes mass according to the process defined in the continuum equation. Although *Ahlstrom, et al.*, [1977] discuss these kinds of applications, they are for the most part inelegant and will not be considered here.

The term in the step equation (52) representing the divergence of the dispersion tensor $\mathbb{D}$ is one that has not been incorporated in familiar random walk transport models [*Ahlstrom, et al.*, 1977, *Prickett, et al.*, 1981], however its inclusion in the case of a spatially variable $\mathbb{D}$ is necessary to make the forementioned analogy correct. This has recently been recognized in the hydrological literature by *Ackerer and Kinzelback*, [1985] who realized that its absence gives rise to an erroneous accumulation of mass in "stagnation" or low conductivity zones in the groundwater flow systems. The effect of this term in most flow regimes, however, is usually quite minimal, owing to small groundwater velocity gradients, and the consequences of its mistaken exclusion in the above models are often insignificant. The impact and necessity of the divergence term has also been recognized and illustrated by *Uffink*, [1983, 1987].

The term in the step equation (55) representing the influence of the moisture content has also been incorrectly neglected in particle tracking models meant to be used in unsaturated problems [*Ahlstrom, et al.*, 1977]. This term can be basically rewritten in terms of the gradient of the logarithm of the moisture content, $\mathbb{D} \cdot \nabla \ln\theta$. The effect of this term will probably be small in many applications, but

near steep wetting fronts, it may be important.

The next section will deals with the implementation of the random walk algorithm in the large scale problem to be studied, and various ways of interpreting the results will be discussed.

5. Random Walk Model: Computational Aspects

5.1 Moving One Particle: Interpolated Nodal Quantities. We return now to the discretized domain shown in Figure 2. The random walk model is meant to propogate particles through this domain using a step equation of the form (49), (52), or (55) and presumes that continuous velocity and moisture content fields, $v(X,t)$ and $\theta(X,t)$ are available at all points X and times t. In this specific problem, however, the velocities and moisture contents, as well as some of their spatial derivatives, must be derived from discrete nodal distributions of the pressure head $h(X_n,t)$ as given from the flow computations, an appropriate form of Darcy's law, and the state relationship for the moisture content (see §2.1, §2.3, §2.4, and §3.2). This will mean that some sort of interpolation scheme must be adopted. Several possible ways of interpolating functions and their derivatives from the nodal values of the functions are reviewed in Appendix B; these will be referred to below.

The flow computations give nodal values of the pressure head $h(X_n,t)$ from which nodal values of the moisture content $\theta(X_n,t)$ can be derived using (4). The most general step equation (55) will require values of v, $\nabla \cdot \mathbb{D}$ (i.e., ∇v), and $(1/\theta)\nabla\theta$ at arbitrary locations X in the flow field corresponding to the location of any particle. Because these quantities would most generally be evaluated for *each* particle at *each* time step, it will be necessary to compare relative costs and accuracies involved with their estimation. To estimate the velocity, for example, one may consider interpolating the head over 8-noded computational cells using tri-linear "basis" functions (Appendix B; Figure B1) and forming the derivative of this quantity. This would yield a velocity continuously variable within each "cell" volume Ω_e yet discontinuous over the cell boundaries and Ω_c. If the nodal head values were differenced to provide nodal head gradients beforehand, the head gradients could be directly interpolated with the linear functions and manipulated to give a continuous velocity representation over all of Ω_c. Use of differenced numerical results in this manner , however, may be ill-advised and will not be considered further.

Interpolation using the simple basis functions would involve evaluating eight weighting function values and making 8 subsequent additions for each component of the velocity. This could amount to a significant expense when thousands of particles may be moved over hundreds, or perhaps thousands, of time steps. Because the ultimate size of this problem will involve upwards of 10^6 or more cells, the use of cell velocities may be a suitable approximation that will offer considerable savings in terms of computational expense. Evaluation of each component would only involve 8 additions of known nodal head values. This would only have to be done once for each cell in steady flow problems. The flux component $q_{x_1}\big|_e$ for the cell pictured in Figure B1 could be evaluated in terms of the eight surrounding nodal values H_n and some elemental conductivity $K\big|_e$:

$$q_{x_1}\big|_e \approx -K\big|_e \cdot \frac{1}{4\Delta X_1}\left[(H_2-H_1) + (H_3-H_4) + (H_6-H_5) + (H_7-H_8)\right] \tag{56a}$$

The nodal head values are piezometric heads based upon the nodal pressure heads and elevations, $H_n = h_n + z_n$. Another approach would involve evaluating each flux component in terms of mid-node conductivities. That is,

$$q_{x_1}\big|_e \approx -\frac{1}{4\Delta X_1}\left[K_{12}{}^*(H_2-H_1) + K_{34}{}^*(H_3-H_4)\right.$$

$$\left. K_{65}{}^*(H_6-H_5) + K_{78}{}^*(H_7-H_8)\right] \tag{56b}$$

where $K_{ij}{}^*$ is a mid node conductivity computed in terms of the geometric mean of the conductivities at nodes i and j. The latter approach is more consistent with the numerical solution for the pressure heads in terms of mass conservation [*Ababou*, 1987] and is used in the current model.

As the moisture content can be defined nodally in terms of the pressure heads h_n, it could easily be interpolated continuously over all of Ω_c. However, to minimize the computational costs and to be consistent with the *level* of interpolation used above, θ will also be estimated as a cell constant from the expression:

$$\theta\big|_e = {}^1/_8 \sum_{n=1}^{8} \theta_n \tag{57}$$

where θ_n is related to h_n through (4). Thus the first component of the cell velocity would be given from (56) and (57) as

$$v_{x_1}\big|_e = q_{x_1}\big|_e / \theta\big|_e \tag{58}$$

All components of the cell velocity $v\big|_e$ can then be used to evaluate a cell dispersion tensor $\mathbb{D}(\overset{o}{v}\big|_e)$. Notice that the porosity θ_0 can be used in place of $\theta\big|_e$ in saturated problems.

The gradient of the moisture content would also be best evaluated as a cell constant. The first component, for example, can be estimated using the eight surrounding nodal values θ_n (Figure B1), similar to (56a)

$$\frac{\partial\theta}{\partial X_1}\bigg|_e \approx \frac{1}{4\Delta X_1}\left[(\theta_2-\theta_1) + (\theta_3-\theta_4) + (\theta_6-\theta_5) + (\theta_7-\theta_8)\right] \tag{59}$$

Recall that the nodal values θ_n can be determined from the pressure head values h_n through (4). Along with the other components, this can be combined with the cell values $\theta\big|_e$ and $\mathbb{D}(v\big|_e)$ to form the appropriate term required in the step equation (55).

Components of the dispersion tensor gradient are proportional to velocity derivatives (or second derivatives of the pressure head). As alluded to in the previous paragraph, cell-wise constant dispersion components can be defined in terms of neighboring cell velocities, and these could be subsequently used to form dispersion component gradients by differencing cell values . Refering to Figure B1, for example, the component $\partial D_{11}/\partial X_1$ for one element would be approximated by

$$\frac{\partial D_{11}}{\partial X_1}\bigg|_e \approx \frac{1}{2\Delta X_1}\left[D_{11}(v\big|_5) - D_{11}(v\big|_3)\right] \tag{60}$$

This is a simple difference between the cell dispersion components D_{11} in cells 5 and 3 as indicated in Figure B1.

In short, the velocities, moisture contents and related derivatives that appear in the various step equations will all be estimated as cell constants to simplify the computations. The errors incurred by these approximations are thought to be small if a large number of cells are used and an adequate time stepping procedure is adopted (§5.3). The evaluation of these terms is reviewed again here:

- <u>Cell velocities</u>: Estimate each flux component via cell-averaged head differences, such as in (56), and multiply the result by some local cell conductivity. This, in turn, can be divided by a mean porosity or cell moisture content to obtain (58).

- <u>Cell moisture contents</u>: Estimate by a simple 8-noded average as in (57). These can be used for the velocities and the moisture gradient terms.

- <u>Cell tensors: $\mathbb{D}$, $\mathbb{B}$, and $\mathbb{R}$</u>: Each of these quantities is a function of the local velocity components and dispersivities and can thus be approximated in terms of the local cell velocity (58) and a suitable choice of the local dispersivities.

- <u>Cell moisture gradient term</u>: The gradient itself can easily be evaluated using cell-averaged moisture differences, such as in (59). The result can then be divided by the cell moisture found in (57) to find the desired term. It could be equivalently approximated by a cell-averaged difference of nodal $\ln(\theta)$ values by replacing θ_n by $\ln\theta_n$ in equation (59).

• <u>Cell dispersion gradient</u>: This is roughly approximated by a difference of cell values as illustrated in (60). Recall that the magnitude of this term as well as that of the moisture gradient is not likely to be large in comparison with the other terms, so the nature of their approximation may not be too important.

5.2 Moving One Particle: Choice of Time Step. In a problem characterized by spatially and temporally variable velocities, the choice of the time step will be a very important task in the overall simulation process. The general step equations required for this situation may be any of those presented earlier: (49), (52) or (55). Particles are moved through space according to a macroscopic force and a random force, one or both being functions of velocity, and hence, position. If too large a time step is used in these applications, errors could be made that could become significant and distort the results. These effects can be illustrated more clearly by first considering displacement segments produced by spatially variable (yet steady) flows and then by temporally variable flows.

• <u>Advective Displacements in a Steady Flow Field</u>: Ideally, a solute particle would follow a streamline in a pure advection problem. If finite time steps are used with a known, steady velocity field defined at all points (analytically or numerically), then small spatial overshoot errors will occur due entirely to the incremental nature of the time step (Figure 5a). The magnitude of this problem could be reduced by using infinitely small time steps or adopting an improved integration scheme, such as a Runge-Kutta method. A stream function-vorticity approach could also be developed to move particles along streamlines [e.g., *van den Akker*, 1983; *Cole, et al.,* 1985].

In the current problem, the velocities will be numerically evaluated in a discrete fashion over a grid of cells. As similar kinds of overshoot errors can arise in this situation (Figure 5b), similar types of remedies could be suggested. Use of smaller and smaller time steps will be advantageous up to a certain point, after which no improvements can be made. The cell Courant number $C_c = V\Delta t / \Delta x$ indicates the ratio of a typical advective displacement over a time step to a typical grid dimension (over which velocities are constant). Use of time steps that force C_c to be greater than one in *any* cell will imply that discrete "overshoot" problems will arise as illustrated in Figure 5b. Use of time steps that force C_c to be less than one will lessen the chances of these problems occurring. It is important to notice that "overshoot" as shown in Figure 5a can still happen inside of a cell, but there is no way of improving upon this situation as there is no resolution of the velocities finer than the scale of the cell. This is an unavoidable approximation that must be accepted as a consequence of choosing a discretized model with cell-constant velocities. On the other hand, higher order integration schemes could be introduced that may allow use of larger time steps. These would require several velocity derivatives to be estimated from the discrete field. Since the velocities are themselves obtained from derivatives

- 47 -

flow streamlines

new position = $\mathbf{x} + \mathbf{v}(\mathbf{x})\Delta t$

overshoot

actual position = $\mathbf{x} + \int \mathbf{v}dt$
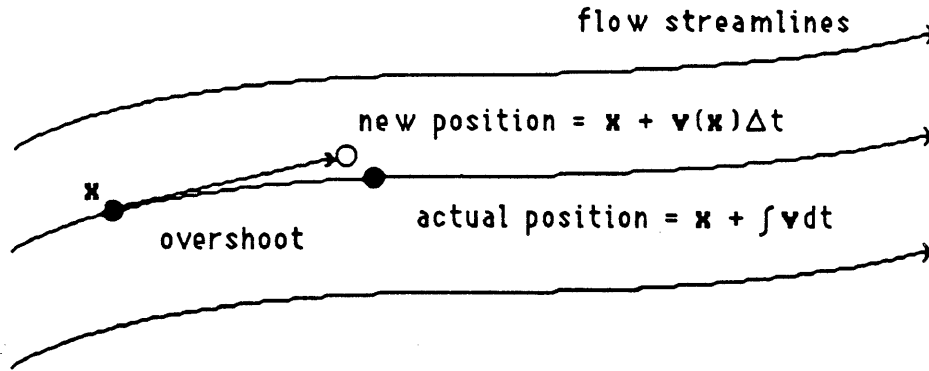
Figure 5a: Advective overshoot due to a finite time step in a completely known velocity field

4

$\mathbf{v}_1\Delta t$

3

overshoot

$\mathbf{v}_2\Delta t_2$

$\mathbf{v}_1\Delta t_1$

1

2

$\Delta t = \Delta t_1 + \Delta t_2$

Δt_1 = time for particle to get
       to cell 1-2 boundary

⟹   cell velocities

——➔O   particle displacements

Figure 5b: Advective overshoot through a computational cell. Use of a time step smaller than Δt_1
cannot improve the error any further (two-dimensions for clarity)

of numerical solutions, taking derivatives of the velocities may lead to additional complicated errors. Higher order schemes of this sort will, therefore, be avoided in the current simulations. Attention will be focused on the former method involving the use of small time steps.

Hence, the optimal choice of time step to advect one particle through space will either be one that is fixed and independent of particle position, or one that is adjustable so that the particle moves from one cell boundary to another. Since a particle could be located anywhere inside of a cell, the choice a time step so that C_c is less than *or* equal to 1 may not be adequate to avoid overshoot into another cell. Picking Δt small so that C_c is always less than, say, 0.1 in all cells will ensure the maximum overshoot is no more than $0.1 \Delta x$ (as the particle could be located initially just upstream of a cell boundary). This approach could lead to many computations to move the particle across the cell (in which the velocity is constant). Another approach would be to simply compute the time needed for a particle to reach the boundary (in the direction of the velocity vector) and move the particle to the boundary or just inside of the next cell (Figure 5). Then, the process could be repeated using the velocity of the neighboring cell. This would minimize errors and computational costs for the advective problem, but makes the time step dependent on the particle's location. Notice that in both of these approaches, the cell Courant number C_c will always be approximately one or less.

Observe that in the special case of a constant velocity field over all Ω_c, no time step restrictions would be needed for the advective problem. However, if the field is spatially constant yet changing in time, a sort of temporal overshoot similar to that described above could occur. This will be examined under a separate heading below.

• <u>Random Dispersive Displacements in a Steady Flow Field</u>: In cases where the dispersion tensor $\mathbb{D}$ or scaling tensor $\mathbb{B}$ are dependent on the velocity field, similar considerations must 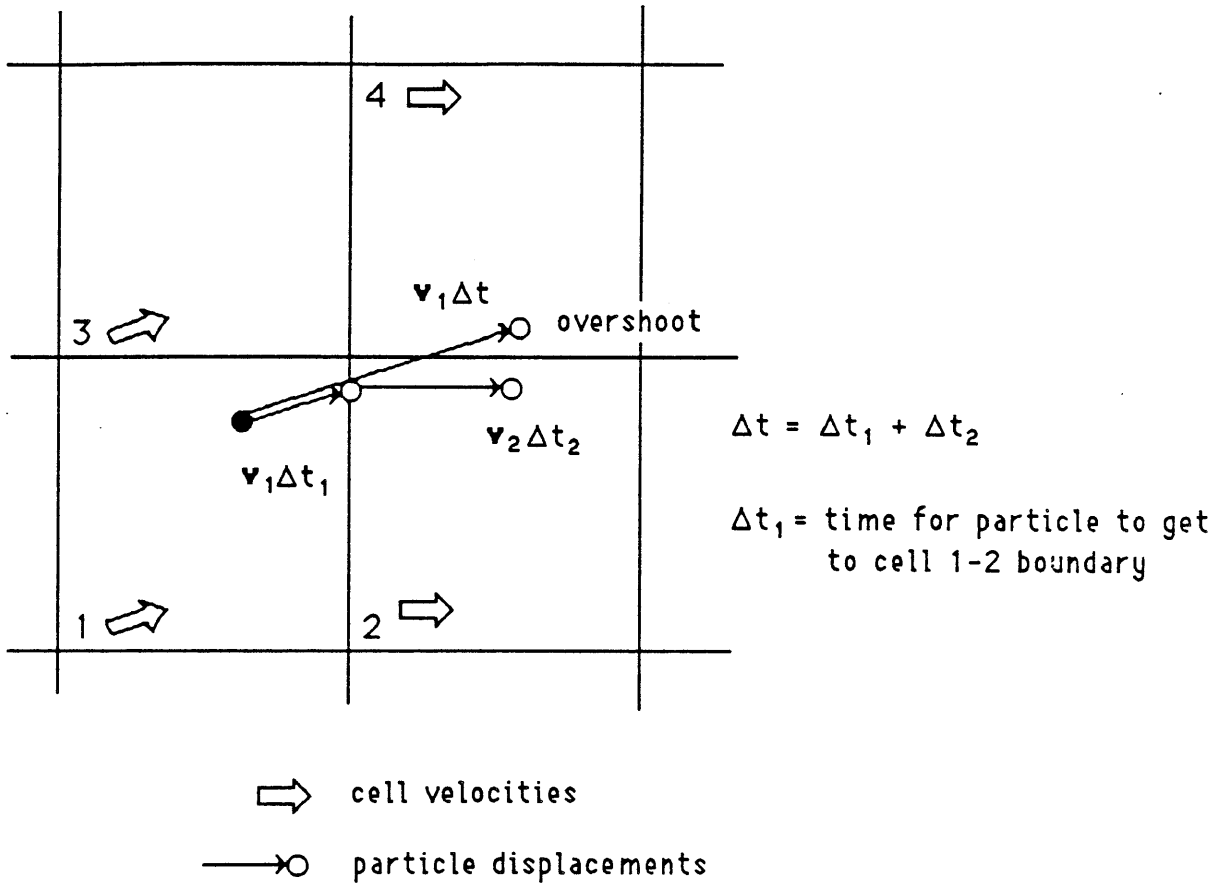be made as above. Over the length of one displacement, the velocity can change and consequently affect the size of the random displacement. It will be useful here to study the expected (root-mean squared) magnitude of this displacement d_i at a given point in the flow field. As used in equations (49), (52) or (55), $d_i = B_{ij}(X_{n-1})Z_{j,n}\sqrt{\Delta t}$, and its mean squared magnitude can be gauged most generally from the matrix $<d_i d_j>$:

$$\langle d_i d_j \rangle = \langle B_{ik} Z_k B_{jm} Z_m \Delta t \rangle \tag{61}$$

$$= B_{ik} B_{jm} \Delta t \langle Z_k Z_m \rangle$$

$$= B_{ik} B_{jk} \Delta t$$

$$= 2D_{ij} \Delta t$$

where (48b) and (51b) have been used. Using its diagonalized form (Appendix A), a typical component of this matrix is $2\alpha_L V \Delta t$, so the magnitude of the typical random displacement is $\sigma_d = \sqrt{2\alpha_L V \Delta t}$. Clearly this displacement will be affected by the same kinds of factors discussed above. Normalizing the random step σ_d with the typical avdective displacement $V \Delta t$ (ignoring the correction terms related to dispersion or moisture gradients) gives $\sqrt{2\alpha_L / (V \Delta t)} = \sqrt{2/C_\alpha}$, where C_α is the dispersive Courant number. If C_C is chosen near 0.1 as discussed above, then this ratio becomes $\sqrt{20\alpha_L / \Delta x} = \sqrt{20/Pe_G}$, where Pe_G is the grid Peclet number. Since Pe_G will range anywhere from 10 to 100 (§ 3.3), this ratio will be on the order of one at most, but probably much smaller. This means that overshoot problems in the dispersive step would be dominated by those of the advective step, and that the optimal approaches suggested previously would be best here also.

In the special case when the velocity field is *spatially* constant, there should be no restrictions on the size of Δt. Consider a one-dimensional problem where simulations will be carried out for a period of n equal time steps up to a maximum time of $n \Delta t = T$. The expected value of the entire displacement of one particle (after many small steps) is simply the average of the sum of the small displacements. Since V is spatially constant, and assuming D is also, this can easily be computed:

$$\langle \Sigma \Delta X_i \rangle = \langle \Sigma (V \Delta t + Z_i \sqrt{2D \Delta t}) \rangle = V n \Delta t = V T \tag{62}$$

The root mean displacement away from the mean is

$$\sigma_d = \langle (\Sigma Z_i \sqrt{2D \Delta t})^2 \rangle^{1/2} \tag{63}$$

$$= \sqrt{2D \Delta t} \langle \Sigma (Z_i^2) \rangle^{1/2}$$

$$= \sqrt{2Dn \Delta t} = \sqrt{2DT}$$

If, on the other hand, a single time step of T is used, the mean or expected displacement of the particle is still VT, and the root mean displacement from it is $\sigma_d = \langle(Z\sqrt{2DT})^2\rangle^{1/2} = \sqrt{2DT}$. Thus, in the case of constant velocities, the first two moments of the particle distributions are unaffected by the size of Δt.

- Correction Terms: In the more general step equations (52) and (55), two "correction" terms appear which modify the advective step according to local velocity or moisture content gradients. As an example, consider the injection of water into a confined aquifer of constant thickness H. The flux in the radial direction at a point located a distance r from the well is

$$q_r = Q/(2\pi H r) \tag{64}$$

where Q is the constant input flow and q_r is the radial Darcy flux. As long as conditions are steady, this relationship will be valid under both saturated and unsaturated conditions. In this situation, the spatially variable radial velocity $v_r(r)$ is just $q_r(r)/\theta(r)$ and a typical radial dispersion coefficient is $D_r(r) = \alpha_L v_r(r)$. To understand the contributions of each of the correction terms to the entire deterministic displacement (denoted here by a), consider the radial component a_r from equation (55) normalized by the pure advection step length $v_r\Delta t$:

$$\frac{a_r}{v_r\Delta t} = 1 + \frac{1}{v_r}\frac{\partial D_r}{\partial r} + D_r\frac{1}{v_r\theta}\frac{\partial\theta}{\partial r} \tag{65a}$$

$$= 1 + \frac{\alpha_L}{v_r}\frac{\partial v_r}{\partial r} + \frac{\alpha_L}{\theta}\frac{\partial\theta}{\partial r}$$

For the steady profile given by (64), this reduces to

$$\frac{a_r}{v_r\Delta t} = 1 - \frac{\alpha_L}{r} \tag{65b}$$

The total contribution of the correction terms in this case would only be significant within a distance of α_L of the well source. The injection problem represents an extreme case in terms of large velocity gradients. Most situations to be encountered are expected to be much less severe. *Uffink* [1987] presents some other examples of the effect of the dispersion gradient correction term in saturated problems.

In more general (unsteady, unsaturated) situations, the last term in the first or second line of (65a) may be interpreted as a normalized moisture gradient displacement. It may be approximated as $\alpha_L\Delta(\ln\theta)/\Delta r$, where Δr might be thought of as a typical grid size Δx used earlier. This term is

roughly equal to $\Delta(\ln\theta)/Pe_G$ where the grid Peclet number is of the order of 10 to 100 (§3.3). For this term to be significant with respect to 1, the change in $\ln\theta$ over one grid spacing would have to be on the order of 10 or more. As $0 < \theta < 1$, this situation may exist near an extremely sharp wetting front in which case a very small time step would be in order. Practically speaking, however, this may be an unlikely prospect in most of our applications.

• Temporally Variable Flows: The examples used above considered overshoot errors that can be introduced by not properly tracking spatially variable streamlines when moving a particle. It is important to recognize that the same kind of error can happen in a temporal sense if the velocities change considerably over a time step Δt. The key point to understand here is how the time scale of the time-variable velocity relates to the time step for the particle movements.

Suppose fluctuations in the flow and moisture fields occur over a characteristic time scale ΔT_f, i.e., updated values are found over time intervals of ΔT_f. For a given snapshot of a flow field, an optimal time step Δt_{opt} for moving a particle may be identified in some manner (see above) by restricting some typical cell Courant number C_c to be smaller than one. If $\Delta t_{opt} << \Delta T_f$, then there is no chance of any temporal overshoot errors as the flow field appears steady over time scales of Δt. If $\Delta t_{opt} \approx \Delta T_f$, then the flow dynamics may be shifting over time scales close to Δt, but since no finer resolution of the flow in time is available, any overshoot errors accumulated by using a Δt less than or equal to Δt_{opt} must be accepted as an approximation (as in the spatial case above). If $\Delta t_{opt} > \Delta T_f$, then a temporal overshoot will occur that can be improved upon by lowering Δt_{opt} to a value of ΔT_f or less.

5.3 Moving Many Particles: Time Stepping Procedures. The discussions in the previous section were concerned with the choice of the time step and the resulting magnitudes of the various component displacements involved with moving one particle using (49), (52) or (55). The main issue was to keep the various step motions small enough to minimize overshoot errors when spatially or temporally variable velocity fields are present. Under most conditions it was found that the largest contribution to the particle motion over one time step comes from the purely advective displacement $v\Delta t$. Controlling the magnitude of this step through a judicious choice of Δt would effectively control all other component displacements to a similar degree. One can choose a very small, fixed value of Δt for all displacements in all cells, or one can choose a variable Δt based upon a particular particle's position such that it consistently moves from one cell boundary to the next. Although the latter method is the more efficient for a *one-particle* system, it may not be ideal for a system with many particles. Our applications will focus on problems that involve moving large numbers of particles through the flow domain Ω_c (§4.2, Figure 4c). Below, we briefly consider two possible time stepping

schemes for our simulations.

* Time Stepping Method 1: Given N particles distributed in the flow domain Ω_C at some arbitrary time t_0, this approach simply involves choosing a fixed time step Δt and moving all N particles sequentially to new positions using an appropriate step equation (49), (52) or (55). The same time step is meant to be used for the displacement of all particles at once so the distribution of solute mass is known at *each* time level (Figure 6a). To avoid overshoot problems, Δt must be chosen with respect to the largest cell velocity in Ω_C whose magnitude V_{max} gives a maximum cell Courant number $C_{c,max}$. Ensuring that $C_{c,max}$ is less than, say, 0.1 will mean that overshoot will be quite small for all particles. Of course, this is a very conservative procedure which might be modified if necessary to lessen computational costs. If the velocity field is unsteady, the value of Δt would, in a strict sense, have to be modified at each time level as well as adjusted downward if large in comparison with the flow update interval ΔT_f.

* Time Stepping Method 2: The first procedure described above is a more traditional approach in that the entire ensemble of particles are moved together with the same time step giving a complete picture or snapshot of the solute mass at *every* computational instant. The method presented here is somewhat different and takes advantage of the intrinsic nature of the particle tracking approach. It is best used when *approximately steady* velocity fields are available (when $\Delta t_{opt} << \Delta T_f$). Given the same N particles distributed in Ω_C at t_0, this technique involves choosing single particles and moving them individually over many time steps up to some fixed *rendezvous* time T_1. In other words, particle 1 is moved from its postion X_0^1 at time t_0 over many time steps to its postion X_1^1 at time T_1. Then particle 2 is moved over many steps from (X_0^2, t_0) to (X_1^2, T_1), and so forth (Figure 6b). Once all the particles have progressed to time T_1, they can be moved again in the same manner to another fixed rendezvous time T_2. The difference here is that complete snapshots of the particles can only be obtained at the preselected times T_1, T_2, etc. The advantage of this method is that time steps used for each particle will differ and must repeatedly be chosen and adjusted according to the local flow conditions. For example, the time step for a given particle i in cell L at time t_0 can be fixed such that the particle is moved just inside the next cell via pure advection (§5.2) and then displaced via the other (presumably smaller) mechanisms. Thus, a particle would not have to be moved incrementally through a cell of constant velocity; it can be moved to the next cell quickly with minimal spatial overshoot error. This approach would ostensibly save computational time in a global sense, however it necessitates careful thought in terms of applying boundary conditions (§5.4) and its use in unsteady problems. If the characteristic update interval for the unsteady flow field ΔT_f is much greater than a typical Δt used in the step equations, then the simulation periods T_1, T_2, etc.,
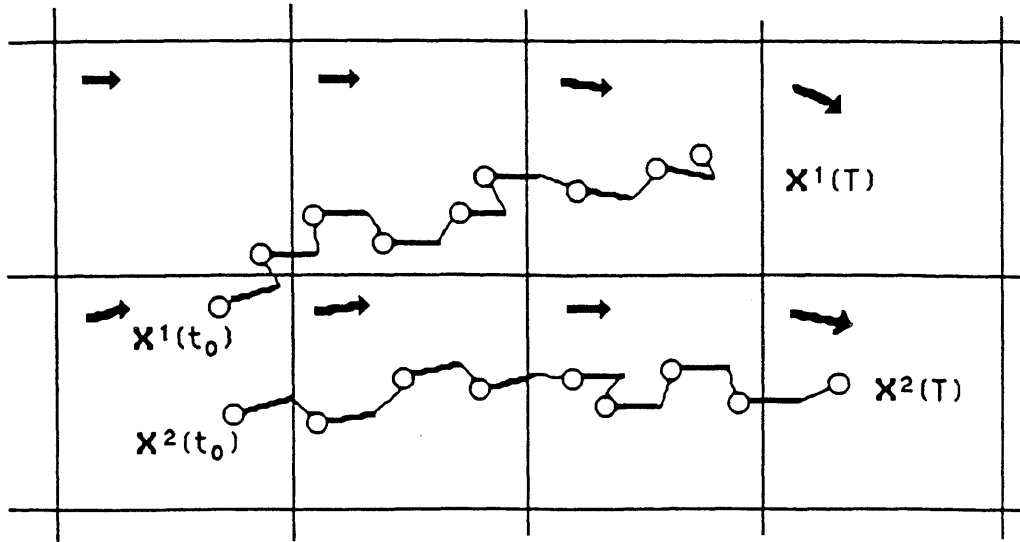
Figure 6a: Movement of two particles in a two-dimensional domain using the first time-stepping method. Bold segments indicate 'advective' displacements; lighter segments, random, dispersive displacements. The time step is fixed and the cell velocities are indicated.
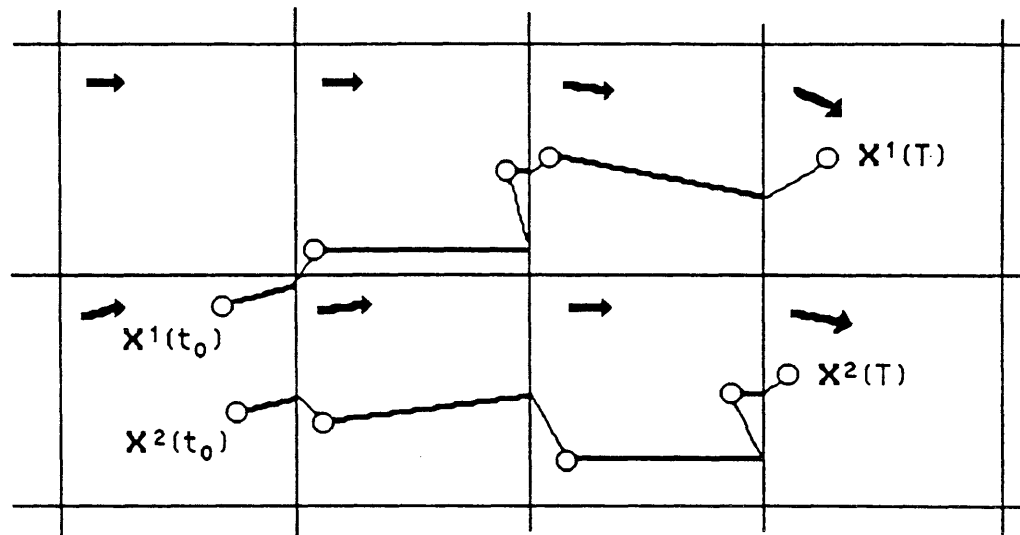

Figure 6b: Movement of two particles in a two-dimensional domain using the second time-stepping method. Particle 1 is moved from (X_0^1, t_0) to (X_1^1, t_1) first; then particle 2 is moved from (X_0^2, t_0) to (X_1^2, t_1)

may be just chosen as times of flow updates, $n\Delta T_f$. Otherwise, if $\Delta T_f < \Delta t$, the advantage in moving particles completely across cells would be lost to accumulating temporal overshoot errors.

- **Number of Particles**: The idea of simulating the motions of a large number of particles at once comes from the desire to see a developing plume of solute move throughout the flow domain in time. The solute mass is divided among a hypothetical group of N particles free to move independently in time through Ω_C according to the step equations (49), (52) or (55). *How many particles should be used?* The more particles used for a given amount of solute, the smaller the mass each particle has and the more "fluid" the body of particles becomes. A better idea of the potential spread can be had. It would be much easier to identify smaller fractions of the solute mass in remote parts of Ω_C. Although *Ahlstrom, et al.* [1977] recommend the use of 10^4 to 10^5 particles in large problems, it should not be forgotten that the results of two or more identical simulations can be superposed since the motions of the individual particals are independent. This is why the simultaneous motion of N particles is equivalent to N combined one-particle experiments. The interpretation of the spread of a given number particles is addressed further in §5.5 and §5.6 and will shed additional light on the choice of N.

5.4 Auxiliary Conditions. The kinds of auxiliary conditions usually applied in transport simulations were briefly examined in §2.6. Our simulations are meant to take place in a computational domain Ω_C which may be though of as a subset of a larger domain Ω in which the random walk equations were developed and where the total solute mass M remains constant (thus conserving the probability, f: Figure 2). The total mass in Ω_C could thus be allowed to vary, if need be, by allowing it to flow in or out through some boundary freely or in some controlled manner. Notice, however, that the mass is conserved on the larger scale of Ω even though its distribution external to Ω_C is not modeled. The boundaries of Ω_C may be hypothetical or represent some actual physical structure.

Initial conditions for the concentration $c(X,t_0)$ or mass fraction $\omega(X,t_0)$ for X in Ω_C must be translated or thought of in terms of initial distributions of particles (§4.2) inside Ω_C. This can be done in the current model configuration in a number of ways. As the cell volumes Ω_e are relatively small in comparison with the entire domain volume Ω_C, groups of particles can be assigned to distinct cells and distributed within them in a random, uniform fashion (Figure 7a). The use of the small volumes allows the distribution of particles within each to be construed as a concentration or a mass fraction associated with that cell. Using the volume of the cell, initial moisture content, mass of each particle, or some other normalization procedure (§5.5), an initial concentration $c(X,t_0)$ or mass fraction $\omega(X,t_0)$ can be converted into an approximate number of particles according to some adopted convention (§4.2). Particles can also be assigned to simulate "exact" sorts of conditions such as a point

Figure 7a: Distribution of 10 particles randomly in cells L_1 and L_3; 20 in cell L_2
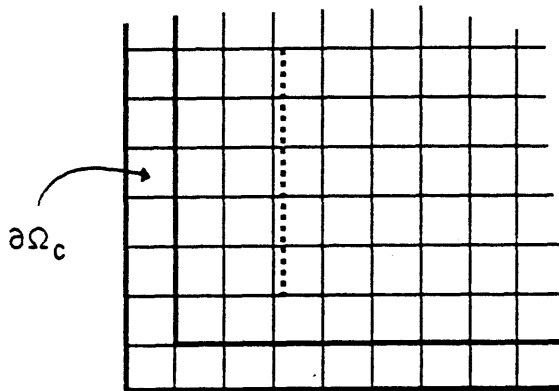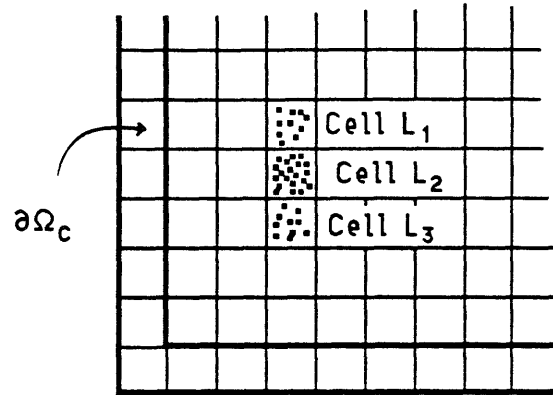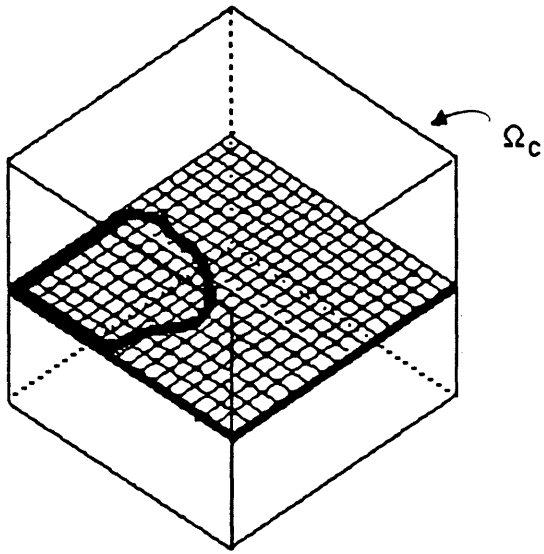

Figure 7b: Line source of particles

source (assign all particles to one position X_0 at t_0), a line or plane source (done similarly), or any other spatial distribution (Figure 7b). Also, it is not really necessary to think of converting concentrations to particles if the distribution of particles itself will serve the purpose of the simulation. It all depends on the manner of interpretation of the results (§ 5.5).

Boundary conditions would normally include specification of $c(X,t)$ or $\omega(X,t)$ or the normal mass flux $F = n \cdot (\rho v \omega + J)$ for points X on the boundary $\partial \Omega_C$ of Ω_C. This mass flux is usually specified to be zero (representing a no-flux boundary) or some positive *inflow* quantity. For convenience in applying these conditions in terms of particle distributions, the outermost shell of cells of Ω_C will be considered as the boundary, or, more precisely, a boundary layer, in which particles will be distributed to mimick fixed concentrations or flux conditions (Figure 8a). Dynamic variables such as velocities and moisture contents will still be associated with these cells. Let us denote by $\partial \Omega_1$ the cells on the boundary (layer) associated with a constant c, ω, or particle count (Dirichlet condition); by $\partial \Omega_2$ those boundary cells used to specify a nonzero mass influx condition; by $\partial \Omega_3$ the boundary cells where a zero-mass flux condition is enforced; and by $\partial \Omega_4$ the remainder of the boundary cells where mass is essentially allowed to flow out of the domain into Ω. Clearly, $\partial \Omega_C = \Sigma \, \partial \Omega_i$. Application of conditions on these boundaries will be explained in turn:

- Dirichlet Boundary $\partial \Omega_1$: Consider the case using the first time stepping method described in §5.3. To each cell in $\partial \Omega_1$ assign a number of particles that represent the specified particle count or a translated concentration or mass fraction value based upon the volume of the cell as discussed above. These should be distributed uniformly and randomly inside the cells. During the next time step, these particles along with all others inside Ω_C are moved according to the time stepping procedure. Some of the particles put into $\partial \Omega_1$ will move into the core of Ω_C (that part of Ω_C excluding the boundary layer), some will remain inside $\partial \Omega_1$, and some may actually move out of $\partial \Omega_1$ into other parts of the boundary or outside of Ω_C completely (Figure 8b). At the end of this time step and before the next, all particles outside of the *core* of Ω_C are removed and all active boundary conditions are reinstated. In other words, all remaining particles outside of Ω_C and $\partial \Omega_C$ are removed. In the case of $\partial \Omega_1$, the remaining particles are taken out and a "fresh" batch is put in again as described above. This serves to maintain the average number of particles or concentration in $\partial \Omega_1$ over the discrete time steps at the same, prescribed level.

In this time stepping approach, the time increments Δt will be small in comparison with total simulation time, so the decrease in the boundary concentration between the start of successive steps and its affect on the solution is minimal. The only way to apply this condition in the second time stepping method would be to reinstate the particles after each rendezvous time T_i. As the time span between these points can conceivably be quite large, the change in the boundary concentration between
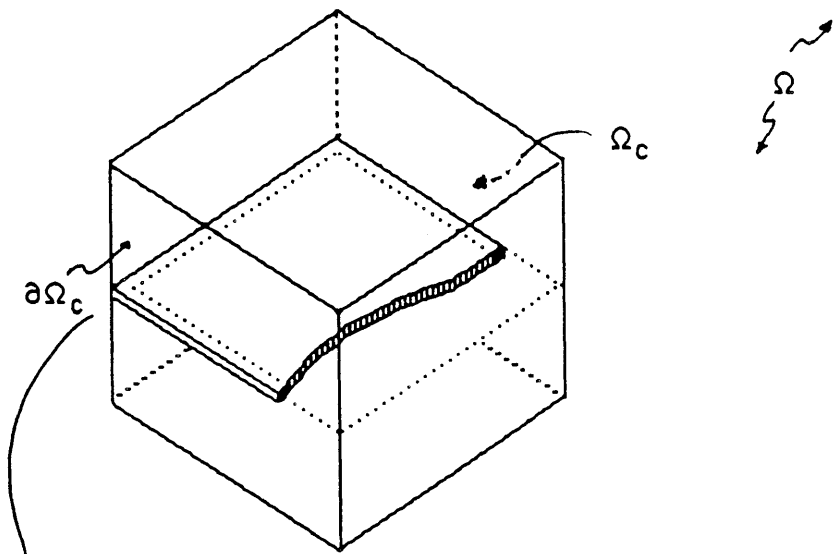
Figure 8a: Boundary layer $\partial\Omega_C$ and domain Ω_C
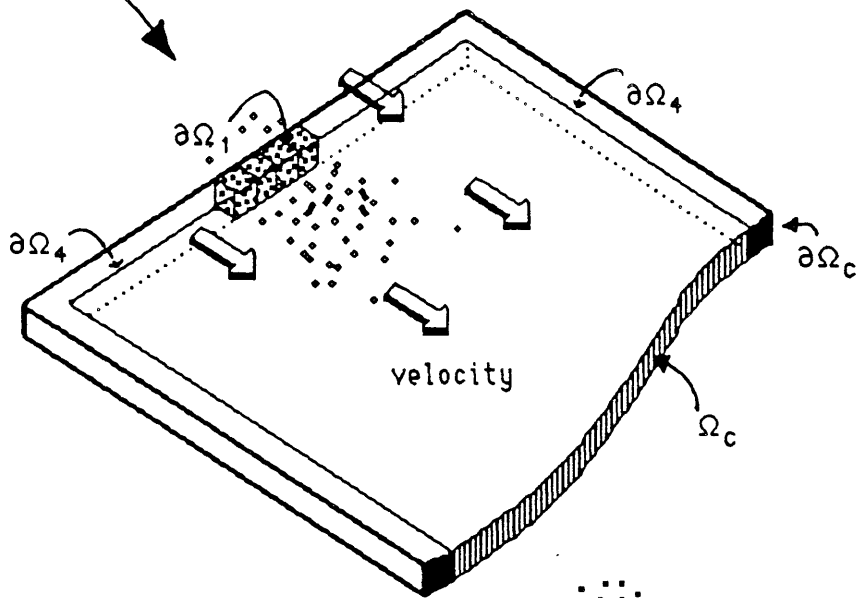
: Initial particle locations

: Particle locations after one time step

Figure 8b: Dirichlet boundary $\partial\Omega_1$

velocity

reflection plane

$\partial\Omega_c$

Ω_c

$\partial\Omega_2$

$\partial\Omega_4$

$\partial\Omega_3$

Δx

$\partial\Omega_c$ $\partial\Omega_3$ Ω

α

α

δ δ

reflection plane
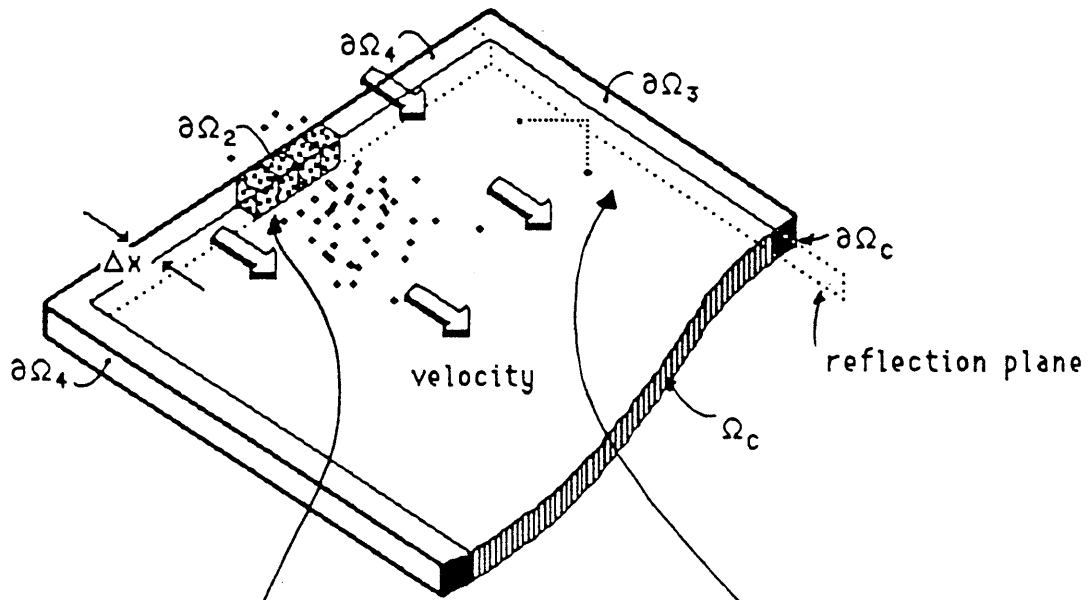
Figure 8d: Zero-flux boundary $\partial\Omega_3$

$\partial\Omega_2$

n normal direction

$v\Delta t$ Δx Ω_c
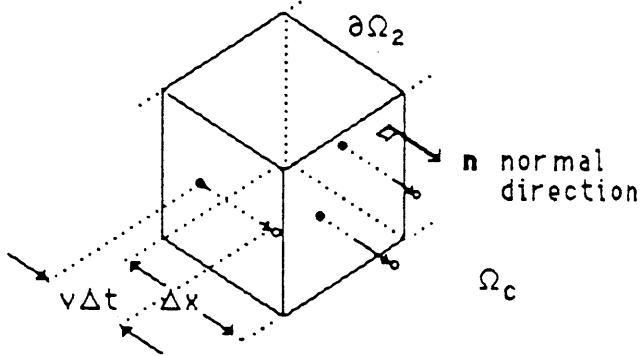
Figure 8c: Mass flux boundary $\partial\Omega_2$

Particles before displacement

Particles after displacement

these increments could influence the solution significantly. As there is no other easy way of implementing this kind of boundary condition for this time marching method, it is recommended to use conditions on $\partial \Omega_1$ with the first time stepping scheme only.

- Mass Influx Boundary $\partial \Omega_2$: The treatment of this boundary condition can be done in a fashion similar to that above. It is important to see that the physical boundary statement involves specifying a certain amount of mass (i.e., number of particles) that must flow into the system through a certain area over some span of time. It is assumed that the velocity at this boundary flows into Ω_c and is consistent with the concept of inflowing solute mass. Suppose that the influx rate is F [mass/area·time]. Then, consider an individual cell L that is part of $\partial \Omega_2$ (Figure 8c). If the area of the side of this cell facing inside toward Ω_c is denoted by A, then the mass expected to flow into Ω_c in a direction normal to the surface A over some time interval Δt is $M_c = F A \Delta t$. This corresponds to $N_c = F A \Delta t / m$ particles that must come through A into Ω_c over Δt, where m is the mass of one particle. The best way to introduce these particles into the domain is to place them uniformly and randomly into cell L and let the velocity component normal to A advect them in over a given period of time Δt (and ignore other velocity components, dispersion and the gradient correction terms). It is, in fact, best to specify this normal velocity component V_n (and ignore the real value) to be $\Delta x / \Delta t$ where Δx is the depth of cell L or the boundary layer (Figure 8c). This will guarantee that all the particles come out of L uniformly over Δt into Ω_c at the desired rate F. This procedure should be applied in all cells that belong to $\p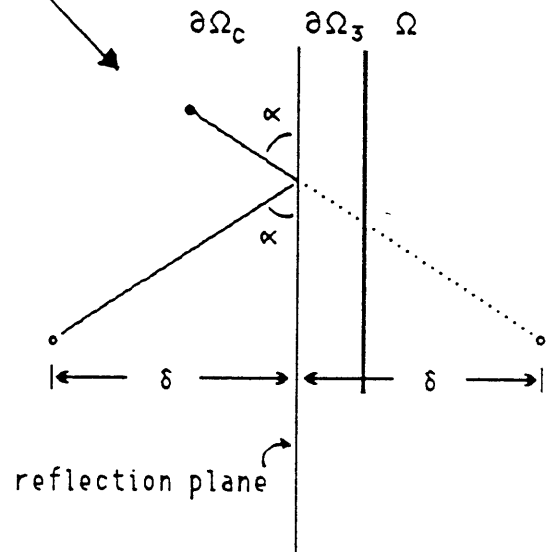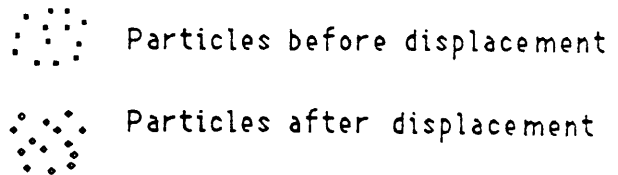artial \Omega_2$. It can be used in either time stepping method; it should be based upon the optimal time step Δt_{opt} in method one, and on the interval between rendezvous times in the second method. The cells would be refilled during each interval.

- Zero-Flux Boundary $\partial \Omega_3$: By definition, this is a boundary across which no mass can cross. Such a boundary will likely be one where the normal velocity is zero. Particles in the vicinity of such a boundary may be "urged" to move across the boundary as part of a diffusive displacement. Any particles moving into a zero-flux boundary cell will be reflected back into the domain in the manner illustrated in Figure 8d, a sort of "billiard ball" bounce. Boundaries such as this are often called *reflective* [Gardiner, 1985].

- Outflow Boundary $\partial \Omega_4$: The remaining cells comprising the boundary layer $\partial \Omega_c$ are loosely classified as free-flow or outflow boundary cells. Particles that enter these cells (or cross through to outside of Ω_c) during a time step will be removed from consideration. They simply exit the system or region of interest. If the boundary of Ω_c is thought of simply as an imaginary line without physical influence through a much larger flow system in Ω, then it is conceivable that a particle

that crossed over this line could find its way back through winding velocities and dispersive motions. This possibility, albeit slight, is excluded from consideration in this model. In other applications, when a theoretical boundary such as this has a physical meaning, it is often labeled as *absorbing* [*Gardiner*, 1985] because of its properties of removing the particles from the flow. This would correspond to $\partial\Omega_4$ being a part of the boundary of Ω, where specification of the probability f to be zero indicates no chance for a particle to be situated there.

A summary of these auxiliary conditions is presented in Table 1.

Table 1
Review of Boundary Types

Boundary	Type	Characteristics	Usage Time Step 1	Time Step 2
$\partial\Omega_1$	Dirichlet	Specified # particles in or on boundary for some time period. (Figure 8b)	OK	Difficult
$\partial\Omega_2$	Specified flux	Specified # particles enter Ω_c from $\partial\Omega_2$ per unit time and unit area facing Ω_c. (Figure 8c)	OK	OK
$\partial\Omega_3$	No-flux	Particles crossing into $\partial\Omega_3$ or beyond (out of Ω_c) reflected back via "billiard ball" bounce. (Figure 8d)	OK	OK
$\partial\Omega_4$	Outflow	Particles crossing into $\partial\Omega_4$ or beyond are extracted from system. (Figures 8b,c,d)	OK	OK
$\partial\Omega_c$	General	$\partial\Omega_c = \partial\Omega_1 + \partial\Omega_2 + \partial\Omega_3 + \partial\Omega_4$		

5.5 Solution Refinement and Sensitivity. In many kinds of applications, it may be desirable to convert particle distributions to concentrations or mass fractions. Suppose we are studying a problem where a fixed amount of solute mass M is represented by some N particles within a large flow domain Ω. Some or all of this mass may be passing through the computational domain of interest Ω_c, but it is only important to realize that M is thought of as being fixed and N is chosen as the number of particles to represent it. The mass of an individual particle will be $m = M/N$ and will depend on the choice of N. Consider some arbitrary sampling region Ω_s of fixed shape, volume V_s, and orientation centered at some point X in Ω (Figure 9a). The following will serve as approximate measures of the local solute mass in Ω_s centered at X at time t:

$$N_S(X,t) \quad = \quad \text{total number of particles in } \Omega_S, \qquad (66)$$

$$MN_S(X,t)/N \quad = \quad mN_S(X,t) \quad = \quad \text{total mass inside } \Omega_S,$$

$$c(X,t) \quad = \quad MN_S(X,t)/N\Theta(X,t)V_S \quad = \quad mN_S/\Theta(X,t)V_S \quad = \quad \text{average mass concentration of solute at } (X,t),$$

$$\omega(X,t) \quad = \quad c(X,t)/\rho \quad = \quad \text{average mass fraction at } (X,t),$$

$$n(X,t) \quad = \quad N_S(X,t)/N \quad = \quad \text{the fraction of the N particles in } \Omega_S \text{ at time } t.$$

Recall, the analogy used with the random walk approach is to represent some known solute mass M with a finite number of N particles, N being selected by the user. In this sense, the individual mass of each particle m will be smaller if N is larger. As pointed out before, the larger N is, the easier it is to (1) represent the distribution of the solute mass through the flow domain, and (2) identify smaller fractions of mass in specific local areas.

The sampling volume Ω_S used to define average concentrations or mass fractions can be of any size or shape, as long as it is used and oriented the same way for all evaluations. Theoretically, it can be moved about the computational domain Ω_C to obtain concentration or mass fraction measurements over a continuum of points (Figure 9b) for a given "snapshot" of the mass at some time t. Qualitatively speaking, the larger Ω_S is, the larger the number of particles found within it will be, and the more smoothly varying the concentration will be. If Ω_S is too large, all of the mass will be found within it and little sense of its spatial distribution will be discerned. On the other hand, if Ω_S is too small, its utility in extracting smooth distributions of mass from numbers of particles will be lost. The whole idea of the volume Ω_S it to provide some sort of continuum measure of the solute distribution. A particularly useful choice of Ω_S will simply be the cell volume Ω_e, whose natural scale is derived from the finite difference flow mesh size. This volume will be representative of the local (REV) scale used in this investigation and is essentially that used to define local hydraulic parameter values and velocities. It is attractive because it can be used to define a local concentration field on a scale corresponding to the local velocities and parameters. Use of non-overlapping cells (Figure 9b) is certainly allowed and provides a convenient framework for estimation of these continuum measures over a regularly spaced set of points.

If the cell volumes Ω_e are adopted to be the sampling volume Ω_S, then control of defining smoothly varying continuum measures of the solute distribution will rest in the choice of N. Because of the finite nature of N, "noisy" solutions such as that pictured in Figure 10 can be obtained. To quantify this noise, we refer to *Ahlstrom, et al.*, [1977] who define a standard normal error ϵ to represent the degree of this problem. Consider the motions of one particle and a random variable Z which takes on the value of 1.0 if the particle lies in a small sampling region Ω_S of volume V_S centered around X
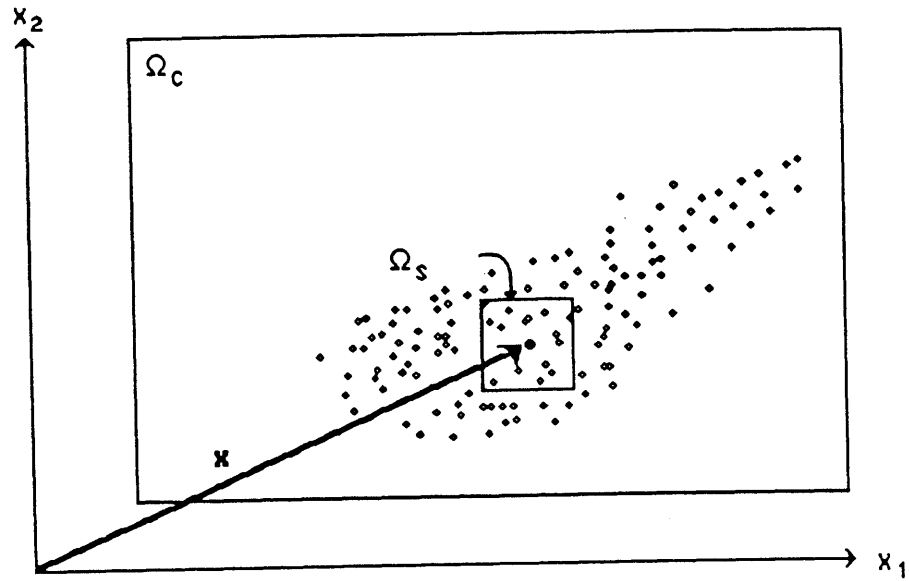
Figure 9a: Location of sampling volume Ω_S in Ω_C (two-dimensional for clarity)
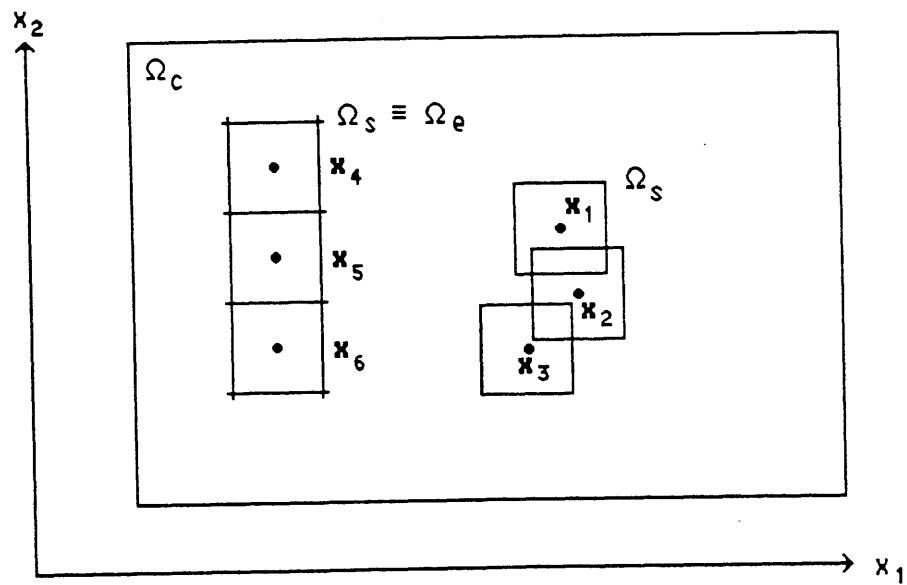
Figure 9b: Location of overlapping volumes Ω_S: choice of cell volume Ω_e as sampling volume Ω_S.
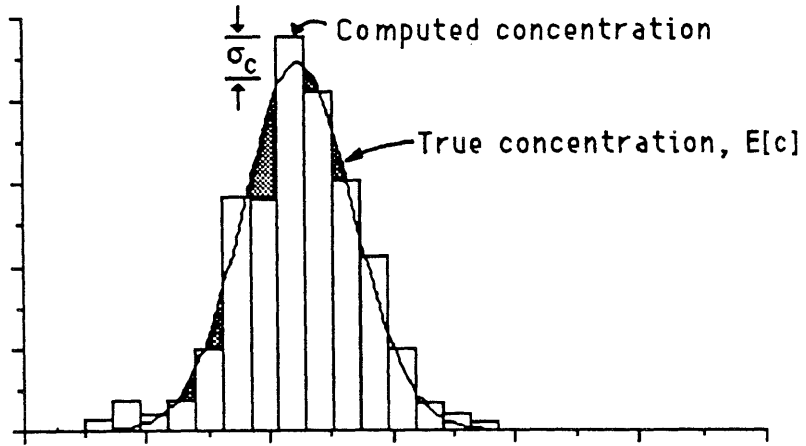
Figure 10:   'Noise' in calculated concentrations

at time t and zero otherwise. For simplicity, suppose Ω_S is, in fact, a small, general sample volume Ω_S of volume V_S as discussed above. If V_S is much smaller than the volume of the region Ω_C, the *expected* value of Z at (X,t) is simply $E[Z] = f(X,t)V_S$ and its variance σ^2_Z is $f(X,t)V_S(1 - f(X,t)V_S)$. If N particles are in Ω_C, the expected number $E[N_S]$ of particles to be found within V_S at any point X and time t is given from (42):

$$E[N_S] = Nf(X,t)V_S \tag{67}$$

with variance σ^2_{Ns},

$$\sigma^2_{Ns} = Nf(X,t)V_S(1 - f(X,t)V_S) \tag{68}$$

If V_S is small, then fV_S small and its square can be removed from (68) to give

$$\sigma^2_{Ns} \approx Nf(X,t)V_S \tag{69}$$

With a fixed total mass M, a cell concentration c_S can be defined using (66) whose mean and variance at (X,t) become

$$E[c_S] = E[MN_S/N\theta V_S] = (M/N\theta V_S) E[N_S] = Mf(X,t)/\theta(X,t) \tag{70}$$

$$\sigma^2_c = Var[MN_S/N\theta V_S] = (M/N\theta V_S)^2 \sigma^2_{Ns} \approx (M/\theta(X,t))^2 f(X,t)/NV_S$$

$$= E[c_S]\cdot(M/NV_S\theta(X,t)) \tag{71}$$

where (67) and (69) were used. Notice that the expected concentration at X and t is independent of the number (N) of particles and the size V_S of the volume used to formulate it, as long as it is small. The variance, on the other hand, is dependent on the mean. Integration of $\theta(X,t)E[c_S]$ over Ω yields the total mass:

$$\int_\Omega \theta(X,t)E[c_S] \, dX = M \int_\Omega f(X,t) \, dX = M\cdot1 \; . \tag{72}$$

The variance σ^2_c does, however, depend on N and V_S, as well as X and t. A more useful measure of the variability is the global squared error ϵ^2 found from integrating $\theta(X,t)^2\sigma^2_c(X,t)$ over X:

$$\epsilon^2 = \frac{M^2}{NV_s} \int_\Omega f(X,t) \, dX = \frac{M^2}{NV_s} \cdot 1 \tag{73}$$

whence the standard normal error is $\epsilon = M/\sqrt{NV_s}$. This result is essentially a global measure of all random noise illustrated in Figure 10 and shows that it is reduced by a factor of two for a four-fold increase in the number of particles N or a four-fold increase of the volume of the sampling region Ω_s from which concentrations are estimated.

As mentioned above, the local cell volume Ω_e was chosen to be Ω_s for these investigations to maintain the scale of the concentration estimates. Improvement of any random noise error in this model will thus be limited to increasing the number of particles used to represent the solute mass, or using some post-process filtering algorithm to find a smooth measure of the resulting particle distributions. The concentration estimates associated with the cell centers can be considered to be corrupted by this random noise and written as

$$z(X,t) = c(X,t) + s(X,t) \tag{74}$$

where $z(X,t)$ is the raw concentration estimate, or measured value, $c(X,t)$, the true, expected, or sought-after value, and $s(X,t)$ is the noisy component with zero mean and variance is given by (71). The random nature of s can be considered a spatial process, dependent on the mean signal $c(X,t)$, yet independent at different times. The measurements, z, are therefore random in this way also. In most situations, the signal would be considered deterministic or coherent in space. *Ahlstrom, et al.,* [1977] discuss a method of filtering the z measurements in the spectral domain to remove what they consider to be the contaminating high frequency spectral components. Their approach consider a very simple problem where $c(X,t)$ is known *a priori* so that it is clear what the corrupting components are. In a general situation, the form of $c(X,t)$ is not know ahead of time, and it is not clear what sort of cutoff frequency to use in their low frequency bypass. This approach is a specific case of a more general smoothing situation where z, s, as well as c are considered to be random in space, and a filter to estimate $c(X,t)$ can be constructed by convoluting the measured signal z with a transfer function based upon the spectra of c and s [*Papoulis,* 1984; *Pratt,* 1978]. This method can be problematic because of the dependence of the noise, σ^2_c, on the signal strength, $E[c_s]$.

On the other hand, simpler smoothing algorithms to find $c(X,t)$ may also work just as well. Some methods exist that are not plagued by a dependence of the magnitude of the noise to the signal magnitude. A familiar least-squares fit can also be used. Furthermore, alternative approaches for defining the concentration can be pursued. A technique based on the concept of smoothing windows used in spectral estimation [*Press, et al.,* 1986] can be used, where the contribution of a particle at X_i to

the concentration $c(X,t)$ at X is controlled by a more smoothly varying "window" or weighting function. This is a generalization of the simple volumetric concept discussed above and illustrated in Figure 9. Although these filtering schemes are intellectually elegant and very interesting from a theoretical point of view, their only potential value here would be to filter the solution to a given degree (measured by a reduction of ε) at a cost less than that associated with using a larger number of particles to achieve a comparable improvement.

The effects of the number of particles can also be illustrated in simple, constant velocity problems by evaluating the second moments of a spreading particle distribution about the mean displacement of its center of mass and comparing this with an exact result. This will be discussed further in the next section in a broader context of measuring the spreading characteristics of a solute plume in a spatially variable velocity field. Examination of the nature the heterogeneous particle distributions in this way is meant to help us understand larger scale behavior of spreading solute as induced by spatially variable velocity, moisture, and hydraulic parameter fields. It will also allow for comparisons to be made with predictions of larger scale stochastic models.

5.6 Detection of Larger Scale Behavior. One approach for comparison of the numerical results found here with stochastic theories (e.g., model equations 10 and 14) will involve analysis of our solutions to detect mean or larger scale Fickian dispersive behavior as evidenced by constant, asymptotic macrodispersivity components (see §2.2). Apparent large scale dispersivities of a heterogeneous medium can be measured in many cases by calculating the second-order spatial moments of a spreading solute mass about its moving center of mass. These measured quantities and their behavior can be compared with their theoretical counterparts derivable from the model *mean* equations such as (10). Agreement between the measured behavior found from the local particle tracking experiments and its theoretical counterpart will tend to corroborate the predictions of stochastic models.

Given a distribution of solute mass $\rho\omega\theta$ in a large three-dimensional domain Ω at some time, its general p-th order spatial cross moment is defined by [*Freyberg et al.*, 1983]

$$M_{lmn} = \int_{\Omega} \rho\omega\theta X^l Y^m Z^n \, d\Omega \tag{75}$$

where $p = l + m + n$. Notice that the solute mass is simply $M \equiv M_{000}$. The center of mass of the solute plume is simply the normalized set of first moments $\overline{X} \equiv (M_{100}/M)i + (M_{010}/M)j + (M_{001}/M)k$. This can be written in a more compact form as

$$\overline{X} = \frac{1}{M} \int_{\Omega} \rho\omega\theta X \, d\Omega \tag{76}$$

- 67 -

One measure of the general three-dimensional *spread* of solute about the center of mass $\overline{X}$ is the normalized second order moment matrix, corrected for the center of mass:

$$\varnothing^2 = \frac{1}{M} \int_\Omega \rho\omega\theta (X - \overline{X})(X - \overline{X})^T \, d\Omega \tag{77}$$

$$= \frac{1}{M} \int_\Omega \rho\omega\theta X X^T \, d\Omega - \overline{X}\overline{X}^T$$

The three components of the first row of $\varnothing^2$ are, for instance,

$$\begin{aligned}
\sigma^2_{11} &= M_{200}/M - (M_{100}/M)^2 \\
\sigma^2_{12} &= \sigma^2_{21} = M_{110}/M - M_{100}M_{010}/M^2 \\
\sigma^2_{13} &= \sigma^2_{31} = M_{101}/M - M_{100}M_{001}/M^2
\end{aligned} \tag{78}$$

As a simple application, consider transport in a saturated domain with a spatially constant velocity V and scalar dispersion coefficient. In this case, the solute balance equation is given by (46) where the porosity θ_0 has been factored out. If a fixed amount of solute mass M remains completely inside Ω_c, then multiplication of (46) by $\theta_0 X X^T$ and integration over all of Ω_c (or Ω) yields the relationship between $\varnothing^2$ and the dispersion components [*Gelhar et al.*, 1979]:

$$\frac{d\varnothing^2}{dt} = 2D \, \mathbb{I} \tag{79a}$$

A similar procedure using $\theta_0 X$ to multiply (46) yields

$$\frac{d\overline{X}}{dt} = V \tag{79b}$$

If a problem is conceived where a plug of N particles is introduced into a small region in Ω_c and allowed to move such that all mass remains inside Ω_c, then the overall spatial characteristics of the resulting solute plume can be measured in the same way as perceived above. In this case, the spatial distribution of solute "particle" mass can be approximated by

$$\rho\omega\theta \approx \sum_{i=1}^{N} m \, \delta(X - X^i(t)) \tag{80}$$

where $m = M/N$ is the mass of one particle and $X^i(t)$ is the position of the i-th particle at time t. The mass, M_*, center of mass, $\overline{X}_*$, and second-order moment matrix $\varnothing^2_*$ of this *particle distribution* can be evaluated using (80) in (75), (76), and (77):

$$M_* = \int_{\Omega_c} \rho \omega \theta \, d\Omega_c \approx \sum_{i=1}^{N} m = mN \tag{81}$$

$$\overline{X}_* = \frac{1}{M_*} \int_{\Omega_c} \rho \omega \theta X \, d\Omega_c \approx \frac{1}{M_*} \sum_{i=1}^{N} mX^i = \frac{1}{N} \sum_{i=1}^{N} X^i \tag{82}$$

$$\varnothing^2_* = \frac{1}{M_*} \int_{\Omega_c} \rho \omega \theta X X^T d\Omega_c - \overline{X}\,\overline{X}^T \approx \frac{1}{N} \sum_{i=1}^{N} X^i X^{iT} - \overline{X}_* \overline{X}_*^T \tag{83}$$

The star subscripts signify statistical measurements based upon an experimental particle distribution. As long as all particles remain in Ω_c, repeated measurements of components of $\varnothing^2_*$ can be plotted against time and the resulting slopes compared with the theoretical values, such as (79a). Deviations from the exact slope will be indicative of the finite number of particles used in the simulation. The same can be done with values of $\overline{X}_*$ to estimate the velocity components.

In the same manner as above, the large scale, mean solute balance equation (10) can be manipulated to form theoretical relationships between moments based upon the mean solute mass distribution $\overline{\rho \omega} \, \overline{\theta}$ and the dispersivity components of $\mathbb{A}$ as well as the the local dispersion coefficients. Consider a saturated flow problem where $\overline{\theta}$ becomes the constant porosity θ_0 or a *steady* unsaturated flow problem where $\hat{R}$ and $\hat{E}$ are zero and $\overline{q}$ can be approximated by $\overline{V}\theta_u$, θ_u being an approximate saturation level. Equation (10) can be written as

$$\frac{\partial}{\partial t}(\rho \theta \overline{\omega}) + \nabla \cdot (\rho \theta \overline{V}\, \overline{\omega}) - \nabla \cdot [\rho\, (\mathbb{E}_{local} + \theta \overline{V}\mathbb{A}(t)) \cdot \nabla \overline{\omega}] = 0 \tag{84}$$

where Θ is θ_0 or θ_u, and $\overline{V}$ is $|\overline{V}|$. Let us assume further that conditions are such that the mean velocity $\overline{V}$ (and hence $\mathbb{A}(t)$ and $\mathbb{E}_{local}$) as well as Θ can be considered constant over space. If a fixed amount of solute mass M remains completely inside Ω_c, then multiplication of (84) by $X X^T$ and integration over Ω_c (or Ω) yields the relationship between $\varnothing^2$ and the large scale dispersion components [*Gelhar et al.*, 1979]:

$$\frac{d\varnothing^2}{dt} = 2(\overline{V}\mathbb{A}(t) + \mathbb{E}_{local}) \tag{85a}$$

Similarly, multiplication of (84) by X yields

$$\frac{d\overline{X}}{dt} = \overline{V} \qquad\qquad (85b)$$

Suppose a corresponding *local* problem is conceived where a plug of N particles is introduced into a small "upstream" region of Ω_c and allowed to move such that all mass remains inside Ω_c. Since the spatial distribution of solute "particle" mass can be still approximated by (80), the overall spatial characteristics of the resulting solute plume can be measured in the same way as above using equations (81) - (83). Because the local velocity field is heterogeneous, the spreading as measured by (83) will be more marked. This will be true especially at larger times when the initially small plug has moved through a significant portion of the variable environment. Initially, the statistical measurements (81) - (83) will vary with time and may not necessarily reflect the mean velocity and dispersive characteristics in (84). Some period of development time will be required for this to occur, and this may be dependent on the variability of the flow field as well as the magnitude of local dispersion effects. Nevertheless, measurements of $\overline{X}_*(t)$ and $\varnothing^2_*(t)$ can be made, plotted, and analyzed over time to see if mean or asymptotic effects can be identified, quantified, and compared with theoretical predictions.

If the simulated small scale velocities correspond to a spatially constant mean velocity $\overline{V}$, then the time derivative of the measured displacement $\overline{X}_*(t)$ can be used to compute an apparent plume velocity $\overline{V}_*(t)$ using (85b). The magnitude and direction of $\overline{V}_*$ may initially vary in time until the plume is spread out sufficiently to sample all velocities; $\overline{V}_*$ would ultimately be expected to approach $\overline{V}$. Similarly, repeated measurements of components of $\varnothing^2_*(t)$ can be used to compute an experimental value of $\mathbb{A}_*(t)$ using (85a). In this case, it would be most appropriate to use a measured velocity magnitude $\overline{V}_*(t) = \left| \overline{V}_*(t) \right|$ and not an overall field average (even though $\overline{V}_* \longrightarrow \overline{V}$ in time). The primary axis and components of $\mathbb{A}_*(t)$ can be computed as time varying quantities and can be analyzed for asymptotic behavior in the form of macrodispersivity components. These can then be compared with theoretically derived values [e.g., *Gelhar and Axness*, 1983, *Dagan*, 1984] corresponding to this problem.

When $\overline{V}$ in (85a) is interpreted as $\overline{V}_* = \left| d\overline{X}_*/dt \right|$, then (85a) can be rewritten in the form [*Gelhar and Collins*, 1971]

$$\frac{d\varnothing^2_*}{ds} \approx 2[\mathbb{A}_*(t) + \mathbb{E}_{local}/\overline{V}_*] \qquad\qquad (86)$$

where the incremental path length $ds \equiv \left| d\overline{X}_* \right|$. This suggests an alternative way to measure the components and primary directions of spreading variance and dispersivity tensor, i.e., in a curvilinear

coordinate system aligned with the measured, traced-out path of the plume.

In the context of this problem, comparison of the measured dispersivity tensor or velocity using (85) or (86) with their theoretical counterparts can only be made in an asymptotic sense, after a sufficient amount of local particle mixing has taken place. Since the mean, theoretical results are *ensemble* averages, they can only be compared, in a strict sense, with ensemble measurements, made over many realizations of an experiment. Early measurements of apparent dispersivities or velocities based upon (85) or (86) would be essentially different for repeated realizations of the same problem with the same sort of variability structure and cannot be individually compared with the theoretical values. However, after some amount of travel time in a heterogeneous (yet stationary) medium, measurements from different replicate problems would become similar; results from one experiment could then be safely used in comparisons. The spreading of the solute mass would then have taken place over regions whose dimensions are representative of the larger scale in this investigation. One would expect that the measured dispersivities eventually reach the predicted asymptotic values.

Other comparisons between the local transport simulations and their mean characteristics could be made and are mentioned here for completeness. They include: (1) investigating the effects of *locally* variable dispersion coefficients on the observed macrodispersion coefficients; (2) examining what sort of influence the underlying parameter correlation structure has on the mean simulation results; or (3) developing methods to estimate a mean concentration field from the simulations such that corresponding perturbation fields can be studied and compared in the spectral domain with the results of *Gelhar and Axness*, [1983], *Mantoglou and Gelhar*, [1987a,b,c], and *Vomvoris*, [1986].

5.7 Summary of Approximations. For completeness, the primary approximations built into the model and discussed above will be reviewed below:

- Conservative Mass Transport: The random walk analogy does not naturally allow for sources and sinks of solute mass to be conveniently included in the step equations. The conservation of probability embedded within the Fokker Planck equation translates directly into a necessary conservation of solute mass. Sources or sinks of mass can be included via post-processing algorithms, which is essentially equivalent in concept to the application of nonzero flux or Dirichlet boundary conditions on the surface of a closed computational region Ω_c, itself a subset of a larger region Ω over which the equations were developed and the mass M is constant. [§4.6 and §5.4]

- Number of Particles: The random walk equations were based on the independent motions of one particle. The simulation of many particles at once is equivalent to an ensemble of single simulations. By representing a given amount of solute mass M by a distributed number of N particles,

the spread of mass at a later time can be simulated. The larger N is, the more representative the actual distribution is and the less noisy resulting concentration estimates will be. [§ 4.2, §5.3, and §5.5]

- **Evaluation of Continuum Forces**: By these, quantities such as moisture contents and velocities are meant. These are typically required anywhere a particle exists. Because of the discrete nature of the corresponding flow problem, these quantities as well as the gradient correction terms are evaluated as cell constants. [§5.1]

- **Discrete Time Step**: If forcing quantities such as the velocities are spatially variable and available at a continuum of points, the necessity of using a finite time step implies overshoot errors will accumulate. These are minimized, in some part, by reducing the size of the time step. If a particle moves within a cell, however, an overshoot will occur than cannot be corrected because velocities and moisture contents within cells are assumed to be spatially constant. If a particle moves through several cells within one time step, additional errors will occur if the velocities vary between the cells. This can be controlled by minimizing particle overshoot across cell boundaries. [§5.2, §5.3, and §5.4]

6. APPLICATIONS OF THE MODEL

6.1 Scope. In this section, the transport model developed in the previous sections will be applied to several test problems. The first example considers a one-dimensional "saturated" problem and is presented to illustrate the effects of the time step and number of particles on concentration estimates. The second example involves a three-dimensional saturated system with a constant velocity. The results will be presented in terms of moment estimates and will also contrast the effects of different time steps and numbers of particles. The third example will involve a preliminary set of local simulations in a three-dimensional, saturated system characterized by a spatially variable velocity distribution. The problem is designed so that the developing dispersive behavior can be easily analyzed and compared with theoretical predictions of stochastic models.

6.2 Example 1: One-Dimensional Simulations. This is a simple problem designed to implement a saturated form of the model in one dimension. The computational flow domain Ω_c consisted of a one-dimensional array of 300 cubic cells of side length $\Delta X_i = 0.5$ placed along the x_1 axis. A constant uniform velocity of $v_1 = 1.0$ was used in a one-dimensional form of (49) to move N particles initially distributed uniformly in the 10th cell located at $4.5 < X_1 < 5.0$. Each end of this domain was treated as a "free" type boundary, $\partial\Omega_4$. A dispersivity $\alpha_L = 1.0$ was chosen so that the dispersion/diffusion constant D takes on a constant value of 1.0. Five different cases were considered to a maximum time of $T_{max} = 40.0$ with varying time steps and numbers of particles. The specifics of each simulation can be found in Table 2. Normalized concentration distributions at $T_{max} = 40.0$ are plotted in Figure 11 against the one-dimensional analytic solution. The concentrations are simply the number of particles found in each cell divided by the total number N used in the simulation; i.e. $c(X,t)\theta V_s/M$ of (66). In Table 2, the standard normal error ε as introduced in (73) is given, where it has been assumed that the total mass M of all N particles is always 1.0 and the sampling volume V_s is $\Delta X_i^3 = 0.125$.

Examples 1.1 to 1.3 were all run with $N = 2000$ particles and various time step sizes. Clearly, the choce of time step did not seem to affect the results in Figures 11a-c. The essential shape of each curve is the same as well as the degree of random "noise". When 20000 particles are used, however, the noise is reduced as illustrated in Figures 11d,e. The improvement is roughly three-fold as indicated by the smaller standard errors associated withe these runs (Table 2).

Table 2
Simulations for Example 1

- One-Dimensional Domain: $L_1 = 150$
  $L_2 = L_3 = 0.5$
  $\Delta X_i = 0.5$

- Initial Condition: Release N particles in uniformly distributed pulse located in $4.5 < X_1 < 5.0$

- Boundary Condition: The two boundaries at each end of the domain are of the free type, $\partial\Omega_4$

- Velocities: $V_1 = 1.0$
  $V_2 = V_3 = 0.$

- Dispersivities: $\alpha_L = 1.0 \Longrightarrow D_{11} = 1.0$

- Time limits $T_{max} = 40.0$
  Δt varies

Run	N	Δt	C_c	$\dot{\varepsilon}$ (M=1, V_s=0.125)	Figure
1.1	2000	0.5	1.	0.0632	11a
1.2	2000	0.05	0.1	0.0632	11b
1.3	2000	0.005	0.01	0.0632	11c
1.4	20000	0.05	0.1	0.0200	11d
1.5	20000	0.5	1.	0.0200	11e

Analytic solution

$$c\theta V_s/M =$$

$$\frac{1}{2}\{erf \quad \frac{[(x_1-v_1T-\ell_1)]}{\sqrt{2\alpha v_1 T}} - erf \quad \frac{[(x_1-v_1T-\ell_2)]}{\sqrt{2\alpha v_1 T}}\}$$

$v_1 = 1$
$T = 40$
$\ell_1 = 4.5$
$\ell_2 = 5$
$\alpha = 1$
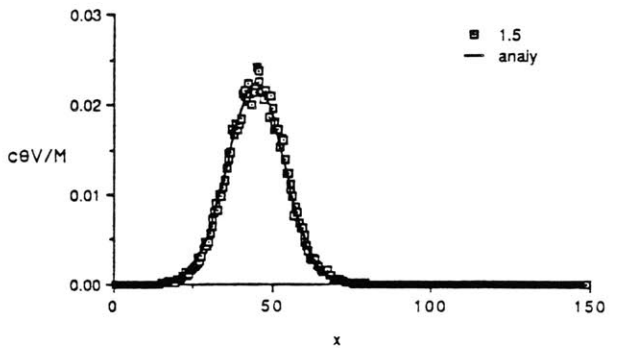
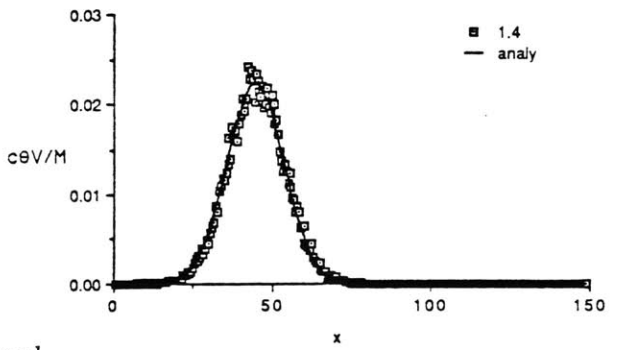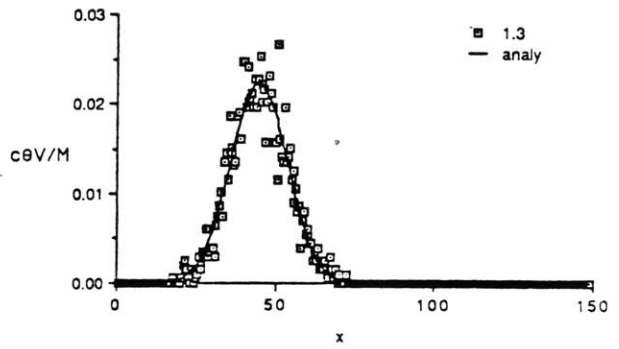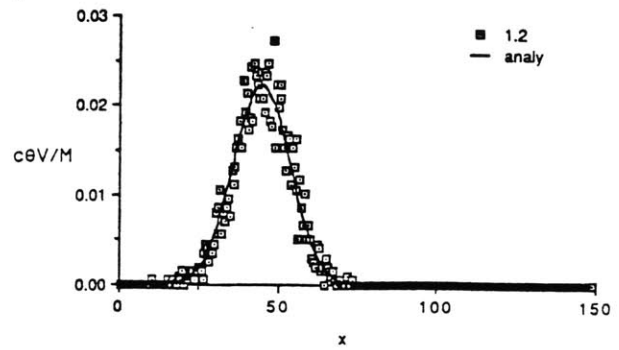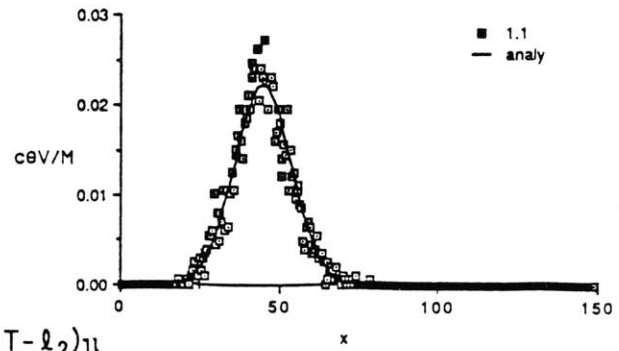Figure 11: Normalized concentration estimates from the one-dimensional runs of example 1

6.3 Example 2: Three-Dimensional Uniform Velocity Simulations. In this example, a three-dimensional, cubic domain composed of a regular grid of 125000 cells was considered (Figure 12). There are 50 cells or 51 nodes along each coordinate direction, and the dimension of each cell in each direction is $\Delta X_i = 0.5$. A constant, uniform velocity field ($V_1 = 1.0$, $V_2 = 0$, $V_3 = 0$) was selected for the entire computational region Ω_c. The dispersivities $\alpha_L = \alpha_T = \alpha = 0.1$ were chosen so that the dispersion tensor could be reduced to a scalar of magnitude $D = 0.1$. For this simple case, the extra gradient terms in the step equations vanish. The appropriate random walk step equation is again given by (49).

As an initial condition, a number of particles were located in the small cubic region consisting of eight cells as shown in Figure 12. All boundaries were considered to be of the fourth or "free" type, $\partial\Omega_4$. The first three simulations used 1000 particles distributed randomly and uniformly in these eight cells (125 each). Each problem was simulated up to a maximum time of $T = 12.5$. It was intended that very few, if any, of the particles would exit the system during this time period; a few may also exit at the start be dispersing upstream through the negative X_1 face of Ω_c. The only difference in each problem was the choice of time step. Three different values ranging from $\Delta t = 0.1$ to $\Delta t = 1.5$ were selected giving a range of cell Courant numbers C_c ranging from 0.1 to 1.5 (§5.2). The second set of three problems was identical to the first group except that 2000 particles were used (250 per cell). A seventh problem involved a choice of 10000 particles (1250 per cell) with $\Delta t = 0.1$. The specifics on all of these examples are summarized in Table 3.

Figure 13 shows the components σ^2_{11*}, σ^2_{22*}, and σ^2_{33*} of the measured second order moment tensor $\mathscr{O}^2_*$ plotted against time for each run. The theoretical behavior is given by equation (79a) and the slope of each experimental line is quite close to the predicted value of $2D = 0.2$. The initial moment distribution at $t = 0$ is easily calculated to be $\mathscr{O}^2(t=0) = {}^1/_{12}\ \mathbb{I}$, so the exact relationship (79a) can be integrated to give

$$\mathscr{O}^2(t) = ({}^1/_{12} + 0.2\,t)\ \mathbb{I} \tag{87}$$

Figures 14a and 14c show a vertical projection of the particles onto the X_1-X_2 plane at $T_{max} = 12.5$ for runs 2.3 and 2.7. Figures 14b and 14d show contours of vertically averaged particle counts normalized by the total number N of particles for runs 2.3 and 2.7. These can be considered as normalized concentrations as in example 1. Notice how noisy the concentration contours for run 2.3 (1000 particles, Figure 14b) are in comparison with those of run 2.7 (10000 particles, Figure 14d). This can be quantified by contrasting the standard normal errors (73) for each case. This error is reduced by greater than a factor of three in going from run 2.3 to 2.7. Although the noise in the concentration contours is significantly affected by the number of particles used, the second moment estimates (Figure

13) do not seem to be as strongly affected. Moment analyses apparently provide a more robust measure of the solute distribution, less susceptible to the effects of small particle counts.

Table 3
Simulations for Example 2

- Three-Dimensional Domain: $\quad L_i = 50$
  $\Delta X_i = 0.5$

- Initial Condition: Release N particles from a uniformly distributed pulse located in a cubic group of 8 cells as shown in Figure 12.

- Boundary Condition: All boundaries of the domain are of the free type, $\partial \Omega_4$

- Velocities: $\mathbf{v} = 1.0\mathbf{i}$

- Dispersivities: $\alpha_L = 0.1$
  $\alpha_T = 0.1 \implies \mathbb{D} = 0.1\,\mathbb{I}$

- Time limits $\quad T_{max} = 12.5$
  Δt varies

Run	N	Δt	C_c	Figures
2.1	1000	1.5	1.5	13a
2.2	1000	1.0	1.0	13b
2.3	1000	0.1	0.1	13c, 14a,b
2.4	2000	1.5	1.5	13d
2.5	2000	1.0	1.0	13e
2.6	2000	0.5	0.1	13f
2.7	10000	0.1	0.1	13g, 14c,d
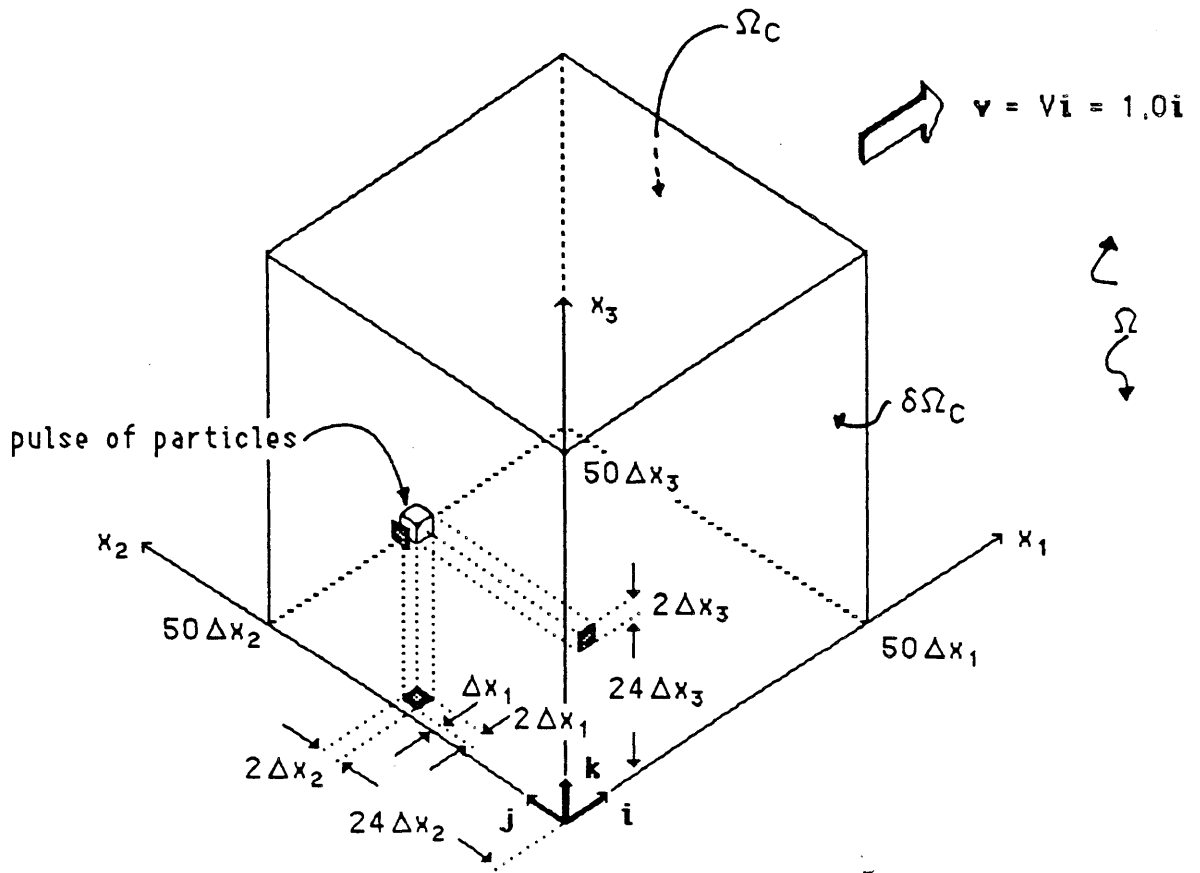
Figure 12: Flow domain for example 2. Initial condition involves N particles released from a $2 \Delta x_1$ by $2 \Delta x_2$ by $2 \Delta x_3$ ($\Delta x_i = 1.0$) region of 8 cells as indicated (table 3)
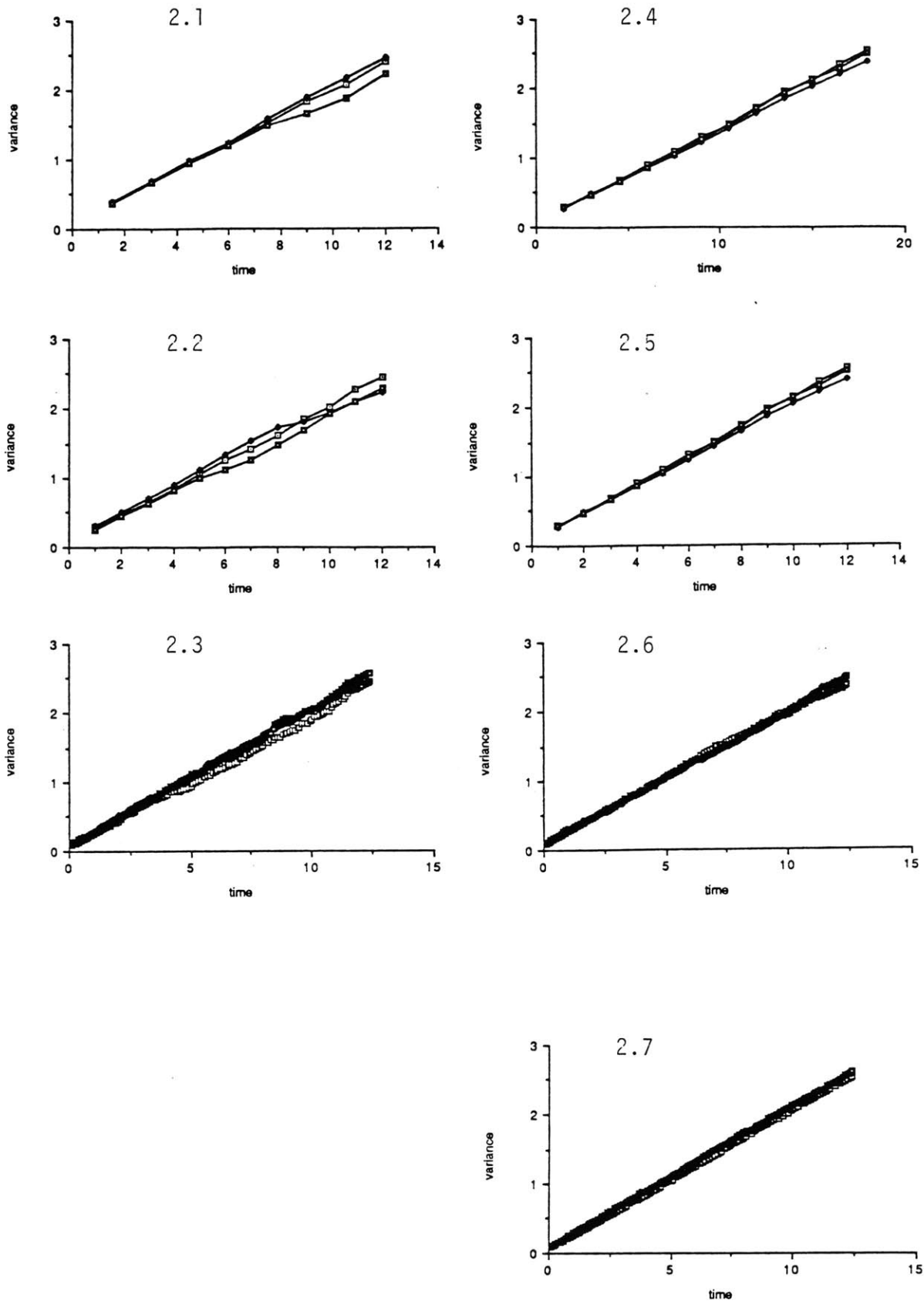
Figure 13: Second moment estimates in the x_1, x_2, and x_3 directions from example 2 (table 3)

Figure 14: (a) vertical projection of particle locations on the x_1 - x_2 plane from run 2.3; (b) Contours of vertically averaged particle counts (normalized concentrations) on this plane

particle tracking, integrated, 2-D contours
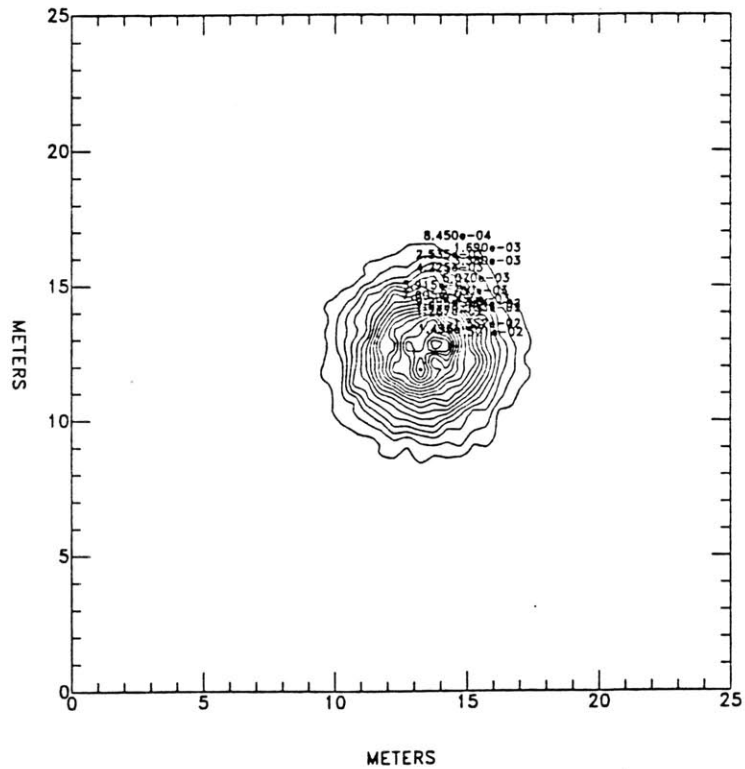
Figure 14:   (c) vertical projection of particle locations on the x_1 - x_2 plane from run 2.7; (d) Contours of vertically averaged particle counts (normalized concentrations) on this plane.

6.4 Example 3: Three-Dimensional Variable Velocity Simulations . These simulations use the same cubic domain as used in Example 2. Spatially variable flow systems corresponding to synthetic heterogeneous conductivity fields were used to move the solute mass under saturated conditions. The spatial distribution of conductivities was generated as a realization of a stationary random field as described in §3.1. This representation of our model heterogeneous system is characterized by the mean, F, of the log-conductivity function $\ell n K_s$ and the associated spatial correlation structure of the perturbation, $f(X)$. Two flow examples have been considered that involve an isotropic, exponential decay correlation model for the fluctuation $f(X)$, with aspecified correlation scale, λ, variance, σ^2_f, and mean conductivity $e^F \equiv K_G$. Within each flow field, several transport simulations were carried out with different values of local dispersivities. The simulated spreading of particle mass is compared with the generic theoretical macrodispersivity results as discussed in §5.6. We emphasize here that these initial simulations and their subsequent analysis should be considered as preliminary in nature.
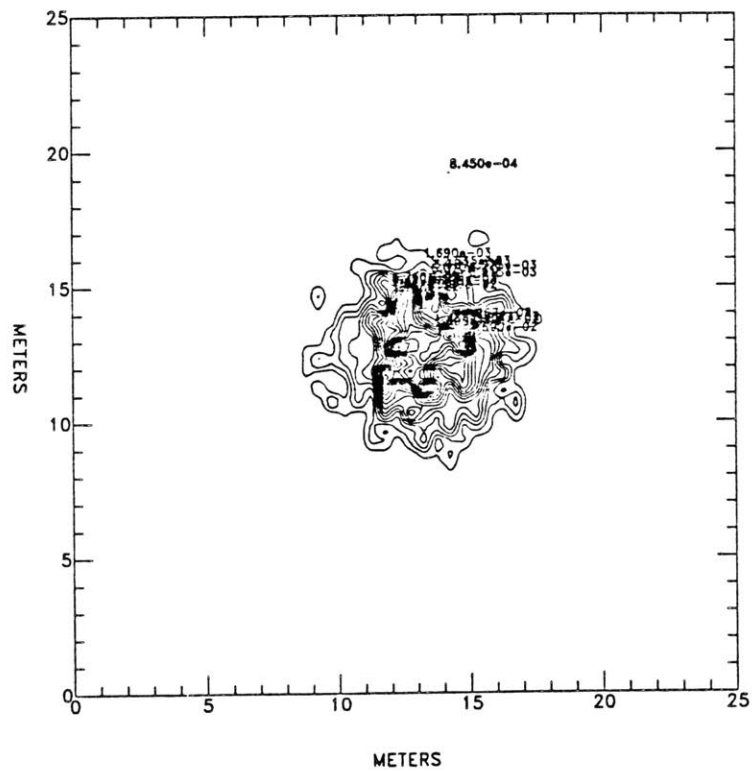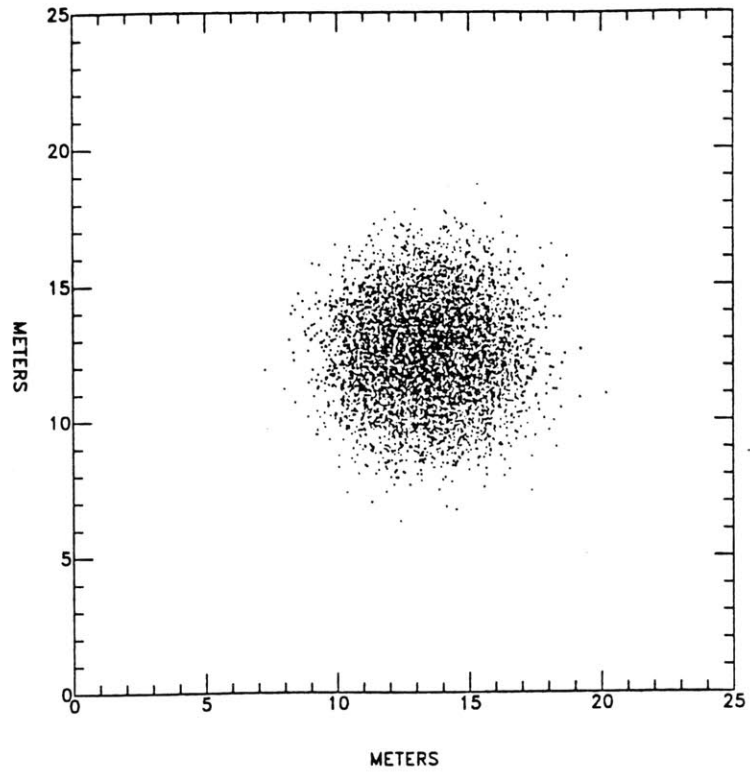
6.3.1 Flow Domain and Boundary Conditions. Each of the problems was developed from a synthetic, spatially variable $\ell n K_s$ field on a grid of 51 × 51 × 51 points (§3.1). In both problems, the spatial discretization ΔX_i was chosen to be 0.5 in all directions, while the isotropic correlation scale λ was set to 1.0 = $2\Delta X_i$. Hence, the computational region Ω_c has a length L_i = 25.0 = 25λ in any direction (Figure 15) and a total of 125000 cells. A total 25 correlelion lengths will fit along length of the domain in any direction. The geometric mean of the conductivity fields $e^F \equiv K_G$ has been set to 1.0 for both problems. The only difference between the flow fields is the degree of heterogeneity of the conductivity distributions as described by the standard deviation, σ_f:

- <u>Flow Problem 1</u>: $\sigma_f = 2.3$ $\lambda = 1.0$ $K_G = 1.0$

- <u>Flow Problem 2</u>: $\sigma_f = 1.0$ $\lambda = 1.0$ $K_G = 1.0$

Note that the two random conductivity fields used were not generated independently. The first field was created as a scalar multiple of the second (i.e., $f_1(X) = 2.3 f_2(X)$). More thorough investigations would use independent conductivity distributions generated with different random "seeds".

In both flow problems, a steady saturated flow is developed (§2.4, §3.2) from specification of an 0.1 drop in the mean head $\overline{h}$ between the the two side faces (1 and 3) intersecting the X_1 axis, as shown in Figure 15. The local head on these faces is maintained at ± 0.05 which corresponds to a mean gradient $J_1 \equiv \partial(h+z)/\partial X_1 = -0.004$. This results in a mean flow in the positive X_1 direction. All other boundaries are treated as no-flow boundaries. Some characteristics of both

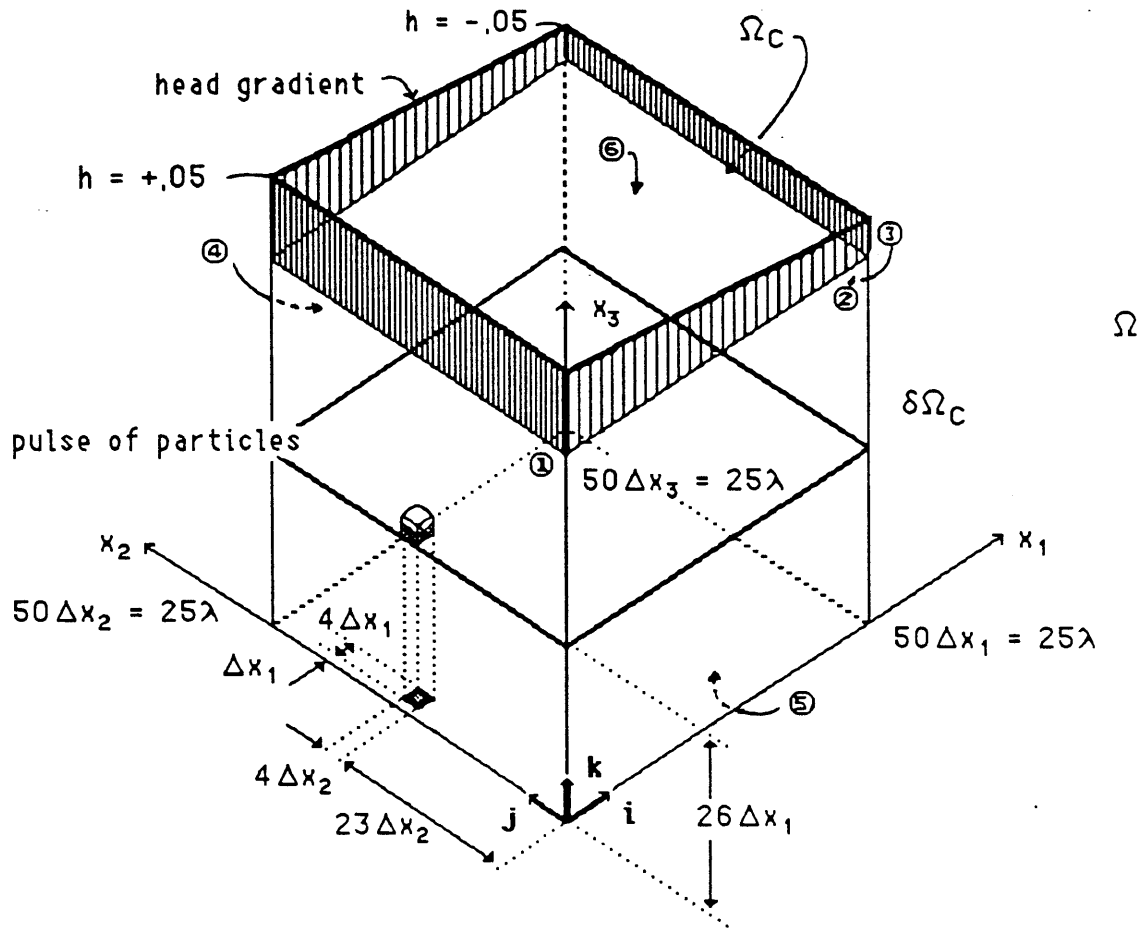Figure 15: Cubic domain Ω_C for example 3 where $\Delta x_i = 0.5$ and $\lambda = 1.0$. Initial pulse location is shown. Circled numbers indicate face number of Ω_C. Dashed $x_1 - x_2$ plane at $x_3 = 26\Delta x_3$ indicates where results in figure 16 are taken from. A mean head difference $\overline{\Delta h} = 0.1$ is maintained between faces 1 and 3 to develop a steady flow solution. Other faces are no-flow boundaries.

velocity fields are given in Table 4. Velocities are derived from the flux components $q_i(X) =$ $\theta_0 v_i(X)$ where the porosity θ_0 has been assigned a constant value of 0.30. For flow problem 1, contours of the head values on an x_1-x_2 plane located at $x_3 = 26\Delta X_3$ (Figure 15) are superimposed on contour maps of the conductivity distribution in Figure 16a.

Table 4
Computed MeanVelocitiy Components, Example 3

	Flow problem 1: $\sigma_f = 2.3$	Flow problem 1: $\sigma_f = 1.0$
$\overline{v_1}$ †	0.0523	0.0174
$\overline{v_2}$	0.0080	0.00080
$\overline{v_3}$	0.00056	-0.000095
$v_{1,max}$	10.73	0.214
$v_{2,max}$	3.90	0.0839
$v_{3,max}$	5.30	0.0699
$v_{1,min}$	-0.96	
$v_{2,min}$	-1.56	
$v_{2,min}$	-1.76	

† $\overline{\overline{v_i}}$ are arithmetic averages of all computed velocity components within Ω_c.

6.4.2 Transport Problems and Auxiliary Conditions. Eight distinct transport problems were run, four in the first flow field ($\sigma_f = 2.3$), and four in the second ($\sigma_f = 1.0$). All problems involved an initial distribution of 8000 particles within a 4×4×4 cube of 64 cells centered near face 1 of Ω_c (Figure 15). The center of this cube is located at (1.5, 12.5, 12.5) = ($3\Delta X_1$, $25\Delta X_2$, $25\Delta X_3$). The particles in each problem were displaced in time according to (52) to simulate development of a solute cloud in the heterogeneous velocity field. Each boundary was treated as a "free" type ($\partial\Omega_4$) so that particles could freely cross any external boundary face of the domain. When this occurred, they were removed from consideration and the total mass in the domain was reduced accordingly. Generally, particles exited the domain for one of two reasons:

- <u>Upstream dispersion near t = 0</u>: Because the initial solute distribution was so near face 1 (Figure 15), a small amount of mass may disperse upstream out of the computational domain Ω_c according to the assumed local Fickian dispersion mechanism. Because these particles are removed, they cannot reenter the flow domain as might be expected. Also, because of the extreme heterogeneity of the medium, it is possible that local velocities in the negative x_1 direction could also arise (table

4) and enhance early particle loss through the upstream face. In most cases, however, the initial loss of mass (if any) will occur for small periods of time near $t = 0$. Afterwards, the mass in the domain remains constant for longer periods of time, allowing measurements of a constant mass distribution to be made.

• Outflow at downstream boundaries: As the particle plume moves through the domain, it will widen and disperse. Because the mean flow direction is in the positive x_1 direction, most particles will eventually exit through the positive x_1 face (face 3, Figure 15). If the plume is wide enough, some particles may exit through the sides of the domain (faces 2,4,5, and 6, Figure 15) via the dispersion mechanism, even though these faces are treated as no-flow boundaries. When either process begins to occur, the total mass in the domain Ω_c will decrease with time. In this case, statistical measurements of the particle distribution inside the domain Ω_c will no longer reflect the same amount mass over time, and cannot be used in measuring statistical characteristics of the overall plume (§5.6). Breakthrough curves, on the other hand, can be constructed and used to illustrated the solute distribution.

In order to minimize overshoot errors (§5.2), the computational time step Δt in these problems was selected to meet the Courant number condition $C_c = V\Delta t / \Delta X < 1$ so as. Based upon the magnitude of the largest positive velocity component in each flow domain (Table 4), the following values were used in the simulations:

• Flow Problem 1, $\sigma_f = 2.3$: $\Delta t = 0.10$

• Flow Problem 2, $\sigma_f = 1.0$: $\Delta t = 1.0$

Most simulations were run for a long enough period of time such that a relatively complete breakthrough curve through the downstream boundary could be constructed.

The four problems considered in each flow differed only in the choice of the local dispersivities α_L and α_T. In each flow domain, one problem used $\alpha_L = \alpha_T = 0$, while the remaining three used $\alpha_L / \alpha_T = 10$, with $\alpha_L = 0.005$, 0.05, and 0.5. All problem characteristics are summarized in Table 5. In Figure 16b, the projected $x_1 - x_2$ positions of the 8000 particles used in run 3.2 illustrates the method and the extreme heterogeneity of the first flow field.

Contours:

-4	$log_{10}K(\mathbf{x}) = -2$	
-3	$log_{10}K(\mathbf{x}) = -1.5$	
-2	$log_{10}K(\mathbf{x}) = -1$	
-1	$log_{10}K(\mathbf{x}) = -0.5$	
0	$log_{10}K(\mathbf{x}) = 0$	
1	$log_{10}K(\mathbf{x}) = 0.5$	
2	$log_{10}K(\mathbf{x}) = 1$	
3	$log_{10}K(\mathbf{x}) = 1.5$	
4	$log_{10}K(\mathbf{x}) = 2$	
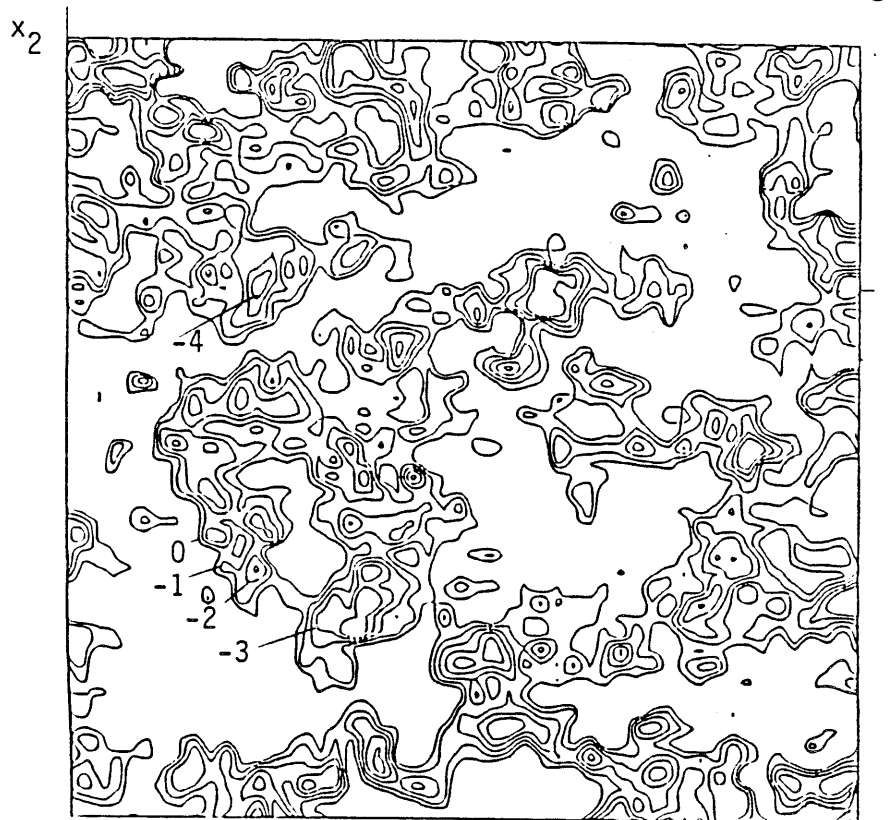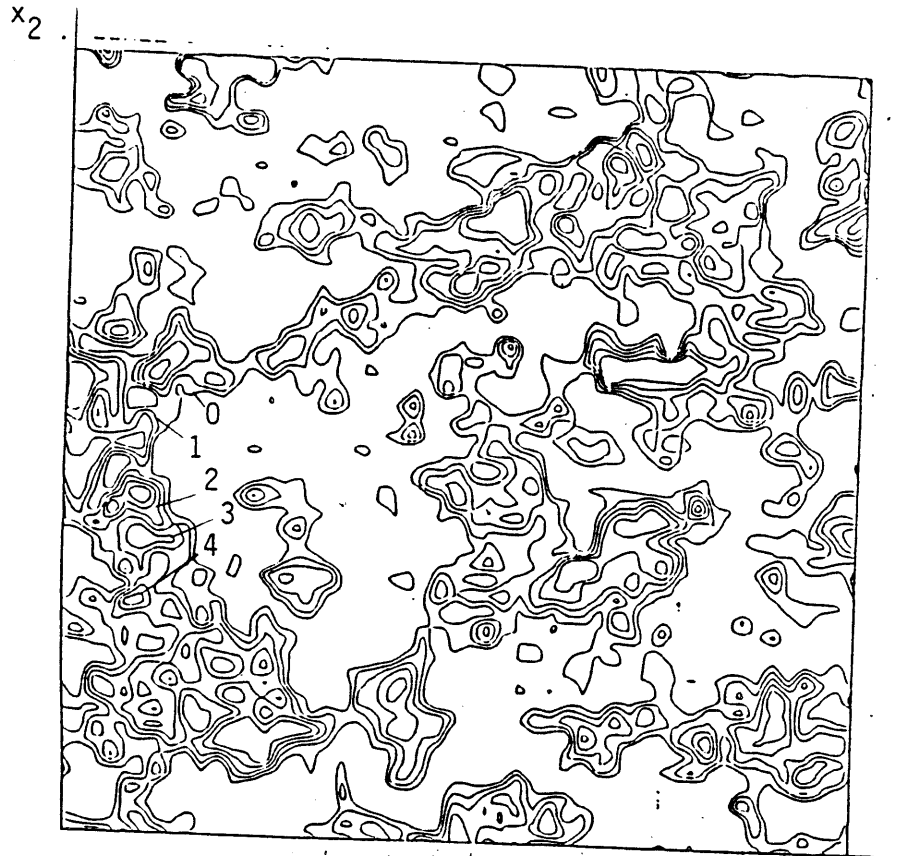
Figure 16a: Low and high $\ln K_s(\mathbf{x})$ contours and head contours for flow problem 1 as outlined in table 4. These values correspond to the $x_1 - x_2$ plane located at $x_3 = 26\Delta x_3$ in figure 15.
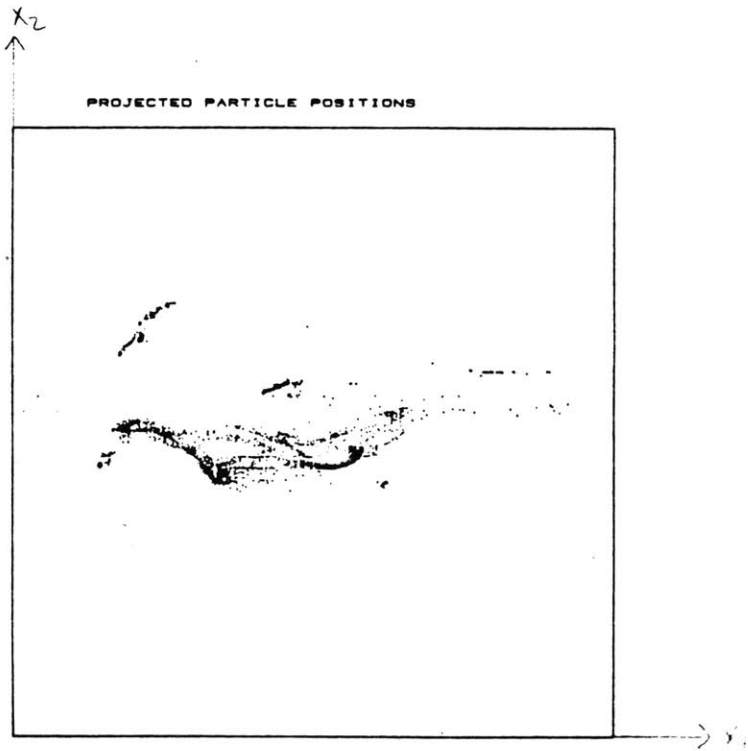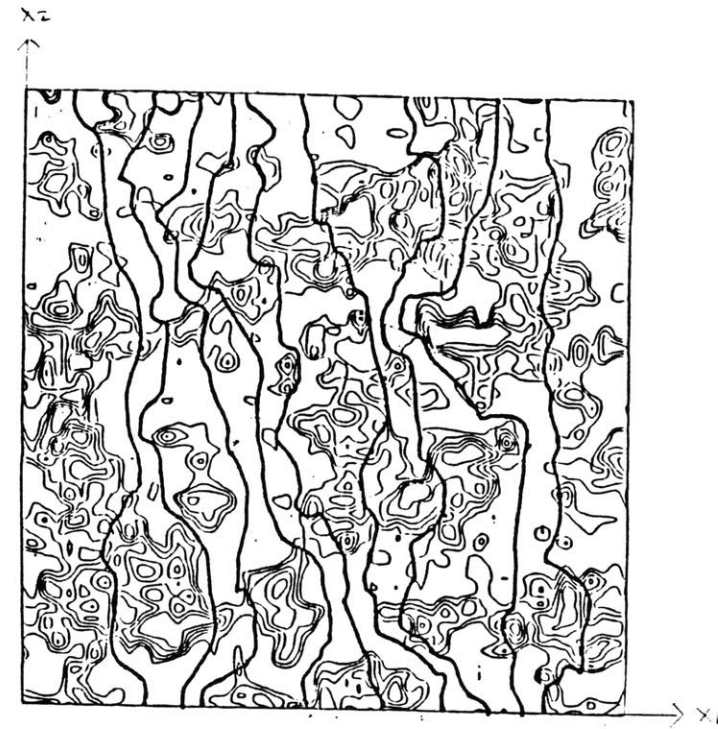
Figure 16b: Superposition of the head and high conductivity fields at $x_3 = 26 \Delta x_3$ from flow field 1, Table 4, along with projected particle positions in the $x_1 - x_2$ plane from run 3.2 at T = 250.

Table 5
Simulations for Example 3

- Three-Dimensional Domain: $L_i = 50$
  $\Delta X_i = 0.5$

- Initial Condition: Release 8000 particles from a uniformly distributed pulse located in a cubic group of 64 cells as shown in Figure 15.

- Boundary Condition: All boundaries of the domain are of the free type, $\partial \Omega_4$

- Conductivities: As derived from a realization of an isotropic, exponentially correlated random field; e.g.,

$$\ell n K_s(X) = F + f(X)$$

where $\lambda_i = 1.$, $F = 0.$, and variance of $f(X) \equiv \sigma^2_f$

     flow problem 1: $\sigma_f = 2.3$
     flow problem 2: $\sigma_f = 1.0$

- Velocities: As derived from an applied head gradient $J = -0.004i$ (Figure 15) across each conductivity field with $\theta_0 = 0.30$.

- Dispersivities α_L, α_T vary (see below)

- Time limits T_{max} (see Table 6)
  Δt varies (see below)

Run	σ_f	α_L	α_T	Δt	Figures
3.1	2.3	0.	0.	0.10	16a; 17, row 1
3.2	2.3	0.005	0.0005	0.10	16a,b; 17, row 2
3.3	2.3	0.05	0.005	0.10	16a; 17, row 3
3.4	2.3	0.5	0.05	0.10	16a; 17, row 4
3.5	1.0	0.	0.	1.0	18, row 1
3.6	1.0	0.005	0.0005	1.0	18, row 2
3.7	1.0	0.05	0.005	1.0	18, row 3
3.8	1.0	0.5	0.05	1.0	18, row 4

6.4.3 Statistical Computations. For each problem, the following statistics of the mass distribution were computed (§5.6) at a time increment ΔT, where $\Delta T = 10$ for flow field 1 and $\Delta T = 5$ for flow field 2:

- <u>Center of mass in the x_i coordinate direction</u>: $\overline{X}_*(t)$

- <u>Spreading variance about center of mass</u>: $\mathcal{O}^2_*(t)$

- <u>Mass exiting face i of the flow domain between t and $t - \Delta T$</u>: $m_i(t)$

The center of mass data can be used to compute the trajectory of the plume. The average velocity of the plume can be computed by estimating time derivatives of $\overline{X}_*(t)$. The variance data can be used to calculate the rate of spreading of the plume about its center of mass (§5.6). Breakthrough data (especially $m_2(t)$) can be used, alternatively, to reflect the mixing in the plume. The first and second moments will be useful only if the mass within the domain remains constant during the time period considered. This will occur for $t_1 < t < t_2$, where t_1 is the time when upstream mass loss ceases and t_2 is the time when the first particle leaves a downstream boundary (§6.4.2). The particular values for t_1 and t_2 in each problem are listed in Table 6.

Table 6
Estimated Plume Velocities, Example 3

Run	$d\overline{X}_1*/dt$	t_1	t_2	$\overline{V}_1$ (Table 4)
3.1	0.00930	0.	290.	0.0523
3.2	0.0100	10.	270.	0.0523
3.3	0.0206	10.	150.	0.0523
3.4	†	70.	80.	0.0523
3.5	0.0128	0.	780.	0.0174
3.6	0.0125	0.	640.	0.0174
3.7	0.0131	15.	575.	0.0174
3.8	0.0143	320.	450.	0.0174

t_1 = time when upstream mass loss ceases
t_2 = time when first particle exits any downstream boundary
† $t_2 - t_1$ = the period when mass within Ω_c remains constant and statistical measurements can be made (not possible in run 3.4)

6.4.4 Plume Trajectory and Longitudinal Macrodispersivities A_{11}. The computed values of the mean displacement $\overline{X}_*(t)$ and spreading variance $\mathscr{O}^2_*(t)$ can be used to estimate a mean velocity $\overline{V}_*(t)$ and dispersivity tensor $\mathbb{A}_*(t)$ of the plume using (85) and (86). In turn, these quantities can be compared with theoretically derived counterparts [e.g., *Gelhar and Axness*, 1983; *Gelhar*, 1987] . Because this problem involves only one simulation on a large domain, comparisons between numerical measurements and (ensemble) theory cannot be made at early times (§5.6). Instead, theoretically derived asymptotic values will be compared with perceived asymptotic behavior in the model results. For the isotropic, exponentially correlated conductivity fields are used in these simulations, the following limiting behavior is predicted from the asymptotic theory of *Gelhar and Axness* [1983]:

- $d\overline{X}/dt \longrightarrow \overline{V}$ as $t \longrightarrow \infty$

- $\mathbb{A}(t) \longrightarrow \mathbb{A}(\infty)$ as $t \longrightarrow \infty$

In addition, the primary axis of $\mathbb{A}(\infty)$ is predicted to be parallel with that of $\mathbb{E}_{local}$, or, in other words, colinear with with $\overline{V}$. Hence, $\mathscr{O}^2$ should take on an asymptotic value and also have a primary axis colinear with $\overline{V}$.

For the example problems, measured components of $\overline{X}_*$ are plotted against t in the first column in of Figures 17 and 18, where t is always less that t_2. Run 3.4 has been been omitted because there was only a very small time period $t_2 - t_1$ in which the mass in Ω_c remained fixed. It appears in all cases that the center of mass comes to move in a direction parallel to the x_1 axis after an initial small negative x_3 displacement. In runs 3.5 to 3.8 there appears to be a slight continual negative x_3 component to this motion. In most cases, it seems that the speed of the center of mass has achieved an approximate asymptotic value (Table 6, Figures 17, 18). The average measured plume velocities $d\overline{X}_*/dt \equiv \overline{V}_* \approx \overline{V}_*i$ in the second flow field ($\sigma_f = 1$) match the field average $\overline{V}$ (Table 4) much more closely than do those of the more-heterogeneous flow field ($\sigma_f = 2.3$) in the first problem. The size of the domain may be, in fact, too small in the first problem to allow for the plume to develop sufficiently to reflect the overall average field velocity.

Because $\overline{V}_*$ always appears to be parallel (in the developmental limit) to the x_1 axis, we will simplify our macrodispersivity calculations by assuming *a-priori* that $\mathscr{O}^2$, $\mathbb{A}$, and $\mathbb{E}_{local}$ achieve asymptotic limits that are diagonal in form (in this coordinate system). In other words, we assume their primary axes come to be aligned with x_1 so that estimates of the longitudinal macrodispersivity $A_{11}*(\infty)$ need only be based on measurements of $\sigma^2_{11}*(t)$ and $\overline{X}_1*(t)$ through simplified forms of (85a) or (86):
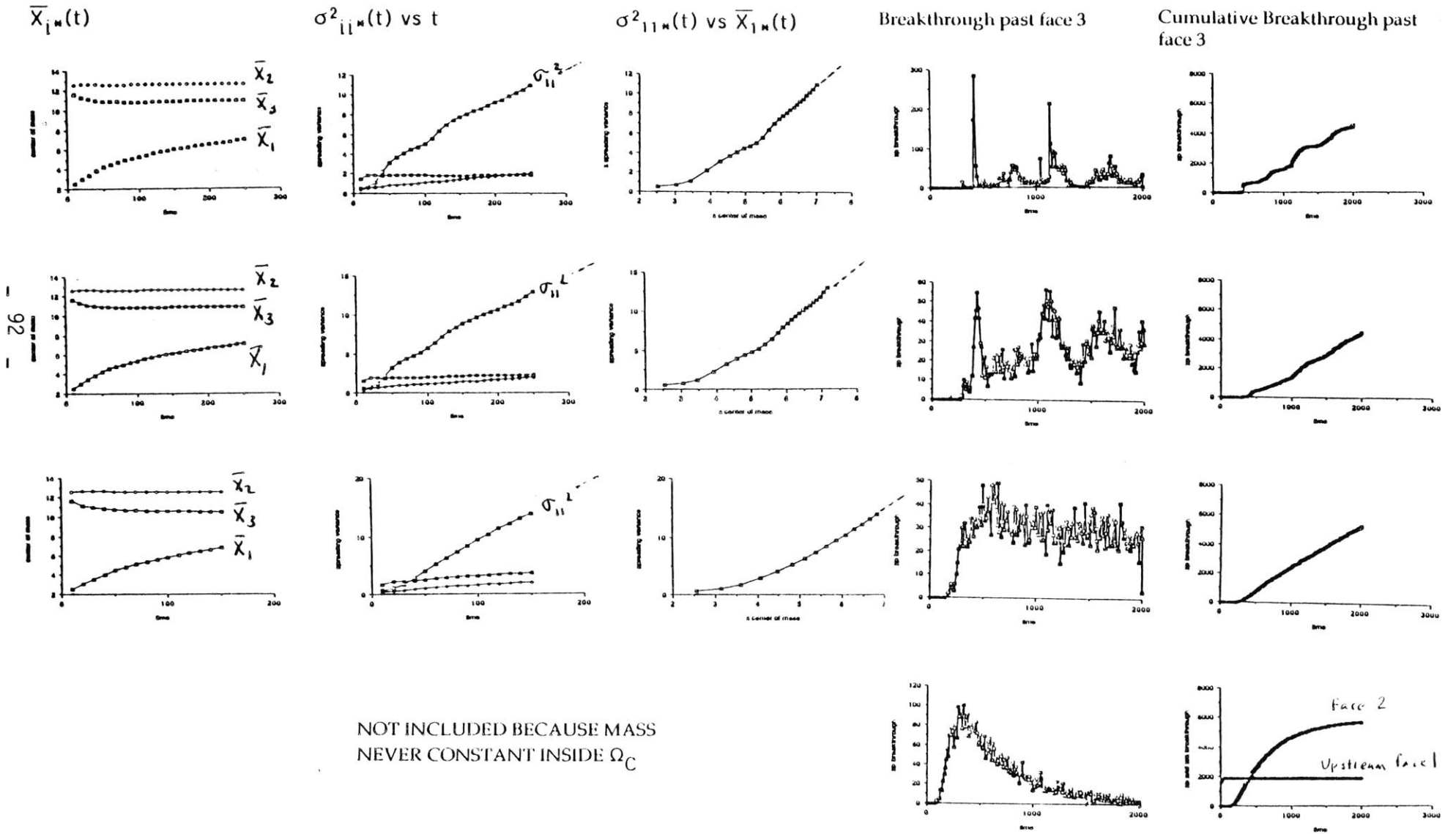
$$\frac{d\sigma^2_{11}*}{dt} = 2 \; \frac{d\overline{X}_1}{dt}*(A_{11}* + \alpha_L) \tag{88a}$$

$$\frac{d\sigma^2_{11*}}{dX_{1*}} = 2(A_{11*} + \alpha_L) \tag{88b}$$

Notice in (88a) that the measured plume velocity $\overline{V}_* = d\overline{X}_{1*}/dt$ is used in place of the overall field velocities as listed in Table 4. Plots of $\sigma^2_{11*}(t)$, $\sigma^2_{22*}(t)$, and $\sigma^2_{33*}(t)$ for $t < t_2$ are shown for all problems in column 2 of Figures 17 and 18, while plots of $\sigma^2_{11*}(\overline{X}_{1*}(t))$ for $t < t_2$ are shown in column 3 of the same Figures. Data for run 3.4 were neglected again because there was very little time in which the mass remained constant within the flow domain. In all cases, the σ^2_{11*} curves appear to take on constant asymptotic slopes, $d\sigma^2_{11*}/dt$ and $d\sigma^2_{11*}/d\overline{X}_{1*}$. Calculations of the longitudinal macrodispersivity $A_{11*}(\infty)$ were made using both (88a) and (88b) and approximate measurements of the constant slopes. These values are summarized in Table 7.

The data for σ^2_{22*} and σ^2_{33*} in column 2 of Figures 17 and 18 could also be analyzed to obtain estimates of $A_{22}(\infty)$ and $A_{33}(\infty)$ using relationships similar to (88a). However, because the slopes are so much smaller, it was thought that measurement errors may lead to large relative errors in their estimation. In addition, slight irregularities in the σ^2_{11*} curves were observed in runs 3.5 - 3.8. These seem to be associated with decreasing σ^2_{22*} and σ^2_{33*} values as well as the slight negative X_3 drift in the center of mass estimate $\overline{X}_*$. It is thought that these perturbations are all manifestations of a slight shift of the principal direction of $\mathcal{O}^2_*(t)$ away from the X_1 axis. This "shift" is not believed to be a permanent asymptotic result, but rather a remnant of the development process. Only inspection of the cross components of $\mathcal{O}^2_*(t)$ as well as analysis of experiments carried out in larger domains can clarify the issue. For this investigation, it will be assumed that the shift is small and that the representative slopes in Figures 18 and 19 can lead to approximate values of $A_{11*}(\infty)$.

Figure 17:   FLOW PROBLEM 1 $\sigma_f = 2.3$

Rows 1 to 4 correspond to Runs 3.1 to 3.4, respectively

$\overline{X}_{i\ast}(t)$ $\sigma^2_{ii\ast}(t)$ vs t $\sigma^2_{11\ast}(t)$ vs $\overline{X}_{1\ast}(t)$ Breakthrough past face 3   Cumulative Breakthrough past face 3

NOT INCLUDED BECAUSE MASS
NEVER CONSTANT INSIDE Ω_C

Figure 18:   FLOW PROBLEM 2 $\sigma_f = 1.0$

Rows 1 to 4 correspond to Runs 3.5 to 3.8, respectively

$\overline{X}_{i*}(t)$

$\sigma^2_{ii*}(t)$ vs t

$\sigma^2_{11*}(t)$ vs $\overline{X}_{1*}(t)$

Breakthrough past face 3

Cumulative Breakthrough past face 3

$\sigma^2_f \lambda$ $(\gamma^2 = 1)$
e.g., Neuman, et al. [1987]

Simulations

$\sigma^2_f \lambda / \gamma^2$ $(\gamma = \exp(\sigma^2_f/6))$
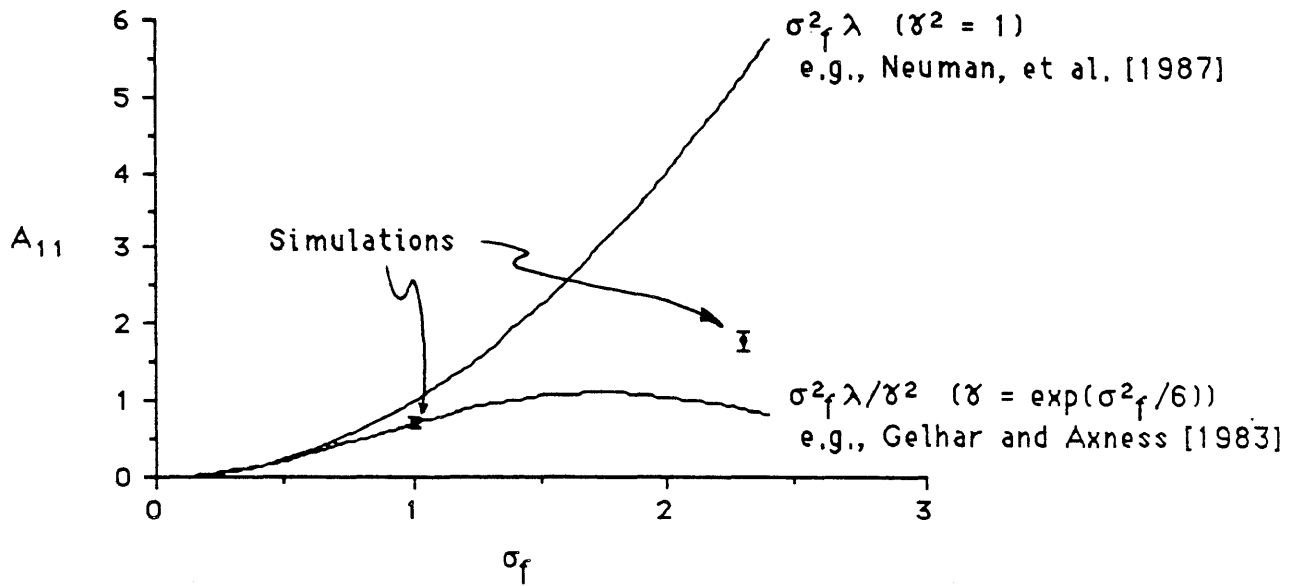e.g., Gelhar and Axness [1983]

A_{11}

σ_f
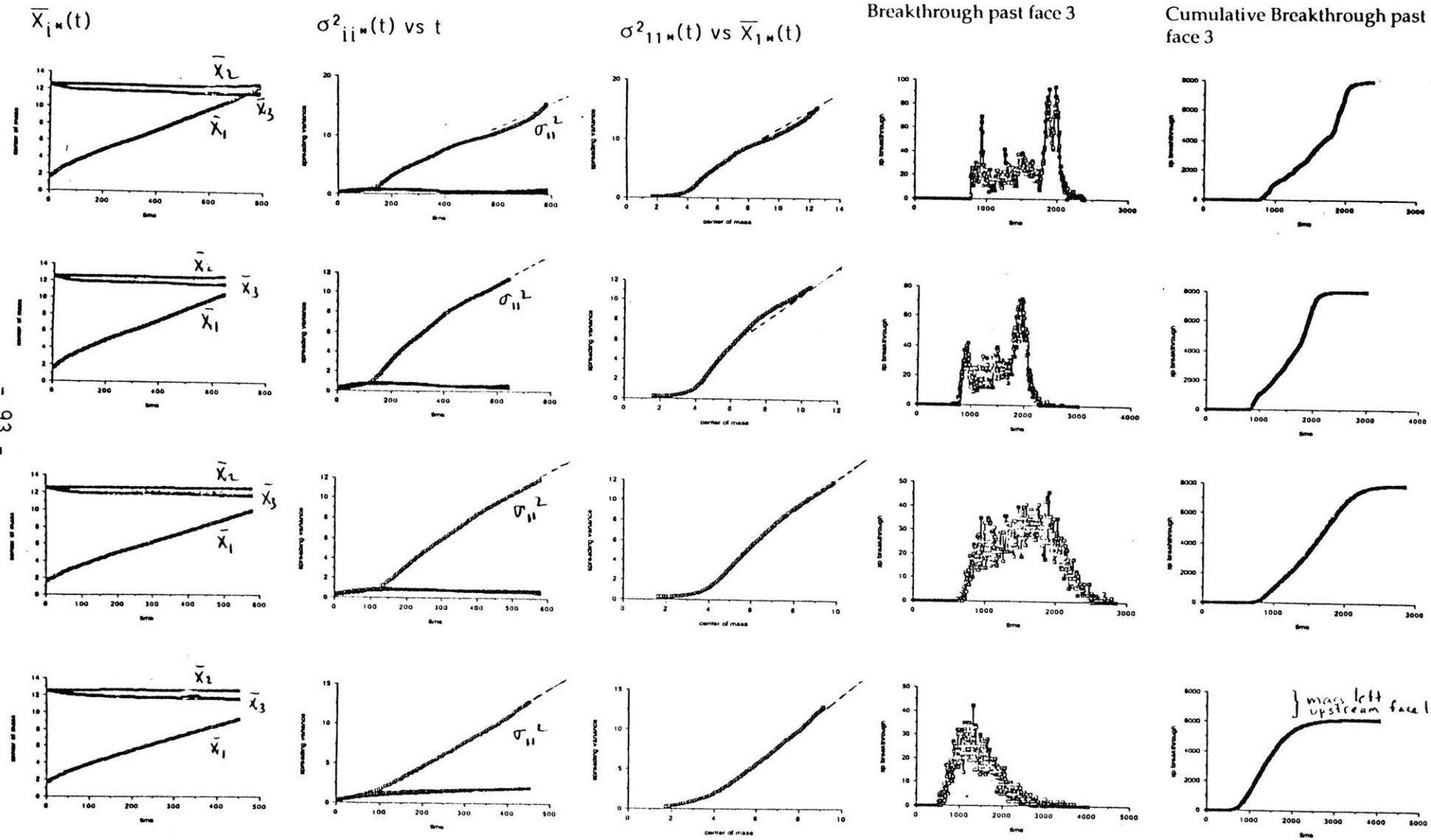
Figure 19: Summary of macrodispersivity results, $A_{11}(\infty)$. Estimates of $A_{11*}(\infty)$ based on example 3 are located within distribution bars at $\sigma_f = 1$ and 2.3. Two theoretical curves for $A_{11}(\infty;\sigma_f)$ are also shown.

6.4.5 Comparisons with Theory. The measured macrodispersivities can be compared with some theoretical results. For a steady saturated flow system in a heterogeneous domain characterized by an isotropic, exponentially correlated $\ell n K_s$ distribution, *Gelhar and Axness*, [1983] predict the following constant, asymptotic components of $\mathbb{A}$:

$$A_{11}(\infty) \;=\; \sigma^2_f \lambda / \gamma^2 \tag{89a}$$

$$A_{22}(\infty) \;=\; A_{33} \;=\; \sigma^2_f \alpha_L (1 + 4\alpha_T/\alpha_L)/15\gamma^2 \tag{89b}$$

$$A_{ij}(\infty) \;=\; 0, \quad i \neq j \tag{89c}$$

where $\gamma \approx \exp(\sigma^2_f/6)$. It is important to realize that these results were developed for systems with small variances ($\sigma^2_f < 1$) and small dispersivities (α_L, $\alpha_T \ll \lambda$). In addition, they were generated from local equations based upon constant local dispersion coefficients (§2.2) and are valid when the x_1 axis is aligned with the mean flow direction (as it approximately is here). Notice that A_{11} is independent of the local dispersivities in this case and that the ratio A_{22}/A_{11} is very small, perhaps in an unrealistic fashion because of the forced isotropy [*Gelhar*, 1987]. When $\alpha_L = \alpha_T = 0$, these results agree with those *Dagan*, [1984] whose Lagrangian approach neglects the influence of the local dispersivities altogether [*Gelhar*, 1986b]. Theoretical values of A_{11} based upon (89a) are included in Table 7. Theoretical values of A_{11} based upon an alternative theory of *Neuman, et al.* [1987] are also shown in Table 7. These results were developed using a set of assumptions slightly different from those of *Gelhar and Axness* [1983], and amount to evaluation of (89a) with $\gamma \equiv 1$.

Table 7
Estimated Longitudinal Macrodispersivities A_{11}, Example 3

Run	— Measured $A_{11*}(\infty)$ — Eq.(88a)	Eq.(88b)	—— Theoretical $A_{11}(\infty) = \sigma^2_f \lambda / \gamma^2$ —— Gelhar and Axness [1983]	Neuman, et al. [1987]
3.1	1.68	1.67	0.91	5.3
3.2	1.90	1.90	0.91	5.3
3.3	1.77	1.86	0.91	5.3
3.4	†	†	0.91	5.3
3.5	0.71	0.67	0.72	1.0
3.6	0.73	0.66	0.72	1.0
3.7	0.79	0.52	0.72	1.0
3.8	0.77	0.77	0.72	1.0
			$\gamma \equiv \exp(\sigma^2_f/6)$	$\gamma \equiv 1.0$

† not calculated because mass in Ω_c never remained constant long enough to make suitable statistical measurements.

The experimental and theoretical results of Table 7 can also be compared as shown in Figure 19. Here, the experimental values of $A_{11*}(\infty)$ at $\sigma_f = 1$ and 2.3 are superposed on top of the two theoretical curves for $A_{11}(\infty)$ vs. σ_f. The agreement of the experiments at $\sigma_f = 1$ with the work of *Gelhar and Axness* [1983] is surprisingly good. They are very close to the predicted values and clearly illustrate an insensitivity to the values of the local dispersivities used. The simulations for $\sigma_f = 2.3$ show results differing significantly from both theories, but the *Gelhar and Axness* [1983] expression is much closer. This result is still regarded as a positive one, given the approximate nature of the theory in such a severely heterogeneous system as well the limited size of the experimental flow domain.

6.4.6 Breakthrough Curves. In column 4 of Figures 17 and 18, the breakthrough behavior at the downstream face (face 2, Figure 15) is shown for all runs for $0 < t < T_{max}$. In some cases (runs 3.1 - 3.4), some particle mass remained in the domain at $t = T_{max}$. Each point is separated by a time interval ΔT ($\Delta T = 10$ for flow field 1, $\Delta T = 5$ for flow field 2) and represents the number of particles that exited that face during that time. The mass flow through this face accounts for more than 99% of all the mass that leaves the system Ω_c, except in the large dispersion cases (runs 3.4 and 3.8) when a large amount will disperse upstream near $t = 0$. Observe the very scattered nature of the breakthroughs when σ_f is large and/or α_L and α_T are small (runs 3.1, 3.2, 3.5, and 3.6). Increased values of the local dispersivities for a fixed σ_f tend to increase the diffusive nature of the plume as

seen in the smoother breakthroughs. For the largest dispersivities, a skewed curve is obtained, indicative of the growth of the plume between the first and last breakthroughs. Although this "smoothing "effect becomes more pronounced when the larger dispersivities are used, it seems to have little or no connection with the measured values of $A_{11*}(\infty)$ which proved to be insensitive to the dispersivity values used.

The curves in column 4 of Figures 17 and 18 can be integrated to give the cumulative breakthrough behavior past face 3, as shown in column 5 of the same figures. Many of the points mentioned above can be seen again in these curves, such as their smoother nature when σ_f is small and/or when the dispersivities are large. It is very easy to see the upstream dispersion effect that occurs in runs 3.4 and 3.8 in these curves.

7. SUMMARY AND RECOMMENDATIONS

In this closing section, we will briefly review some of the major points and findings of the report and will conclude by suggesting some additional avenues for future research. The primary goal of this study was to develop and initially apply a transport model for the study of conservative solute migration through large, three-dimensional, heterogeneous flow systems in porous media under both saturated and unsaturated conditions. These simulations were to be used to examine the temporal and spatial effects of the variable flow field on developing solute plumes, and in particular, to investigate the nature of their large scale dispersive behavior. This could, in turn, be compared with theoretical predictions of such phenomena, such as those included in several recent analyses based upon stochastic methods.

To be consistent with the fundamental hypotheses of the stochastic theories, flow fields would be developed in large, three-dimensional domains characterized by hydraulic parameter distributions that are realizations of spatially correlated random fields. They would then be used as input for the transport model. Both the flow and transport studies would be carried out in one realization of the hydraulic parameter field(s) and would not be part of any Monte Carlo analysis. Variabilities in the local solutions would thus be measured in a spatial sense, much as they are in real field situations. From a computational point of view, this effort would require a grid resolution smaller than a typical fluctuation scale of the input parameter field(s) yet a domain much larger than a typical fluctuation scale of any of the output hydraulic fields. In three dimensions, problems with as many as 10^6 to 10^7 nodes could be envisioned, which would make it imperative to build a transport model as computationally efficient as possible.

A particle tracking, or "random walk" method was chosen as the basis of the transport model. These methods typically represent the solute mass as a large collection of particles, each of which is moved via individual deterministic and random displacements over discrete increments of time. The magnitudes of each displacement depend directly on the velocity and dispersion tensor. At the heart of the method lies an analogy between the familiar solute transport balance equation, a continuum representation, and a certain Fokker-Planck equation which conserves the density of the particles as they are moved in space and time with the discrete "step" equation. In their original form, particle methods are meant to be applied to conservative problems, and as such, conserve mass exactly. They do not suffer from familiar oscillatory problems associated with large grid Peclet numbers. In addition, they can be very cost effective in large, multidimensional, densely-gridded problems. On the other hand, they require the user to think of the application problem in terms of particle distributions and not point concentrations (this can be, in fact, advantageous in many circumstances). This gives rise to issues regarding initial and boundary conditions, interpolation of particle

velocities, choice of time step, and conversion of solutions to meaningful units, such as concentration.

A prototype particle tracking code was developed and tested on several one- and three-dimensional problems. It was then applied to two three-dimensional, saturated heterogeneous flow systems. Both cubically shaped flow domains consisted of roughly 50^3 = 125,000 cells. The two flow systems were developed from specification of a simple head gradient across the domain. The hydraulic conductivity distribution in the first problem was chosen as a realization of an isotropic, exponentially correlated random field with $K_G \equiv 1$ and $\sigma_f \equiv 2.3$. The distribution in the second problem was merely obtained as a multiple of the first such that $\sigma_f \equiv 1.0$. Eight problems involving the release of 8000 particles were run (four in each flow system) and the results were analyzed statistically using moment estimates of the resulting particle distributions. Analysis of the first-order moments indicated mean plume trajectories were roughly parallel with the applied gradient in all problems. Additional analyses based upon measurements of the second ooments of the particle distributions allowed for approximate estimates the longitudinal macrodispersivity component $A_{11}(\infty)$ to be made. Although they can only be considered preliminary in nature, these results compared quite well with their theoretical counterparts, given the various levels of approximation used in the theory, model implementation, and analysis of results.

It should be stressed once again that the model applications in heterogeneous flow systems presented here are provisional, and should be used as a framework to plan more comprehensive simulations. Several particular avenues for additional work include:

- Larger Domains: Simulations in larger domains may shed additional light on the developmental aspects of extremely variable problems, such as those in runs 3.1 to 3.4. They may also tend to minimize effects of the boundary on the internal flow and transport solutions.

- Improved Analyses and Anisotropic Media: Although a number of important data analysis issues were sidestepped in the initial simulations conducted here, a number of more careful, generalized procedures must be adopted in future applications. In particular, examination of the second-order spreading variance must include identification of its principal directions and components as a function of time. These can be compared with estimates of the trajectory (as a function of time) to gauge the orientation difference between the primary direction of the macrodispersivity tensor and mean flux (or trajectory) vector. These differences are predicted by stochastic models, particularly when the underlying conductivity distribution is anisotropic. Anisotropic simulations will also prove to be more realistic in nature.

- <u>Unsaturated Flow Systems</u>: Application of this model to transport in heterogeneous, unsaturated flow systems is also possible under the framework of this investigation, although the comparable theoretical results are much less well developed.

In addition, we should also emphasize that since the particle tracking model has worked very well in the simulations to date, it should be regarded as a viable alternative to conventional models in many kinds of applications (especially in larger problems). Some particular topics for future research may include:

- <u>Multispecies Simulations</u>: This particular model is well suited for simulation the motions of many species at one time. These kinds of simulations are usually of interest when interaction or reaction effects are taking place (see next point).

- <u>Inclusion of Nonconservative Effects</u>: These include any kind of source or sink term due to adsorption or reaction effects and must usually be treated in a post-processing environment.

- <u>Improvement of Concentration Estimation Methods</u>: There is need for improvement in the way particle distributions can be converted to more useful units, such as concentration. As discussed earlier, the simple approach used here gives rise to a "noisy" component of the solution which can be eliminated by using more particles. There may be some type of spatial or spectral filtering mechanism which may be much less expensive to use.

REFERENCES

Ababou, R. , "Three-Dimensional Flow in Random Porous Media", Ph.D. Thesis, Department of Civil Engineering, MIT, Cambridge, MA, 1987

Ababou, R. , D. B. McLaughlin, L. W. Gelhar, and A. F. B. Tompson, Numerical Simulation of Saturated/Unsaturated Flow Fields in Randomly Heterogeneous Media, *International Symposium on the Stochastic Approach to Subsurface Flow, proceedings*, Montvillargenne, France, 1985

Ackerer, Ph. and W. Kinzelbach, Modelisation du Transport de Contaminant par la methode de marche au hasard: Influence des variations du champ d'ecoulement au cours du temps sur la dispersion, *International Symposium on the Stochastic Approach to Subsurface Flow, proceedings*, Montvillargenne, France, 1985

Ahlstrom, S. W., H. P. Foote, R. C. Arnett, C. R. Cole, and R. J. Serne, *Multicomponent Mass Transport Model: Theory and Numerical Implementation*, report BNWL 2127, Battelle, Pacific Northwest Laboratories, Richland, WA, 1977

Baptista, A., E. E. Adams, and K. D. Stolzenbach, Eularian-Lagrangian Analysis of Pollutant Transport in Shallow Water, Tech. Report #296, R. M. Parsons Laboratory, Department of Civil Engineering, M.I.T., Cambridge, MA, 1984

Bhattacharya, R. N., V. K. Gupta, and G. Sposito, On the Stochastic Foundations of the Theory of Water Flow Through Unsaturated Soil, *Wat. Resourc. Res.*, 20(5), p521, 1984

Baveye, P. and G. Sposito, The Operational Significance of the Continuum Hypothesis in the Theory of Water Movement through Soils and Aquifers, *Wat. Resourc. Res.*, 12(3), p503, 1976

Bear, J., *Dynamics of Fluids in Porous Media*, Elsevier, New York, 1972

Bear, J., Hydrodynamic Dispersion, ch. 4 in *Flow Through Porous Media*, R. J. M. De Wiest, ed., Academic Press, 1969

Chandrasakher, S., Stochastic Problems in Physics and Astronomy, in *Selected Papers on Noise and Stochastic Processes*, N. Wax, ed, Dover Pubs. ,1954

Cole, C. R., H. R. Foote, D. A. Zimmerman, and C. S. Simmons, Understanding, Testing, and Development of Stochastic Approaches to Hydrologic Flow and Transport through the use of the Multigrid Method and Synthetic Data Sets, *International Symposium on the Stochastic Approach to Subsurface Flow, proceedings*, Montvillargenne, France, 1985

Cushman, J. H., On Unifying Concepts of Scale, Instrumentation, and Stochastics in the Development of Multiphase Transport Theory, *Wat. Resour. Res.*, 20(11),p1668, 1984

Dagan, G., Solute Transport in Heterogeneous Porous Formations, *J. Fluid Mech.*, 145, p151, 1984

Ewing R. E., and T. F. Russell, Multistep Galerkin Methods Along Characteristics for Convective-Diffusion Problems, *Advances in Computer Methods for Partial Differential Equations IV*, R. Vichnevetsky and R. S. Stepleman, eds., IMACS, Rutgers Univ, New Brunswick, NJ, 1981

Freeze, R. A., A Stochastic-Conceptual Analysis of One-Dimensional Groundwater Flow in Nonuniform Homogeneous Media, *Wat. Resourc. Res.*, **11**, p725, 1975

Freyberg, D., D. Macay, and J. Cherry, Advection and Dispersion in an Experimental Groundwater Plume, preprint of presentation at the Groundwater Contamination Session of the 1983 National Conference on Environmental Engineering, ASCE, University of Colorado, Boulder, 1983

Gardiner, C. W., *Handbook of Stochastic Methods for Physics, Chemistry and the Natural Sciences, second ed.*, Springer Verlag, 1985

Gelhar, L. W., Stochastic Analysis of Flow in Heterogeneous Porous Media, *Fundamentals of Transport Phenomena in Porous Media*, J. Bear and M. Corapcioglu, eds., Martinus Nijhof, Dordrecht, Netherlands, pp 673-717, 1984

Gelhar, L. W., Stochastic Analysis of Transport in Saturated and Unsaturated Porous Media, *Advances in Transport Phenomena in Porous Media*, J. Bear and M. Corapcioglu, eds., Martinus Nijhof, Dordrecht, Netherlands, pp657-700, 1987

Gelhar, L. W., Stochastic Subsurface Hydrology from Theory to Applications, *Wat. Resourc. Res.*, **22**(9), p135s, 1986

Gelhar, L. W., and C. W. Axness, Three Dimensional Analysis of Macrodispersion in Aquifers, *Wat. Resourc. Res.* **19**(1), p161, 1983

Gelhar, L. W., and M. A. Collins, General Analysis of Longitudinal Dispersion in Nonuniform Flow, *Wat. Resourc. Res.* **7**(6), p1511, 1971

Gelhar, L. W., A. L. Gutjahr, and R. L. Naff, Stochastic Analysis of Macrodispersion in a Stratified Aquifer, *Wat. Resourc. Res.*, **15**(6), p1387, 1979

Haken, H., *Synergetics, An Introduction, third ed.*, Springer Verlag, 1983a

Haken, H., *Advanced Synergetics*, Springer Verlag, 1983b

Hassanizadeh, M. and W. G. Gray, General Conservation Equations for Multi-Phase Systems, 1. Averaging Procedures, *Adv. Wat. Resourc.*, **2**, p131, 1979a

Hassanizadeh, M. and W. G. Gray, General Conservation Equations for Multi-Phase Systems, 2. Mass, Momenta, and Entropy Equations, *Adv. Wat. Resourc.*, **2**, p191, 1979b

Hildebrand, F. *Methods of Applied Mathematics*, Prentice Hall, 1965

Hoeksema, R. J., and P. K. Kitanidis, Analysis of the Spatial Structure of Properties of Selected Aquifers, *Wat. Resourc. Res.*, **21**(4), p563, 1985

Huyakorn, P., and G. F. Pinder, *Computational Methods in Subsurface Flow* , Academic Press, 1983

Jazwinski, *Stochastic Processes and Filtering Theory*, Academic Press, 1970

Konikow, L. F., and J. D. Bredehoft, *Computer Model of Two-Dimensional Solute Transport and Dispersion in Groundwater*, Book 7, ch 2., U. S. Geological Survey, 1978

Lapidus, L., and G. F. Pinder, *Numerical Solution of Partial Differential Equations in Science and Engineering*, Wiley, 1982

Mantoglou, A. and L. W. Gelhar, Large Scale Models of Transient, Unsaturated Flow and Contaminant Transport using Stochastic Methods, Tech. Report #299, R. M. Parsons Laboratory, Department of Civil Engineering, M.I.T., Cambridge, MA, 1985

Mantoglou, A., and L. W. Gelhar, Stochastic Modeling of Large-Scale Transient Unsaturated Flow Systems, *Wat. Resourc. Res.*, 23(1), p37, 1987a

Mantoglou, A., and L. W. Gelhar, Capillary Tension Head Variance, Mean Soil Moisture Content, and Effective Specific Soil Moisture Capacity of Transient Unsaturated Flow in Stratified Soils, *Wat. Resourc. Res.*, 23(1), p47, 1987b

Mantoglou, A., and L. W. Gelhar, Effective Hydraulic Conductivities of Transient Unsaturated Flow in Stratified Soils, *Wat. Resourc. Res.*, 23(1), p57, 1987c

Mantoglou, A., Digital Simulation of Multivariate Two- and Three-Dimensional Stochastic Processes with a Spectral Turning Bands Method, *Math. Geology*, 19(2), p129, 1987

Mantoglou, A. and J. L. Wilson, The Turning Bands Method for the Simulation of Random Fields using Line Generation by a Spectral Method, *Wat. Resouc. Res.*, 18(5), p1379, 1982

Matheron, G., and G. deMarsily, Is Transport in Porous Media Always Diffusive? A Counterexample,*Wat. Resouc. Res.*, 16(5), p901, 1980

Monin, A., and A. Yaglom, *Statistical Fluid Mechanics II*, MIT Press, Cambridge MA, 1975

Mulford, E. F., "The Application of Stochastic Models to Numerical Simulations of Large Scale Unsaturated Flow", M.S. Thesis, Department of Civil Engineering, MIT, Cambridge, MA 1986

O'Neill, K., Highly Efficient, Oscillation Free Solution of the Transport Equation over Long Times and Large Spaces, *Wat. Resouc. Res.*, 17(6), p1665, 1981.

Papoulis, A., *Probability, Random Variables, and Stochastic Processes, second ed.*, McGraw Hill, 1984

Pinder, G. F., and H. H. Cooper, A Numerical Technique for Calculating the Transient Position of the Salt Water Front, *Wat. Resourc. Res.*, 6(3), p875, 1970

Pinder, G. F. and W. G. Gray, *Finite Element Simulation in Surface and Subsurface Hydrology*, Academic Press, 1977

Pratt, W. K., *Digital Image Processing*, WIley Interscience, New York, 1978

Press, W. H., B. P. Flannery, S. A. Teukolsky and W. T. Vetterling, *Numerical Recipes, The Art of Scientific Computing*, Cambridge University Press, Cambridge, 1986

Prickett, T. A., T. C. Naymick, and C. G. Lonnquist, A "Random Walk" Solute Transport Model for Selected Groundwater Quality Evaluations, Illinois State Water Survey Bulletin 65, Champaign, 1981

Schwartz, F. W., Macroscopic Dispersion in Porous Media: The Controlling Factors, *Wat. Resourc. Res.*, **13**(4), p743, 1977

Smith, L. and F. W. Schwartz, Mass Transport, 1. A Stochastic Analysis of Macroscopic Dispersion, *Wat. Resourc. Res.*, **16**(2), p303, 1980

Tompson, A. F. B., R. Ababou, and L. W. Gelhar., Applications and Use of the Three-Dimensional Turning Bands Random Field Generator in Hydrology: Single Realization Problems, Tech. Report #313, R. M. Parsons Laboratory, Department of Civil Engineering, M.I.T., Cambridge, MA, 1987

Uffink, G., A Random Walk Model for the Simulation of Macrodispersion in a Stratified Aquifer, *IUGG 18th General Assembly, Hamburg, Proceedings of the IAHS Symposia, Vol. HS2*, 1983

Uffink, G., Modeling of Solute Transport with the Random Walk Method, *NATO Advanced Workshop on Advances in Analytical and Numerical Groundwater Flow and Quality Modeling*, Lisbon, Portugal, June 2-6, 1987

van den Akker, C., Nunerical Analysis of the Stream Function in Plane Groundwater Flow, Report 83-1, National Institute for Water Supply (RIVM), Bilthoven, The Netherlands, 1983

Van Kampen, N. G., *Stochastic Processes in Physics and Chemistry*, North-Holland pub., Amsterdam, 1981

Vanmarcke, E., *Random Fields. Analysis and Synthesis*. M.I.T. Press, Cambridge, MA, 1983

Vomvoris, E. G., *Concentration Variability in Transport in Heterogeneous Aquifers: A Stochastic Analysis*, Ph.D. Thesis, Department of Civil Engineering, MIT, Cambridge, MA 1986

Wang, M. C., and G. E. Uhlenbeck, On the Theory of Brownian Motion II, in *Selected Papers on Noise and Stochastic Processes*, N. Wax, ed, Dover Pubs. ,1954

Wax, N., ed, *Selected Papers on Noise and Stochastic Processes*, Dover Pubs. ,1954

Wierenga, P. S., L. W. Gelhar, C. S. Simmons, E. A. Jacobson, G. W. Gee, and T. J. Nicholson, Validation of Stochastic Flow and Transport Models for Unsaturated Soils: A Comprehensive Field Study, U. S. Nuclear Regulatory Commission NUREG/CR-4622, PNL-5875, RU, 1986

Whitaker, S., Flow in Porous Media I: A Theoretical Derivation of Darcy's Law, *Trans. Por. Med.*, **1**, p3, 1986

Yeh, T.-C. J., L. W. Gelhar, and A. L. Gutjahr, Stochastic Analysis of Unsaturated Flow in Heterogeneous Soils, 2. Statistically Anisotropic Media with Variable â, *Wat. Resourc. Res.*, **21**(4), p457, 1985a

Yeh, T.-C. J., L. W. Gelhar, and A. L. Gutjahr, Stochastic Analysis of Unsaturated Flow in Heterogeneous Soils, 3. Observations and Applications, *Wat. Resourc. Res.*, **21**(4), p465, 1985b

Yeh, T.-C. J., L. W. Gelhar, and P. J. Wierenga, Observation of Spatial Variability of Soil-Water Pressure in a Field Soil, *Soil Sci.*,142(1), p7, 1986

APPENDIX A: EVALUATION OF THE TENSOR $\mathbb{B}$

The purpose of this section is to determine a relationship between the components of the tensor $\mathbb{B}$ and those of the dispersion tensor $\mathbb{D}$ for use in the random walk step equations (52) and (55). Recall from equation (7) that $D_{ij}(\mathbf{X})$ is given by

$$D_{ij} = (\alpha_T V + D)\delta_{ij} + (\alpha_L - \alpha_T)v_i v_j / V \tag{A1}$$

where $v_i(\mathbf{X})$ is the local groundwater velocity vector of magnitude $V(\mathbf{X})$, $D(\mathbf{X})$ is a molecular diffusion coefficient, and $\alpha_L(\mathbf{X})$ and $\alpha_T(\mathbf{X})$ are local dispersivities. $D_{ij}(\mathbf{X})$ is related to $B_{ij}(\mathbf{X})$ through the expression

$$D_{ij} = {}^1/_2\, B_{ik} B_{jk} = {}^1/_2\, \mathbb{B}\,\mathbb{B}^T \tag{A2}$$

given earlier as equations (51b) or (54b).

As D_{ij} is a symmetric, real valued tensor, it can be represented in terms of its diagonalized form $\mathbb{D}^*$ [*Hildebrand*, 1965]:

$$\mathbb{D} = \mathbb{R}\,\mathbb{D}^*\,\mathbb{R}^T \tag{A3}$$

The diagonal matrix $\mathbb{D}^*$ simply contains the eigenvalues of $\mathbb{D}$ and $\mathbb{R}$ is a matrix of its corresponding orthogonal, normalized eigenvectors (as columns). The eigenvalues of $\mathbb{D}$ are

$$\lambda_1 = \alpha_L V + D \tag{A4}$$
$$\lambda_{2,3} = \alpha_T V + D$$

The normalized eigenvector corresponding to λ_1 is

$$e_1 = (v_1/V,\ v_2/V,\ v_3/V) = (\ell_1,\ m_1,\ n_1) \tag{A5}$$

which corresponds to the direction of the velocity vector $\mathbf{V}$. The remaining two normalized eigenvectors must be mutually orthogonal and lie in the plane perpendicular to $\mathbf{V}$. Their orientation in this plane is arbitrary, however, which corresponds to the equivalent dispersivities in any of these directions. The eigenvectors correspond physically to direction cosines $(\ell_i,\ m_i,\ n_i)$ of a

coordinate transformation that maps the X coordinate system into the X^* system where the X_1^* direction is aligned with the velocity vector V (figure A1). In this sense, the matrix $\mathbb{R}$ is a rotation matrix of direction cosines in the columns:

$$\mathbb{R} = \begin{bmatrix} \ell_1 & \ell_2 & \ell_3 \\ m_1 & m_2 & m_3 \\ n_1 & n_2 & n_3 \end{bmatrix} \quad \text{or} \quad R_{ij} \equiv \cos(X_i, X_j^*) \tag{A6}$$

Equation (A3) can be rewritten as

$$\mathbb{D} = \mathbb{R} \mathbb{A} \mathbb{A}^T \mathbb{R}^T \tag{A7}$$

where

$$\mathbb{A} = \begin{bmatrix} \sqrt{\alpha_L V + D} & 0 & 0 \\ 0 & \sqrt{\alpha_T V + D} & 0 \\ 0 & 0 & \sqrt{\alpha_T V + D} \end{bmatrix} = \mathbb{D}^{*\,1/2} \tag{A8}$$

Thus (A7) can be written as

$$\mathbb{D} = \mathbb{R} \mathbb{A} (\mathbb{R} \mathbb{A})^T \tag{A9}$$

whence from (A2),

$$\mathbb{B} = \sqrt{2} \mathbb{R} \mathbb{A} = \mathbb{R} \mathbb{B}^* \tag{A10}$$

where

$$\mathbb{B}^* = \begin{bmatrix} \sqrt{2(\alpha_L V + D)} & 0 & 0 \\ 0 & \sqrt{2(\alpha_T V + D)} & 0 \\ 0 & 0 & \sqrt{2(\alpha_T V + D)} \end{bmatrix} = \sqrt{2} \mathbb{A} = \sqrt{2} \mathbb{D}^{*1/2} \tag{A11}$$

is the diagonal representation of the matrix $\mathbb{B}$ or the rotated form in the X^* coordinate system.

To completely define $\mathbb{B}$ through (A10) it is only necessary to find two other normal, orthogonal
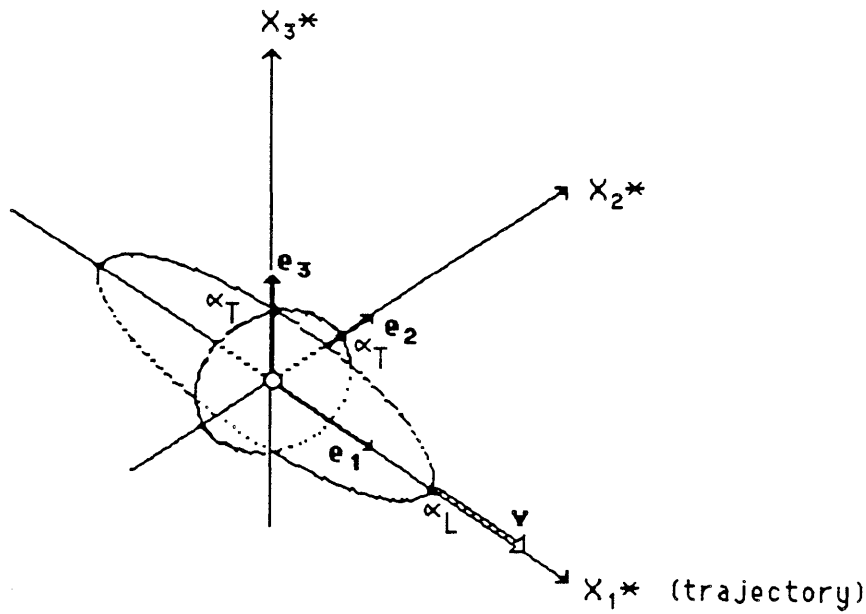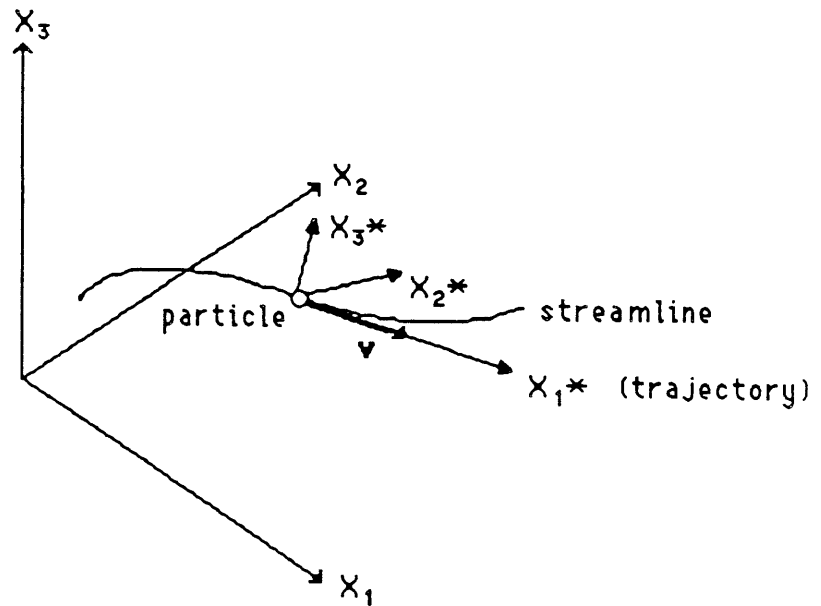
Figure A1: Relationship of eigenvectors to rotated coordinate system X^*. Note the degree of freedom in the orientation of the X_2^* and X_3^* axes (corresponding to the double eigenvalue λ_2, λ_3).

eigenvectors e_2 and e_3 for the rotation matrix $\mathbb{R}$ (as e_1 is given by A5). There are many possibilities for these vectors (Figure A1) as these will correspond to the direction cosines of the rotated axes X_2^* and X_3^*. One choice of a perpendicular direction n to the first eigenvector e_1 is

$$n = (-v_2/V, \ (v_1 + v_3)/V, \ -v_2/V) \tag{A12}$$

which, when normalized, gives $e_2 \equiv n/|n|$. The third normalized eigenvector is then given by the cross product $e_3 \equiv e_1 \times e_2$. The resulting rotation matrix $\mathbb{R} = R_{ij}$ is given by:

$$\mathbb{R} = \begin{bmatrix} v_1/V & -v_2/\beta & -[v_2^2 + v_3^2 + v_1 v_3]/\beta V \\ v_2/V & (v_1 + v_3)/\beta & [v_2(v_1 - v_3)]/\beta V \\ v_3/V & -v_2/\beta & [v_1^2 + v_2^2 + v_1 v_3]/\beta V \end{bmatrix} \tag{A13a}$$

where

$$\beta \equiv \sqrt{V^2 + 2v_1 v_3 + v_2^2} > 0 \quad \text{for} \quad V > 0 \tag{A13b}$$

Notice that $\mathbb{R}$ will most generally be a function of position (as the direction of V may change in space). The choice of e_2 and e_3 used above eliminate the possibility of any computational singularities when evaluating the components R_{ij} as long as the velocity magnitude $V > 0$. This makes computer implementation of the random walk algorithms more simple.

The generalized dispersive displacement d used in equations (52) and (55) will be given by

$$d_i = B_{ij}(X_{n-1})Z_{j,n}\sqrt{\Delta t} \quad = R_{ik}B_{kj}^*Z_{j,n}\sqrt{\Delta t} \tag{A14}$$

where R_{ik} is given above in (A14) and B_{kj}^* is the diagonalized form of B_{kj} given by (A11). This expression reduces to the same one used in the two-dimensional model of *Ackerer and Kinzelbach*, [1985].

Notice that the case $\alpha_L = \alpha_T = 0$, the tensor $D_{ij} \equiv D \, \delta_{ij}$ (which is equivalent to the simple diffusion case, equation 47b). Following the development above, it is found that $B_{ij} = R_{ik}B_{kj}^*$ where B_{kj}^* is simply given by $\sqrt{2D} \, \delta_{kj}$, and the generalized dispersive displacement d is given by

$$d_i = B_{ij}(X_{n-1})Z_{j,n}\sqrt{\Delta t} \quad = R_{ik} \sqrt{2D} \, \delta_{kj} Z_{j,n}\sqrt{\Delta t} \tag{A15}$$

$$= R_{ik} Z_{k,n}\sqrt{2D \, \Delta t}$$

where R_{ik} is given as above. This expression is perfectly correct, except that if one notices that the eigenvectors of the reduced form of D_{ij} possess two degrees of freedom (as opposed to one earlier), then the rotation matrix could also have an arbitrarily oriented e_1 vector. In other words, the absence of the α_L, α_T dependence means that e_1 does not have to necessarily be aligned with v. This implies a greater freedom in finding an R_{ik}, the most obvious choice now being $R_{ik} = \delta_{ik}$. Use of this rotation above reduces (A15) to

$$d_i = \delta_{ik} z_{k,n} \sqrt{2D \, \Delta t} = z_{i,n} \sqrt{2D \, \Delta t} \tag{A16}$$

which is exactly what is used in equation (52).

APPENDIX B: INTERPOLATION FROM NODAL VALUES

Consider a general function $\psi(X)$ for which discrete nodal values on the large regular, three-dimensional prismatic grid of Figure 2 are known, as illustrated in detail in Figure B1. These values may have come, for example, from some finite difference or finite element numerical simulation. The question is: how can approximations be developed for ψ, $\nabla\psi$, and, perhaps, $\nabla\nabla\psi$ at points between the nodes?

Let the flow domain Ω_c be broken up into a number of connecting volumes Ω_e each defined by 8 noded rectangular blocks (or cubes) as shown in Figure B1. In a finite element sense, these will simply be elements; in a finite difference sense, they might be called cells. In any case, none of the cell volumes Ω_e overlap and their union form the complete computational domain Ω_c (Figure 2). For the time being, we will consider one cell and the 8 values of ψ ($= \psi_n$, $n = 1, 2, \ldots 8$) at its corners and be concerned with defining ψ and its derivatives inside of it. Let X_n denote the coordinate of the n-th node, X_c, the center of the cell (easy to define since the cells are rectangular), and X_i, any arbitrary point within Ω_e.

- Interpolation of ψ: One way to interpolate $\psi(X_i)$ inside a cell is to define

$$\hat{\psi}(X_i) = \sum_{n=1}^{8} \psi_n \varphi_n(X_i) \tag{B1}$$

where $\varphi_n(X)$ is the trilinear, Lagrangian polynomial basis or interpolation function associated with node n [*Lapidus and Pinder*, 1982]. The functions φ_n are C^∞ continuous within Ω_e, yet C^0 continuous over all of Ω_c. The approximation (B1) will thus be C^∞ in Ω_e, but only C^0 throughout Ω_c. In some cases, a simpler representation of ψ within Ω_e may be desired. The constant approximation $\psi|_e$ given by

$$\psi|_e = {}^1/_8 \sum_{n=1}^{8} \psi_n \equiv \hat{\psi}(X_c) \tag{B2}$$

is constant within cells and discontinuous across cell boundaries $\partial\Omega_e$. Notice that $\psi|_e$ is just $\hat{\psi}$ evaluated at the center point X_c. Such an approximation may make sense in situations where large
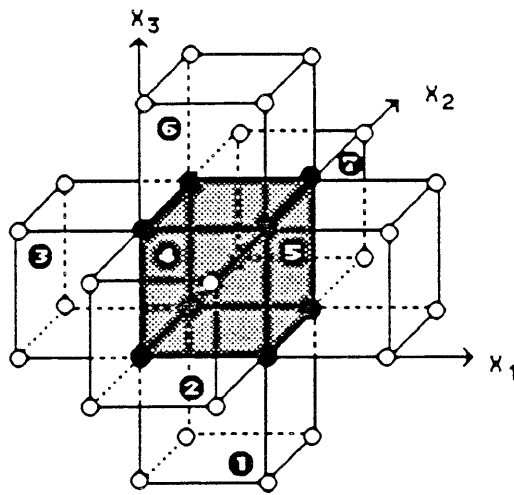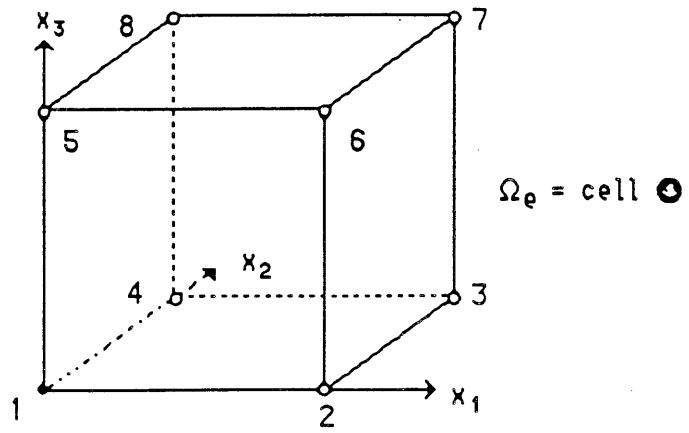
Figure B1:   Cell with 8 nodes (above) and same cell with its six, numbered neighbors.

numbers of cells are considered and / or when computational costs must be minimized.

- Interpolation of $\nabla \psi$: The same interpolation functions φ_n can be used to estimate the gradient $\nabla \hat{\psi} \big|_{X_i}$ using the nodal values of ψ:

$$\nabla \hat{\psi} \big|_{X_i} = \sum_{i=1}^{8} \psi_n \nabla \varphi_n(X_i) \tag{B3}$$

Because the φ_n functions are C^0 continuous, this approximation will vary continuously within the cell volume Ω_e, but it will be discontinuous across the cell boundaries $\partial \Omega_e$ and in Ω_c as a whole. A cell-wise constant value of the gradient $\nabla \psi \big|_e$ based upon the 8 nodal values ψ_n can be approximated (Figure B1) by

$$\nabla \psi \big|_e = \frac{1}{4\Delta X_1} \left[(\psi_2-\psi_1) + (\psi_3-\psi_4) + (\psi_6-\psi_5) + (\psi_7-\psi_8) \right] i +$$

$$\frac{1}{4\Delta X_2} \left[(\psi_4-\psi_1) + (\psi_3-\psi_2) + (\psi_8-\psi_5) + (\psi_7-\psi_6) \right] j$$

$$\frac{1}{4\Delta X_3} \left[(\psi_5-\psi_1) + (\psi_6-\psi_2) + (\psi_7-\psi_3) + (\psi_8-\psi_4) \right] k \tag{B4}$$

$$= \nabla \hat{\psi} \big|_{X_c}$$

which is equivalent to (B3) evaluated at X_c. This is, of course, constant over each cell volume Ω_e and discontinuous over all of Ω_c. Another cell approximation with the same continuity properties $\nabla \psi \big|_{ee}$ can be based upon differences of the approximate neighboring cell values $\psi \big|_e$ defined by (B2). Referring to Figure B1, one way of doing this is

$$\nabla \psi \big|_{ee} = \frac{1}{2\Delta X_1} (\psi \big|_5 - \psi \big|_3) i + \frac{1}{2\Delta X_2} (\psi \big|_6 - \psi \big|_2) j + \frac{1}{2\Delta X_3} (\psi \big|_7 - \psi \big|_8) \tag{B5}$$

To find continuous estimates of $\nabla \psi$ over Ω_c it would be necessary to either use higher order interpolation functions φ_n in (B3) (perhaps defined over cells with 27 nodes) or to have nodal estimates of $\nabla \psi \big|_{X_n}$. Use of the higher order basis functions will be avoided here because of the increased complexity. Although nodal values of the derivatives are not assumed to be available

a-priori from a numerical solution procedure, *estimates* could be made on the regular grid based upon simple differences of the nodal ψ_n values. Although some degree of additional error from differencing numerical solutions for ψ would arise, the differenced values could be considered a new function ζ_n (most generally a vector) and interpolated as done above with the function ψ in (B1) or (B2). If ζ_n is obtained from centered differences of ψ_n, then use of (B1) will give a continuous representation $\zeta(X_i)$ over Ω_c. In this case, the constant representation (B5) will be equivalent to $\zeta(X_c)$. The approximations (B3 - B4) will be based on 8 nodal values of ψ; (B5) as well as (B1 - B2) using ζ will involve 32 values of ψ.

- **Interpolation of $\nabla\nabla\psi$:** In this case, no suitable approximation can be found based upon the 8 nodal values of ψ and the linear interpolation functions φ_n. Given the nodal values of $\nabla\psi = \zeta$ mentioned above, continuous approximations over the cell volume Ω_e similar to (B3) can be developed. Nodal values of $\nabla\nabla\psi$ (or some of its components) might be developed by differencing of ψ values (as above) and used to develop representations of second derivatives of ψ over Ω_c or Ω_e similar to (B1) or (B2). A more practical possibility may be the simple differencing of cell values of $\nabla\psi$ similar to what is done in (B5).